Depositional setting, provenance and tectonic-volcanic setting of Eocene-Recent deep-sea sediments of the oceanic Izu-Bonin forearc, NW Pacific (IODP Expedition 352)

International Geology Review

ISSN: 0020-6814 (Print) 1938-2839 (Online) Journal homepage: http://www.tandfonline.com/loi/tigr20

Depositional setting, provenance, and tectonic-volcanic setting of Eocene–Recent deep-sea sediments of the oceanic Izu–Bonin forearc, northwest Pacific (IODP Expedition 352)

Alastair H. F. Robertson, Steffen Kutterolf, Aaron Avery, Alan T. Baxter, Katerina Petronotis, Gary D. Acton, Claire Carvallo & Julie C. Schindlbeck

To cite this article: Alastair H. F. Robertson, Steffen Kutterolf, Aaron Avery, Alan T. Baxter, Katerina Petronotis, Gary D. Acton, Claire Carvallo & Julie C. Schindlbeck (2017): Depositional setting, provenance, and tectonic-volcanic setting of Eocene–Recent deep-sea sediments of the oceanic Izu–Bonin forearc, northwest Pacific (IODP Expedition 352), International Geology Review, DOI: 10.1080/00206814.2017.1393634

To link to this article: https://doi.org/10.1080/00206814.2017.1393634

INTERNATIONAL GEOLOGY REVIEW, 2017
https://doi.org/10.1080/00206814.2017.1393634

Taylor & Francis
Taylor & Francis Group

ARTICLE

OPEN ACCESS Check for updates

Depositional setting, provenance, and tectonic-volcanic setting of Eocene–Recent deep-sea sediments of the oceanic Izu–Bonin forearc, northwest Pacific (IODP Expedition 352)

Alastair H. F. Robertson[a], Steffen Kutterolf[b], Aaron Avery[c], Alan T. Baxter[d], Katerina Petronotis[e], Gary D. Acton[f*], Claire Carvallo[g] and Julie C. Schindlbeck[b†]

[a]School of GeoSciences, University of Edinburgh, Grant Institute, Edinburgh, UK; [b]Dynamics of the Ocean Floor, GEOMAR Helmholtz Centre for Ocean Research Kiel, Kiel, Germany; [c]Earth, Ocean and Atmospheric Sciences, Florida State University, Tallahassee, FL, USA; [d]School of Rural and Environmental Sciences, University of New England, Armidale, Australia; [e]International Ocean Discovery Program, Texas A&M University, College Station, TX, USA; [f]Department of Geography and Geology, Sam Houston State University, Huntsville, TX, USA; [g]Institut de Minéralogie de Physiques des Matériaux et de Cosmochemie, Université Pierre et Marie Curie, Paris, France

ABSTRACT

New biostratigraphical, geochemical, and magnetic evidence is synthesized with IODP Expedition 352 shipboard results to understand the sedimentary and tectono-magmatic development of the Izu–Bonin outer forearc region. The oceanic basement of the Izu–Bonin forearc was created by supra-subduction zone seafloor spreading during early Eocene (c. 50–51 Ma). Seafloor spreading created an irregular seafloor topography on which talus locally accumulated. Oxide-rich sediments accumulated above the igneous basement by mixing of hydrothermal and pelagic sediment. Basaltic volcanism was followed by a hiatus of up to 15 million years as a result of topographic isolation or sediment bypassing. Variably tuffaceous deep-sea sediments were deposited during Oligocene to early Miocene and from mid-Miocene to Pleistocene. The sediments ponded into extensional fault-controlled basins, whereas condensed sediments accumulated on a local basement high. Oligocene nannofossil ooze accumulated together with felsic tuff that was mainly derived from the nearby Izu–Bonin arc. Accumulation of radiolarian-bearing mud, silty clay, and hydrogenous metal oxides beneath the carbonate compensation depth (CCD) characterized the early Miocene, followed by middle Miocene–Pleistocene increased carbonate preservation, deepened CCD and tephra input from both the oceanic Izu–Bonin arc and the continental margin Honshu arc. The Izu–Bonin forearc basement formed in a near-equatorial setting, with late Mesozoic arc remnants to the west. Subduction-initiation magmatism is likely to have taken place near a pre-existing continent–oceanic crust boundary. The Izu–Bonin arc migrated northward and clockwise to collide with Honshu by early Miocene, strongly influencing regional sedimentation.

ARTICLE HISTORY
Received 30 June 2017
Accepted 14 October 2017

KEYWORDS
Oligocene–Recent; deep-sea sediments; tuffaceous sediments; oceanic crust; magnetic data; biostratigraphy; Izu–Bonin forearc; IODP Expedition 352; northwest Pacific region

Introduction

We synthesize new biostratigraphic, sedimentary, geochemical, and magnetic data with IODP Expedition 352 shipboard results for Eocene–Recent sediments on the Izu–Bonin outer forearc (Reagan *et al*. 2015, 2017) and discuss these in the evolving regional tectonic-volcanic setting. Our results complement and extend previous exploration, especially dredging and submersible studies of the forearc region (Reagan *et al*. 2010, 2013) and recent results from the Izu–Bonin arc (Arculus *et al*. 2015c) and backarc (Busby *et al*. 2017; Tamura *et al*. 2015).

We highlight the provenance and origin of the tuffaceous input to many but crucially not all levels of the drilled sequences. Volcanogenic sediments can be used to indicate the distribution, composition, and temporal evolution of both oceanic and continental margin arcs (Huang *et al*. 1973; Kennett and Thunell 1975; Huang 1980; Sigurdsson *et al*. 1980; Cambray *et al*. 1995; Straub and Schmincke 1998; Bryant *et al*. 2003; Scudder *et al*. 2016). Oceanic forearc basins provide invaluable insights into arc evolution because they are located close to active magmatic arcs but are isolated from continental margin turbidity currents. Forearc

CONTACT Alastair H. F. Robertson Alastair.Robertson@ed.ac.uk School of GeoSciences, University of Edinburgh, Grant Institute, James Hutton Road, Edinburgh, UK, EH9 3FE

*Present addresses: International Ocean Discovery Program, Texas A&M University, 1000 Discovery Drive, College Station, TX 77845-9547, USA
†Universität Heidelberg, Institut für Geowissenschaften, Im Neuenheimer Feld 234-236, 69120 Heidelberg, Germany

Supplemental data for this article can be accessed here.

basins, which are commonly controlled by extensional faulting, preserve the sedimentary record with minimal reworking. During Expedition 352, several fault-controlled depocentres were drilled within <20 km of each other (Reagan *et al*. 2015) allowing unique insights into sediment accumulation in an outer forearc setting (Figures 1 and 2).

Our specific objectives are as follows:

(1) To refine and synthesize existing shipboard nannofossil biostratigraphy (Reagan *et al*. 2015) and provide constraints from new radiolarian biostratigraphy.
(2) To identify the chemical composition and provenance of tuffaceous sediments and related changes through time using bulk sediment and tephra chemical data.
(3) To use new palaeomagnetic data to show that some volcanic breccias that were included within the igneous basement (Reagan *et al*. 2015) instead represent coarse sedimentary detritus (talus).
(4) To use new magnetic property data for selected core intervals, especially to test for presence of fine-grained tuffaceous input in hemipelagic sediments.
(5) To evaluate the relative importance of tectonic and/or volcanic controls compared to palaeoceanographic controls in sediment accumulation, particularly in relation to low-carbonate intervals near or beneath the carbonate compensation depth (CCD).
(6) To synthesize all of the new data and interpretation in the context of the Izu–Bonin outer forearc development through time.
(7) To interpret the combined sedimentary record in the Eocene–Recent geological development of the oceanic Izu–Bonin forearc and the Honshu arc (southern Japan). We also evaluate alternative published tectonic models for the creation of the oceanic forearc and subsequent amalgamation with Honshu in the light of the sedimentary evidence.

The time scale of Gradstein *et al*. (2012) is used in this paper.

Drill locations and chronostratigraphic units

Two sites were drilled within and near a several kilometre-sized basin on the upper forearc slope at water depths of 3128 and 3162 m and another two on the lower forearc slope at 4447 and 4775 m (Reagan *et al*. 2015; Figure 2). The upslope sites (U1439, U1442) form the outer part of a belt of NW–SE trending fault-controlled bathymetric ridges and basins (>5 km across),

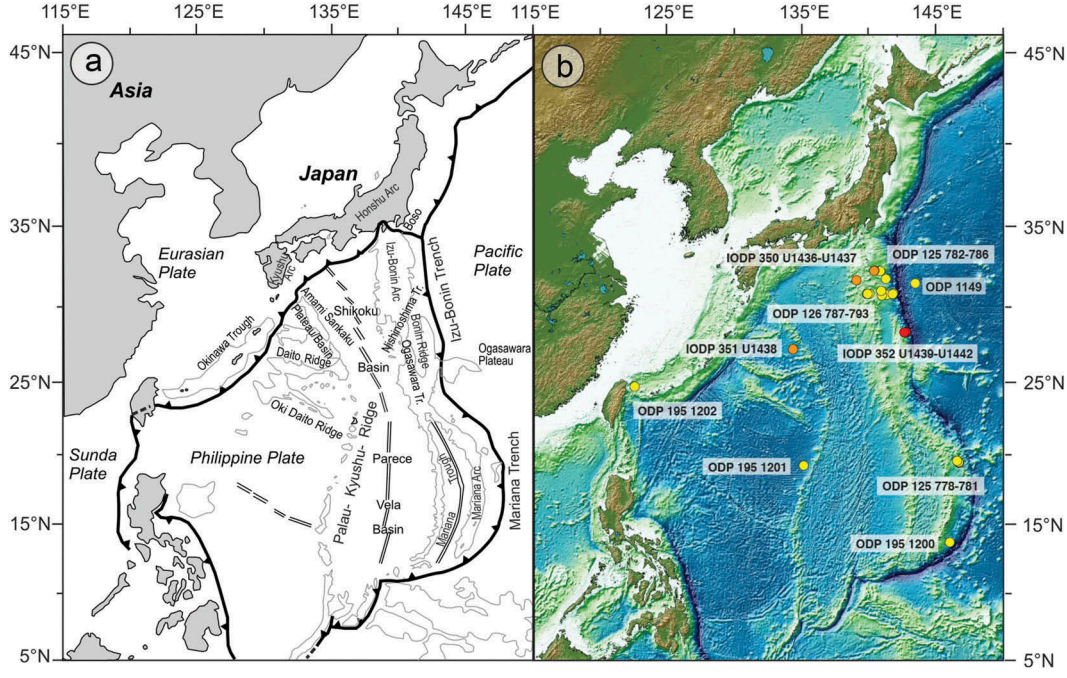

Figure 1. Location maps. (a) Regional tectonic map showing the plate tectonic setting of the northwest Pacific region, including morphotectonic features mentioned in the text; (b) bathymetric map showing the location of the IODP Expedition 352 in relation to other ODP and IODP drill sites in the northwest Pacific region (see Reagan *et al*. 2015 and references) for data sources.

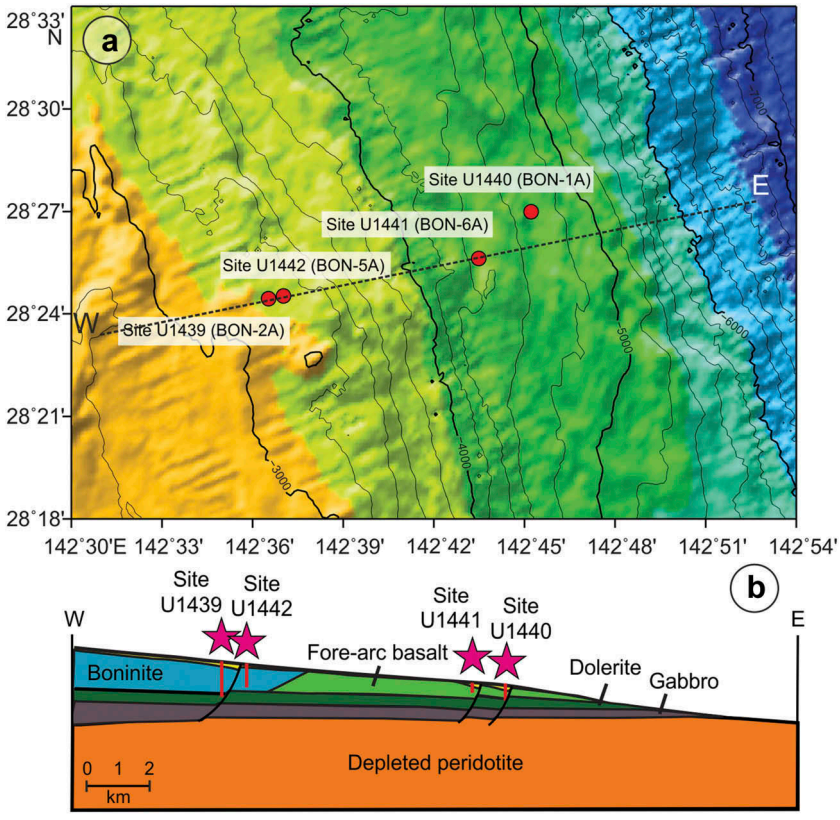

Figure 2. Location of the Expedition 352 drill sites in relation to the regional bathymetry. (a) Bathymetric map showing the Izu–Bonin Ridge and adjacent seafloor (section in Figure 2(b) is shown by the dashed line); (b) schematic section showing the relative locations and penetrations of the drill sites, and the inferred forearc crustal structure (from Reagan *et al*. 2015).

whereas the downslope sites (U1441, U1440) lie within an area of small (<5 km across) fault-controlled basins that extend towards the trench axis (Ishizuka *et al*. 2011a; Figure 1(a)). Site U1439 provided very good overall recovery within a relatively flat-bottomed sediment pond (Figure 3(a,b)), whereas sediment coring at Site U1440 (Figure 3(c)) was compromised by rough sea conditions and proximity (c. 250 m) to the sloping western basin margin (Reagan *et al*. 2015; Christeson *et al*. 2016). Two additional sites (U1441 and U1442) gave relatively poor but useful recovery (Figure 3(c,d)). One of these, Site U1442 (Figure 3(a)), was drilled through a thin sediment drape, c. 200 m east of a small basement high to the east of Site U1439 (Figure 2).

The shipboard division into lithological units (from the top downwards) included relatively coarse-grained sediments and sedimentary rocks (e.g. tuffaceous sand/sandstone, volcaniclastic breccia–conglomerate), which dominate some intervals of the drill cores (Reagan *et al*. 2015). However, post-cruise study, aided by improved biostratigraphy, indicates that intercalated fine-grained sediments (mostly mud/mudstone, clay/claystone, marl, chalk, and limestone) can be correlated across all four drill sites (Figures 4 and 6) using a combination of sedimentary facies, biostratigraphic age, distinctive tephra layers (Reagan *et al*. 2015; Kutterolf *et al*. 2017), and the presence of distinctive spikes or trends in sediment chemical composition. Three main age ranges of background fine-grained sediment deposition are recognized that we term *Time Slices* (Figures 4 and 5). These are most accurately defined for the reference Site U1439. Although less well dated, Time Slices 1–3 can also be recognized in Hole U1440A, Time Slice 1 in Hole U1440B, and Times Slices 2–3 in Hole U1441A. The three time slices help interpret the geochemical evidence and highlight regional to global sedimentary and palaeoceanographic processes.

The biostratigraphically determined ages of the time slices are *Time Slice 1* early Oligocene to early Miocene (c. 35–23 Ma): nannofossil chalk, marl, or limestone, variably mixed with volcaniclastic and tuffaceous sediment (i.e. calcareous siltstone or sandstone). *Time Slice 2* early Miocene to mid-Pliocene (c. 23–4 Ma): clay/claystone and mud/mudstone (variably mixed with silt/siltstone and sand/sandstone). *Time Slice 3* mid-Pliocene to Holocene (c. 4–0 Ma): nannofossil ooze and minor mud (variably mixed with tuffaceous sediment).

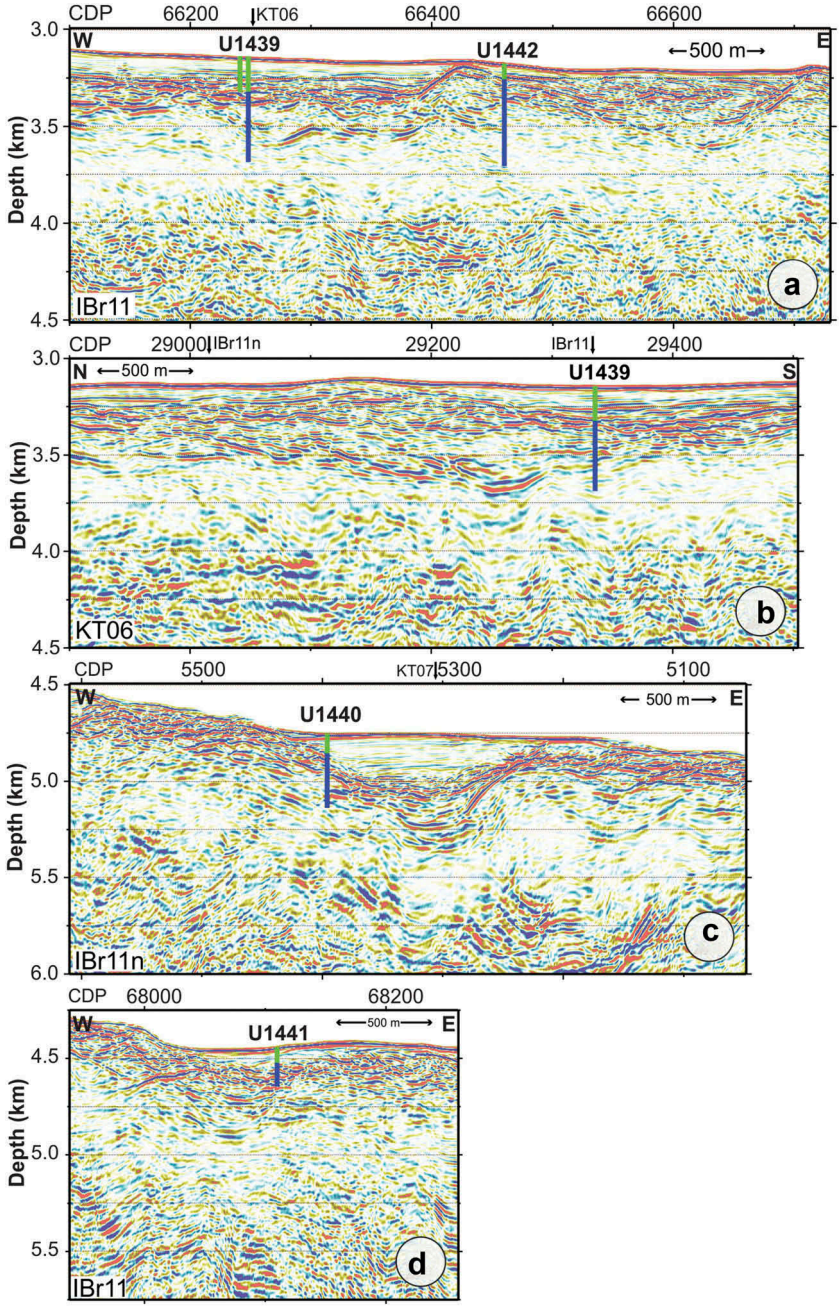

Figure 3. Prestack time migrated images, converted to depth showing the location of the drill sites. (a) Upper forearc basin sites (Sites U1439 and U1442); E–W line; (b) upper forearc basin sites (Sites U1439 and U1442); N–S crossing line; (c) lower forearc basin (Site U1440); E–W line; (d) lower forearc basin (Site U1441); E–W line. Data source Christeson *et al*. (2016) and G. Christeson pers. com. (2015).

Biostratigraphic constraints

Postcruise, approximately 140 samples were studied to produce more accurate calcareous nannofossil datums and an additional 23 samples to provide radiolarian biostratigraphic constraints for key carbonate-poor intervals. These samples helped to refine the shipboard nannofossil age model presented in Reagan *et al*. (2015). The last appearance data (LAD) of nannofossil species in the following section are listed in Supplementary Table 1 and shown in the age model and age/depth plots (Figures 4 and 5). Holes U1439A and U1442A contain the most complete sections while Holes U1441A and U1440A exhibit a limited biostratigraphic record.

For Site U1439, the key reference drill hole, the oldest sediments are slightly younger than previously suggested (Reagan *et al*. 2015). Hole U1439A contains a nearly complete Oligocene–Recent sequence,

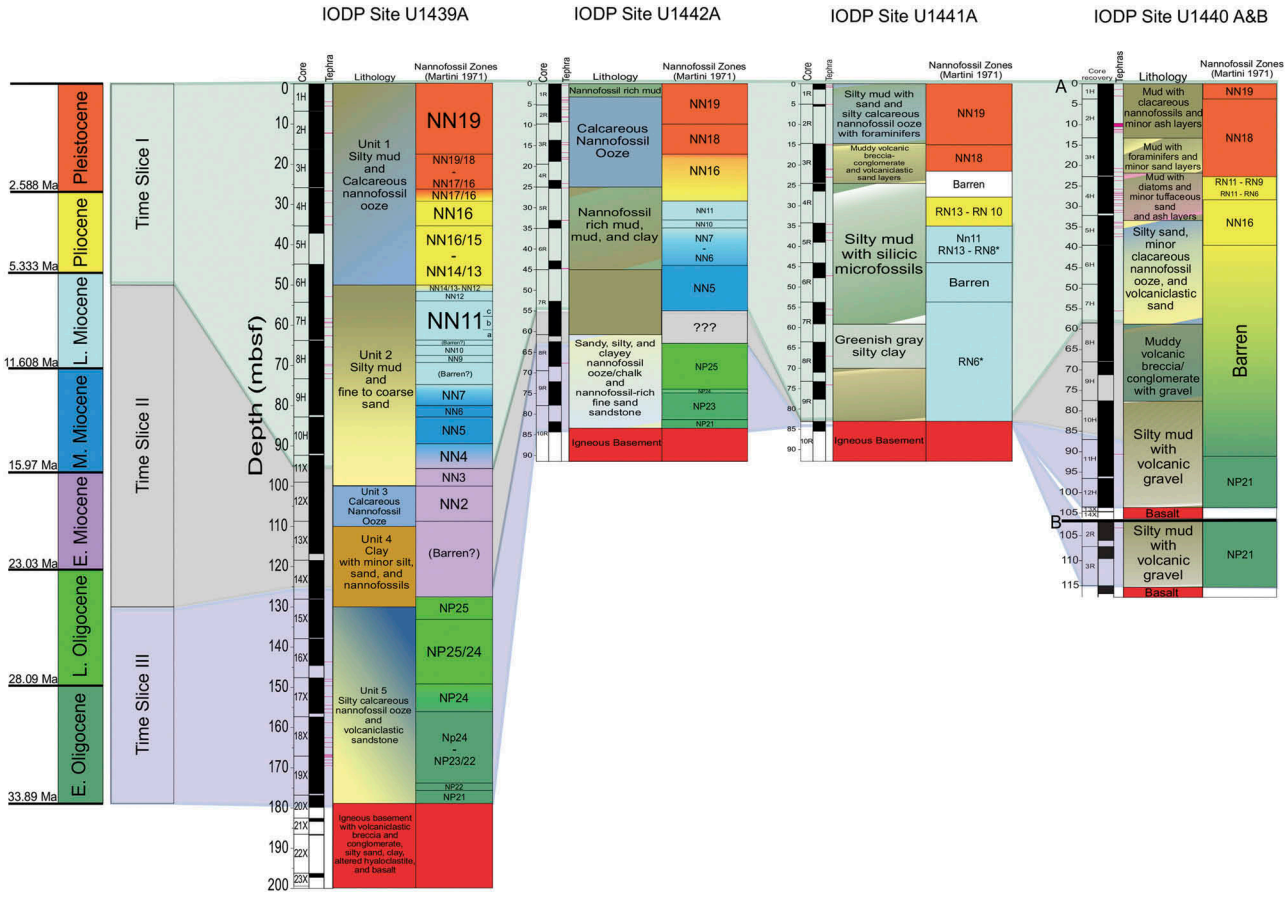

Figure 4. Summary of the combined biostratigraphic data from calcareous nannofossils recovered from carbonate-rich sediments. From left to right, the columns for each site show the age boundaries of epochs, the correlated time slices (used to aid interpretation), depth below seafloor, the shipboard units, the recovery, the inferred ages of tephras (see Kutterolf *et al.*, 2017), the main lithologies, and finally the nannofossil zones. RN values are radiolarian biostratigraphical zonations (see supplementary publication for supporting information).

except for a barren interval of inferred middle Miocene age (Figure 4). The oldest nannofossil-bearing sample is earliest Oligocene (34.44–32.92 Ma) and Oligocene-aged sediments are well represented in Hole U1439A. The exact positioning of the Oligocene/Miocene boundary is difficult to determine owing to the absence of nannofossils (between 107.345 and 125.745 mbsf). The LAD of *Reticulofenestra bisecta* (23.13 Ma) is the best available identification of the Oligocene/Miocene boundary (at 128.01 mbsf), although the true stratigraphic LAD may be located within the barren interval, slightly above this. Above the barren interval, the section is relatively complete. Thirteen (*versus* 7 shipboard) nannofossil biomarkers are recognized, 12 in the Miocene, and a 13th spanning the Miocene/Pliocene boundary (Figure 4).

Hole U1442A contains the secondmost complete section and has many similarities to U1439. The maximum assigned age of earliest Oligocene is identical to Site U1439 but is found ~100 m shallower than at Site U1439. The recovered Oligocene section is also very similar to Hole U1439A in terms of overall abundance and species assemblage. Three Oligocene horizons that were not identified in Hole U1439A are recognized in Hole U1442A. However, the Miocene section is not nearly as complete in Hole U1442A as it is in Hole U1439A, and no early Miocene nannofossils were identified. Only two middle Miocene horizons could be identified at this site, with the younger horizon containing the middle Miocene to late Miocene boundary (between 43.64 and 44.89 mbsf). The late Miocene is represented by two horizons, one of which was not observed in Hole U1439A. The youngest biomarker observed is the LAD of *Helicosphaera sellii* (1.26 Ma).

For Site U1441, the age profile differs considerably. The basal sediments at Site U1441A are inferred to be late Miocene (nannofossil zone NN11a), although the lowest cores lack nannofossils. Neither Oligocene nor early Miocene sediments were recovered. Definitive middle Miocene sediments are also absent. The

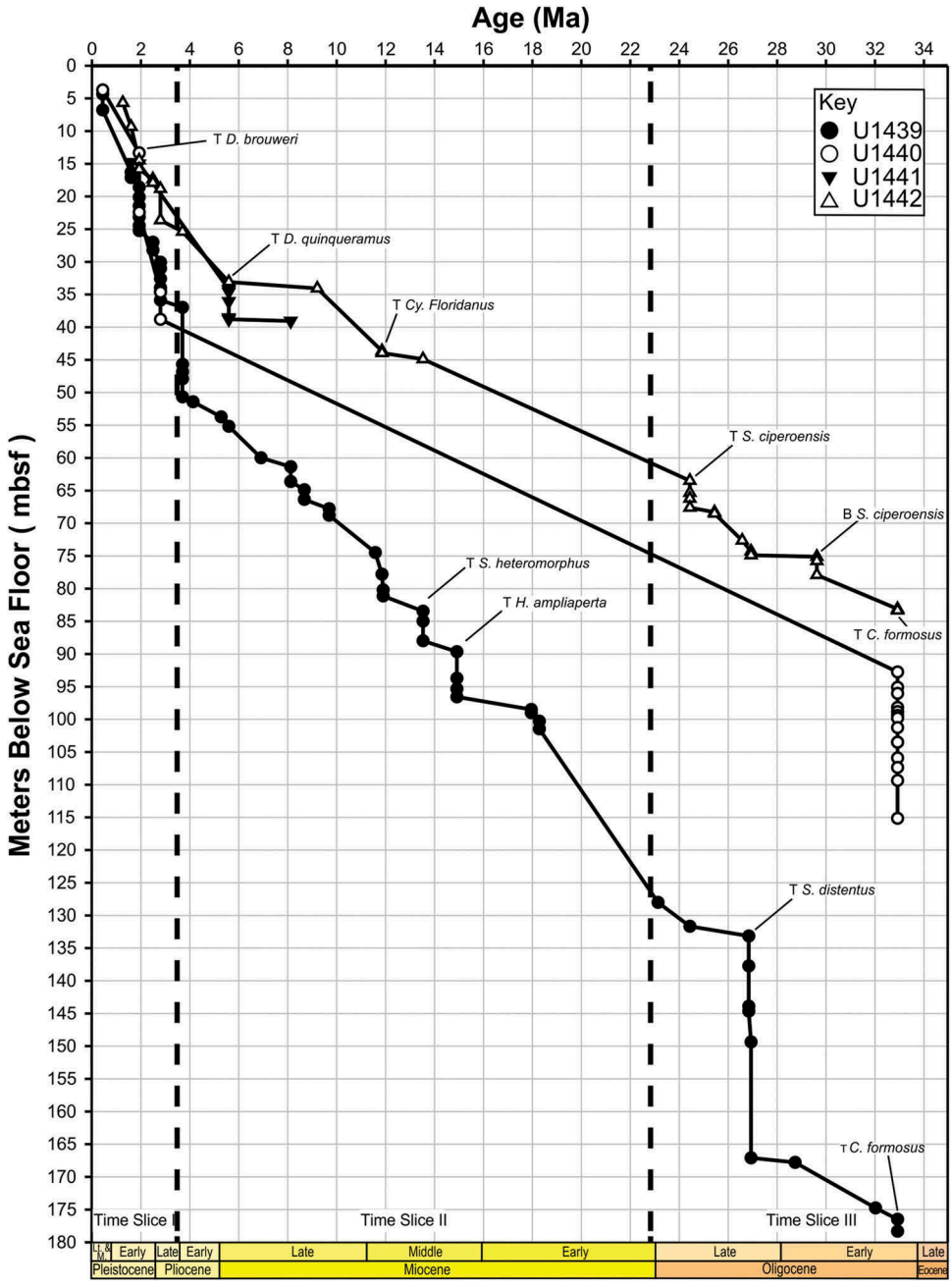

Figure 5. Age/Depth plots with key zonal taxa, also showing the epochs and time slices. The recognized epochs help interpret the geohistory, whereas the time slices aid correlation and interpretation of the hemipelagic sediments.

oldest biostratigraphic age (Cores U1441A 7R through 9R) is from radiolarians assigned a broad late Miocene age. Middle Miocene sediments may be present although there is an absence of definitive markers that could confirm the presence of the middle/late Miocene boundary. No Pliocene-aged radiolarians or calcareous nannofossils were identified although it is likely that a barren interval (Cores U1441A 3R through 4R) is Pliocene. Pleistocene-aged nannofossils are well represented, as in the previously discussed sites.

For Site U1440, the basal sediments in both of the holes drilled (Holes U1440A and U1440B) are constrained as Oligocene by the presence of *Coccolithus formosus* (32.92 Ma), i.e. coeval with the basal sediments at Sites U1439 and U1442. No Miocene nannofossils were recovered due to the presence of a major hiatus from the earliest Oligocene to the Pliocene boundary, amounting to the longest barren interval at any of the four sites. Radiolarian assemblages (Samples U1440A 4H 1W, 90–92 cm and U1440A 4H 4W, 100–102) indicate a broad Pliocene-to-Miocene age for

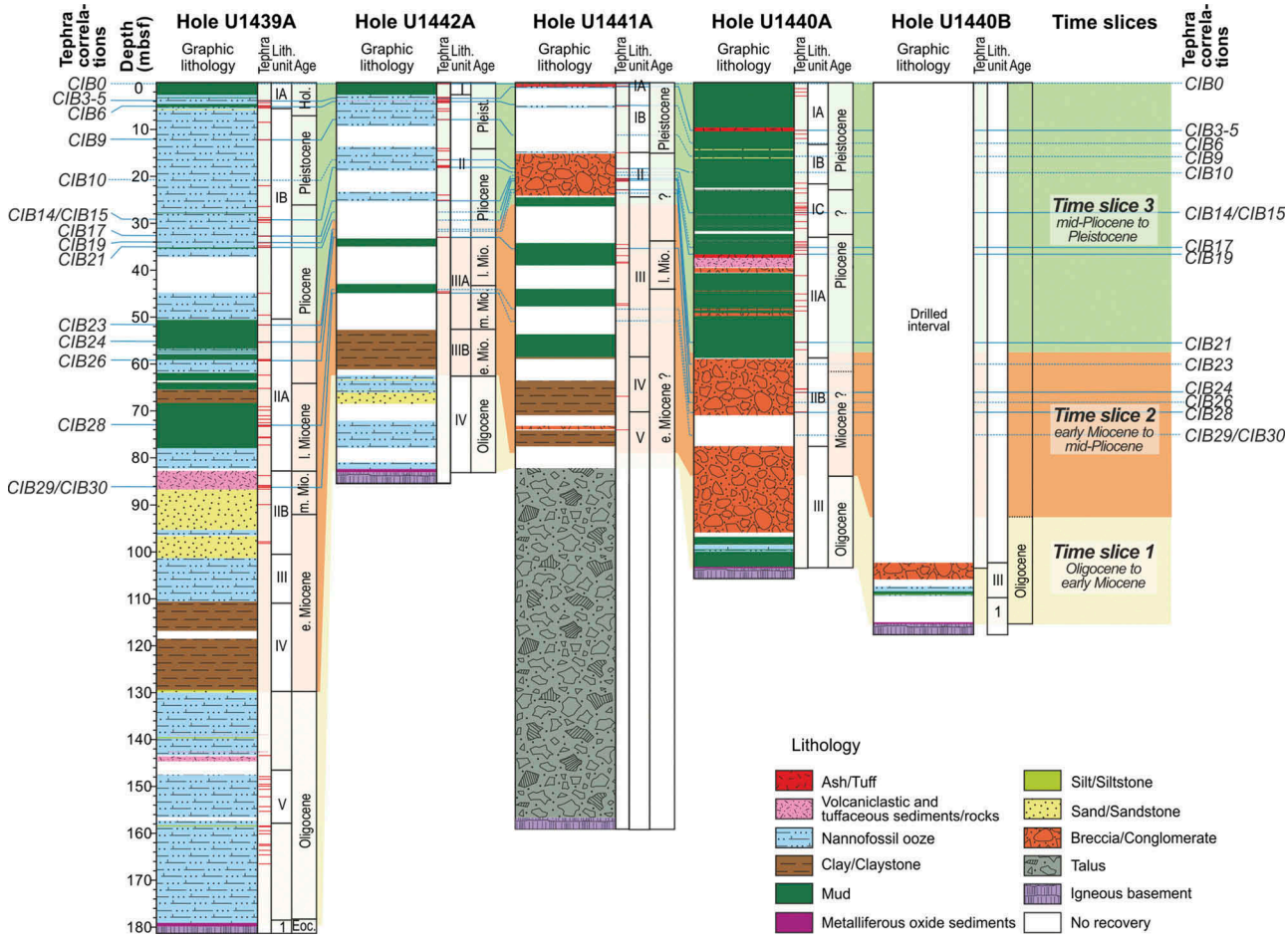

Figure 6. Summary and correlation of the main lithologies recovered during Expedition 352 sites based on shipboard and postcruise data. From left to right, the columns for each site are: numbered tephra layers that can be correlated between sites (blue lines) after Kutterolf *et al*. 2017, depth below seafloor, graphic lithology (see key), main tephra occurrences (horizontal red lines), shipboard units, epochs, and finally the three recognized time slices; a drilled interval without coring in Hole U1440B is also indicated.

the upper part of Hole U1440A. Two additional age constraints (Samples U1440A 8H 7W, 10–12 cm and U1440A 9H 2W, 28–30 cm) suggest that the interval between 67.13 and 69.79 mbsf was deposited in the middle-to-late Miocene.

The resulting biostratigraphy therefore provides a robust basis for interpretation of the geological development of the outer Izu–Bonin forearc through time. Several key inferences are as follows: (1) On the basis of similar nannofossil assemblages and abundances, a similar basal horizon (base of Time Slice 1) can be correlated between Sites U1439, U1440, and U1442. (2) At Sites U1439 and U1442, the barren interval across the Oligocene–Miocene boundary (Time Slice 2) is suggestive of a rise in the CCD that inhibited nannofossil preservation. The occurrence of rare *Discoaster* species within this interval could indicate a near-CCD depth at which monocrystalline nannofossils such as the *Discoaster* group were preferentially preserved whereas other genera were dissolved. (3) Radiolarian assemblages confirm a late Miocene age suggesting accumulation below the CCD at the lower slope sites during a time when the upslope sites (U1439 and U1442) accumulated nannofossil-bearing sediments above the CCD.

Constraints from sediment chemistry

Chemical evidence sheds light on sediment provenance beyond what is possible from shipboard observations (e.g. study of smear slides) (Reagan *et al*. 2105). Hole U1439A is used as a reference because this succession is the longest, most intact, and best dated. One sample of fine-grained pelagic or hemipelagic sediment was taken every 10 m from the seafloor to the top of the igneous basement, supplemented by additional samples that were prepared for shipboard carbonate and XRD. Several samples of sediments within the igneous basement were included (see

Reagan *et al*. 2105). Analysis was carried out by inductively coupled plasma-emission spectrometry for major elements and by ICP-MS (inductively coupled plasma-mass spectrometry) for minor elements (see Electronic supplement table 3). The downhole chemical data were converted from downhole depths to inferred age using the age model (Figures 4 and 6). The explanation below focuses on the three time slices which have contrasting fine-grained sediment compositions and provenance.

Chemical associations and trends through time

Absolute values of chemical abundances are initially plotted against their inferred age for selected major elements, trace elements, and Rare Earth elements (REE) (Figures 7–9). Four main chemical associations, characteristic of specific time intervals are recognized at Site U1439, which reflect differences in depositional processes and/or provenance:

First, during the early Oligocene to early Miocene (Time Slice 1), CaO (Figure 7(a)) and Sr (Figure 7(b)) values are relatively high except close to the igneous basement where metalliferous sediments occur. During the early Miocene to mid-Pliocene (Time Slice 2), CaO and Sr values drop markedly to very low values and then generally rise in the younger part of this time slice (with several spikes). Values are high and variable within Time Slice 3. CaO and Sr co-vary, reflecting substitution of Sr for Ca in calcite (e.g. Rollinson 1993). The low values of CaO and Sr in Time Slice 2 reflect accumulation near or beneath the CCD, consistent with the biostratigraphic evidence (see above). At Site U1440, the analysed values of CaO and Sr are low throughout both Time Slices 1 and 2 although few data are available prior to c. 13 Ma owing to poor recovery.

Second, MgO, TiO_2, SiO_2, K_2O, Al_2O_3, Na_2O, Rb, Sc, Ba, Cs, and Ga (Figure 8(a–g); see also Supplementary Figure 2A–C) show relatively high but variable values during Oligocene to early Miocene time and also relatively high but more constant values during early Miocene to mid-Pliocene time. Time Slice 2 can be generally subdivided into lower and upper parts, in which the lower part has relatively high and constant values of the above constituents and corresponds to an interval of nearly non-calcareous clay/claystone of early Miocene age. In contrast, the upper part of Time Slice 2 exhibits more variable values of these constituents during middle Miocene–early Pliocene time. Absolute values are generally lower but variable during mid-Pliocene to Holocene. The above elemental trends mainly reflect relative downhole variation in aluminosilicate constituents including tephra, ash, or volcaniclastic silt/mud (see below). MgO is not enriched except in the boninitic igneous basement of Hole U1439A (up to 17.5%). Detritus of this composition did not contribute significantly to the overlying sediments.

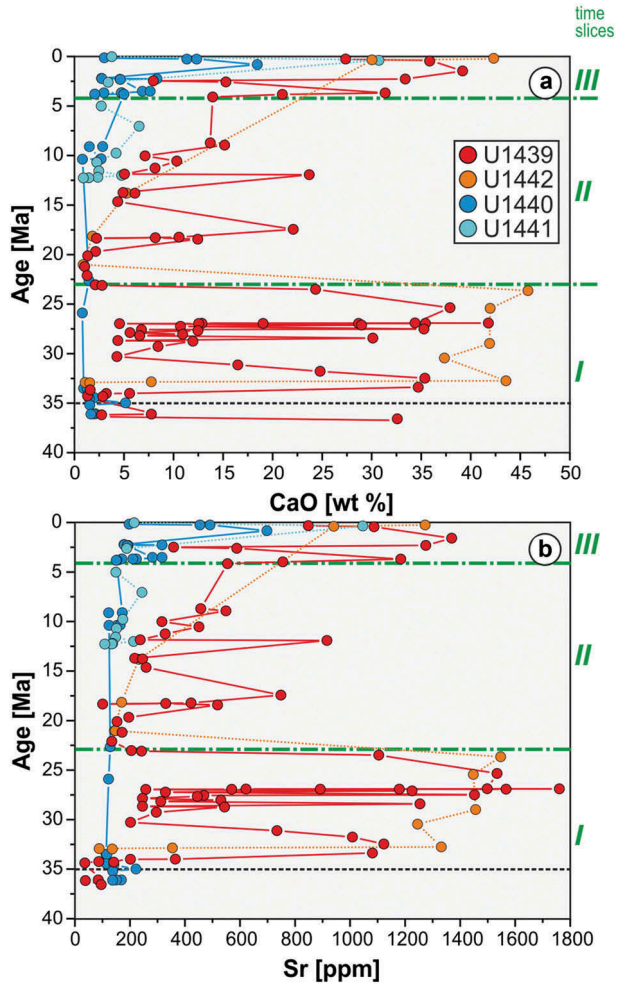

Figure 7. (a,b) Downhole variation in chemical composition through time. (a) CaO as a proxy for carbonate abundance; (b) Sr, an additional proxy for carbonate abundance (correlates with carbonate abundance due to substitution of Sr for Ca). Green broken lines and italic roman numerals indicate the three time slices. See Supplementary Table 3 for analytical data. Additional plots of elements showing similar behaviour are given in Supplementary Figures 2 and 3.

Third, MnO, Fe_2O_3, P_2O_5, Cu, Mo, Pb, Zn, Ni, Co, Hf, Nb, Th, U, Zr, La, and the other REEs (Figure 9(a–g); Supplementary Figure 2D–L) show strong relative enrichment in the basal metalliferous sediments (where present), especially in Hole U1439A (Reagan *et al*. 2015). Similar enrichment is also seen within the early Miocene clay/claystone (Time Slice 2). The relative enrichments of these constituents relate to hydrothermal or hydrogenous accumulation.

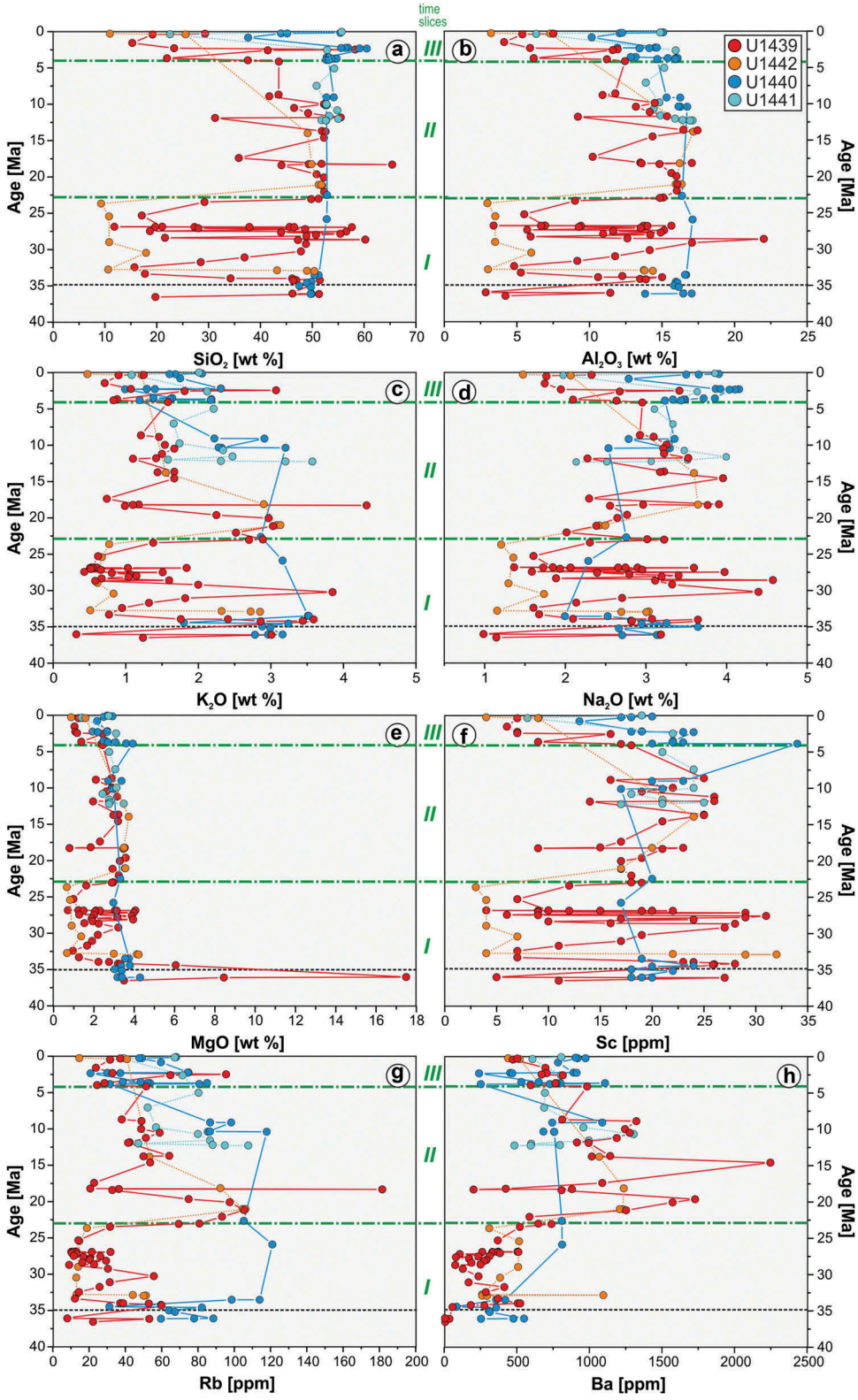

Figure 8. (a–h) Downhole variation in composition through time for selected constituents that show similar chemical behaviour: (a) SiO_2; (b) Al_2O_3; (c) K_2O; (d) Na_2O; (e) MgO; (f) Sc; (g) Rb; (h) Ba. Green broken lines and italic roman numerals indicate the three time slices. See Supplementary Table 3 for analytical data.

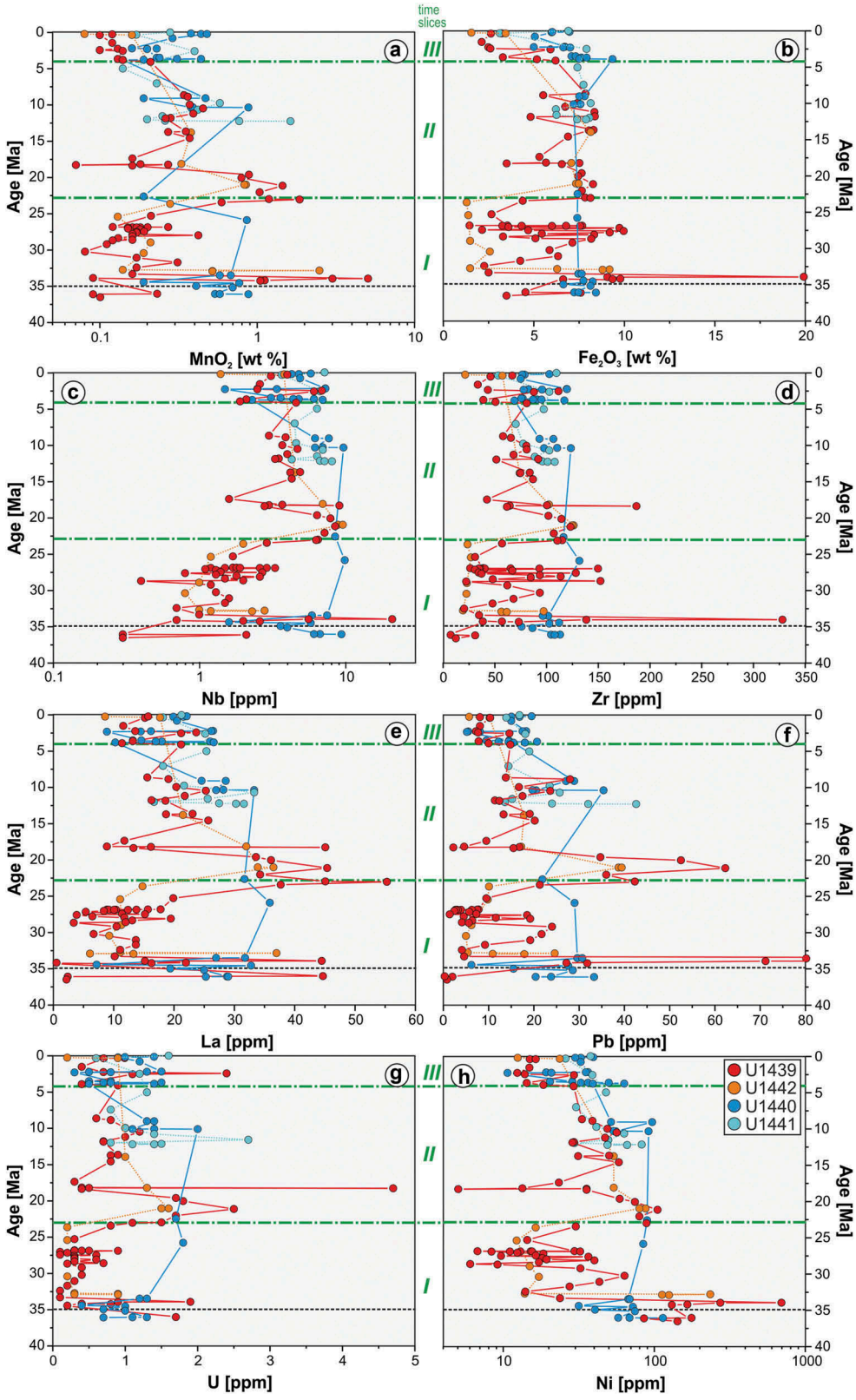

Figure 9. Downhole variation in chemical composition through time for additional constituents that show similar chemical behaviour: (a) MnO; (b) Fe_2O_3; (c) Nb; (d) Zr; (e) La; (f) Pb; (g) U; (h) Ni. These constituents show similarities in chemical behaviour as discussed in the text. See Supplementary Table 3 for analytical data.

Fourth, Fe and V (Figure 9(b); Supplementary Figure 2M) exhibit high values in the basal metalliferous sediments but little systematic variation higher in the succession.

Upslope, Site U1442 shows similar downhole chemical trends and associations to Site U1439 despite much smaller number of analyses (Figures 7–9). The basal sediments there are enriched in both lithogenous (e.g. Al_2O_3, TiO_2, MgO, Zr, Th, Sc, Ga, Rb), hydrogenous, or hydrothermally related constituents (e.g. MnO, Fe_2O_3, P_2O_5, Cu, Mo, U, Co, Sc, Ce). The chemical composition of the early Oligocene–early Miocene interval corresponds to the abundance of tephra-rich, tuffaceous, and volcaniclastic sediments compared to background nannofossil-rich carbonate. Elemental concentrations for this time interval are relatively constant on this topographic high, consistent with pelagic carbonate sedimentation and slope-controlled reworking. In contrast, event-controlled sedimentation (e.g. pyroclastic density currents and ash fallout) coupled with pelagic background sedimentation characterizes the fault-controlled depocentre at Site U1439A. The early Miocene to mid-Pliocene clays/claystones of Time Slice 2 are enriched in many constituents in Hole U1442A, especially during the early Miocene. The absolute values of many chemical constituents (e.g. SiO_2, Al_2O_3, TiO_2, Fe_2O_3, MgO, Cu, Zr, Nb, Th, Co, Sc) are greater in Hole U1442A than in Hole U1439A, which reflects the depositionally condensed nature of the early Miocene clay/claystone in Hole U1442A (c. 10 m) compared to Hole U1439A (c. 20 m). The metal enrichment in Hole U1442A reflects a relatively low sedimentation rate, which favoured hydrogenous accumulation. The generally decreasing abundances of constituents other than $CaCO_3$ and Sr in the Pliocene–Holocene (upper parts of Time Slices 2 and 3) correspond to overall increase in the abundance of nannofossil ooze.

Furthest downslope at Site U1440, several constituents (e.g. K_2O, MnO, Cu, Pb, Ni, Ta, Th) reach relatively high values in the lowermost sediment recovered above the igneous basement. The basal sediments at this site are inferred to lie within Time Slice 2 (early–mid-Pliocene) (Figures 4 and 6). Prominent 'spikes' in many constituents (e.g. Ba, W, K_2O, Na_2O, TiO_2, P_2O_5, Cu, Ni, Ta, Th, U, Y, La, Ce, Nd) characterize the younger part of this time interval (c. 80–50 mbsf). The very low recovery in the younger sediment (Time Slice 1) precludes recognition of downhole trends.

Recovery in the second downslope Site U1441 was restricted to the Pliocene–Holocene (Time Slice 3) for which the element trends are similar to those at adjacent Site U1440.

Chemical evidence of sediment provenance

Previous studies identified several different sediment sources in the northwest Pacific region, including airfall ash (tephra), loess, distal gravity-flow deposits, and hydrogenous (seawater-precipitated) deposits, which are variably mixed with terrigenous sediments (Huang *et al*. 1973; Huang 1980; Minai *et al*. 1986; Hiscott *et al*. 1992; Straub 1997; Plank *et al*. 2007; Ziegler and Murray 2007; Ziegler *et al*. 2007; Scudder *et al*. 2009, 2014; Pickering *et al*. 2013; Schindlbeck *et al*. 2013; Kutterolf *et al*. 2014; Straub *et al*. 2015). In contrast, the isolation of the Izu–Bonin outer forearc from terrigenous turbidites allows fine-grained sediment sources and source changes to be identified more easily than elsewhere.

The Expedition 352 sediments have not been deeply buried beneath a thick sedimentary cover, subjected to high heat flow or deformation and therefore we assume that key elements including potassium have not been significantly altered after deposition. To test this, we calculated alteration indices, (we calculated the Chemical Index of Alteration [CIA]) (see Nesbitt and Young l982 for definition). CIA values range from 6 to 73 (median 57), which is consistent with relatively fresh unaltered sediments (Asiedu *et al*. 2000; Bahlburg and Dobrzinski 2011). We are therefore able to compare our chemically analysed samples with the composition of similar sediments of known origin on land or under the sea, especially in the northwest Pacific region. We utilize several well-tested discriminant diagrams that plot a range of major elements, trace elements, and respective ratios, including rare earth elements (Floyd and Leveridge l987; Bhatia l983; Bhatia and Crook, l986; Plank *et al*. 2007; see also Floyd *et al*. 1991; McLennan *et al*. 1993).

The basal sediments at both Sites U1439 and U1442 are enriched in lithogenous constituents (e.g. Al_2O_3, TiO_2, MgO, Zr, Th, Sc, Ga, Rb), hydrogenous or hydrothermal-related constituents (e.g. MnO, Fe_20_3, P_2O_5, Cu, Mo, U, Co, Sc, Ce, V). In addition, several constituents (e.g. K_2O, MnO, Cu, Pb, Ni, Ta, Th) reach relatively high values in the lowermost sediments recovered near the igneous basement. On the ternary diagram Fe *versus* Mn *versus* (Ni + Cu + Co) × 10 (Figure 10), nearly all of the sediments fall within the compositional range of Pacific non-metalliferous sediments. One sample from beneath the pelagic carbonate sediments at Site U1439 is enriched in Fe and trace metals but relatively depleted in Mn. Several samples of the basal sediments from Hole U1439A and also one sample from beneath the pelagic sediments at Site U1442 plot close to the field of western and eastern Pacific pelagic sediments and also to

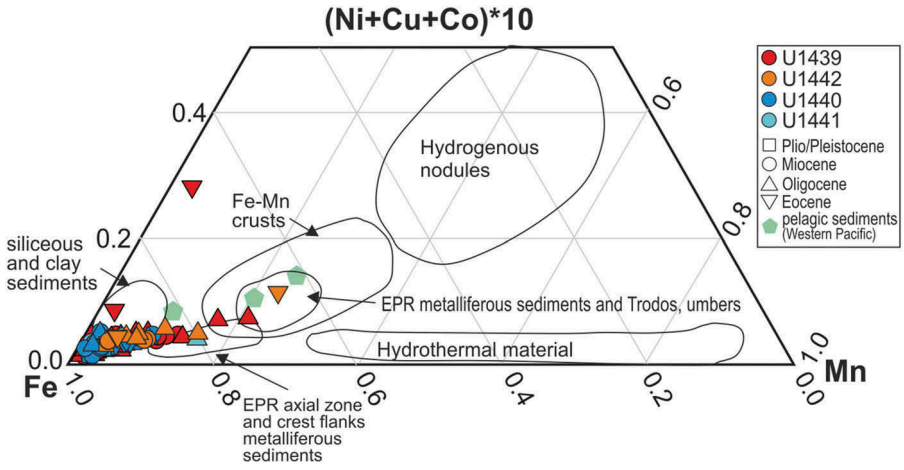

Figure 10. Ternary plot of Fe *versus* Mn *versus* Ni + Cu + Co × 10 for chemical data from Sites U1439A, U1440A&B, U1441A, and U1442A. For our new chemical data, the symbol shape is indicative of the three different time slices, whereas the colours refer to the drill sites (as in previous chemical plots). The diagram highlights the composition of basal metalliferous sediments and some layers and segregations within Time Slice 2 (early Miocene–early Pliocene). Fields: hydrogenous nodules and hydrothermal material, Fe–Mn crusts, East Pacific Rise axial zone and crest flank metalliferous sediments (e.g. Boström *et al*. 1969; Bonatti *et al*. 1972; Cronan *et al*. 1976). Western Pacific pelagic sediments are shown as green polygons (Lin 1992; Cousens *et al*. 1994). The ridge crest metalliferous sediments are chemically similar to the EPR metalliferous sediments from deeper ridge flanks (e.g. Bauer Deep sediments) (Sayles and Bischoff 1973) and ferromanganiferous umbers, for example of the Troodos Massif, Cyprus (Robertson and Hudson 1973) (see Supplementary Table 3 for analytical data).

relatively manganiferous East Pacific Rise metalliferous sediments and Fe–Mn-rich umbers associated with the Troodos ophiolite (e.g. Boström *et al*. 1969; Bonatti *et al*. 1972; Cronan *et al*. 1976; Sayles and Bischoff 1973; Robertson and Hudson, 1973). One sample from Site U1439 that is relatively rich in Ni + Cu + Co could have originated as a hydrogenous nodule that lost manganese owing to chemical mobilization during diagenesis. In support, the overlying sediments show abundant evidence of diagenetic mobilization and migration of metalliferous oxides, as indicated by greyish-to-blackish 'patches' and diffuse segregations of metalliferous oxides (Reagan *et al*. 2015; Supplementary Table 7). The likely cause is upward flow of reducing seawater from the igneous basement.

Generally, high K_2O, Rb/Hf or Zr/Y ratios, together with high Th/Nb or low La/Th ratios, are characteristic of continentally influenced sources, such as loess (airfall dust), tephra from a continental margin island arc setting (i.e. Japan), or terrigenous (redeposited) sediments (Floyd and Leveridge l987, Bhatia l983, Bhatia and Crook, l986; Plank *et al*. 2007; see also Floyd *et al*. 1991; McLennan *et al*. 1993).

The K_2O *versus* SiO_2/CaO diagram (Figure 11(a)) suggests primary compositional variations within the tuffaceous and volcaniclastic sediments. This diagram indicates the relative influence of IBM *versus* Honshu volcanic products because low SiO_2/CaO ratios at low K_2O concentrations reflect IBM sources (e.g. Kutterolf *et al*. 2017; Schindlbeck et al. 2017; average tephra compositions in Figure 11(a) are represented by stars).

The sediments have La/Th ratios from 3.0 to 13, which is indicative of a magmatic arc origin (e.g. Bhatia 1985; Bhatia and Crook 1986; McLennan *et al*. 1993). Potassium is generally higher in volcanics from the Honshu arc than from the IBM arc (exceptions are some IBM backarc volcanics) at given silica contents (Bryant *et al*. 2003; Kutterolf *et al*. 2014; references therein). The La/Th *versus* K_2O discrimination diagram (Figure 11(b)) suggests that the Oligocene–early Miocene sediments (Time Slice 1) predominantly came from the IBM arc, whereas the early Miocene–mid-Pliocene–Holocene sediments (Time Slices 2 and 3) were mostly from the Honshu arc. The Zr/Y *versus* La/Th diagram (Figure 11(c)) further suggests that Oligocene samples from the upslope sites (U1439, U1442) were mostly derived from the Izu arc (although many samples plot in overlap area with Japan). In the Rb/Hf *versus* Th/Nb diagram (Figure 11(d)), which highlights continental sources, only a relatively small number of samples, mostly from the Oligocene of Hole U1439, plot uniquely in the Izu field, suggesting a strong influence of continentally derived sediments (e.g. loess) or volcanic products from a continental margin arc.

Several other well-known diagrams (Floyd and Leveridge l987, Bhatia l983, Bhatia and Crook l986;

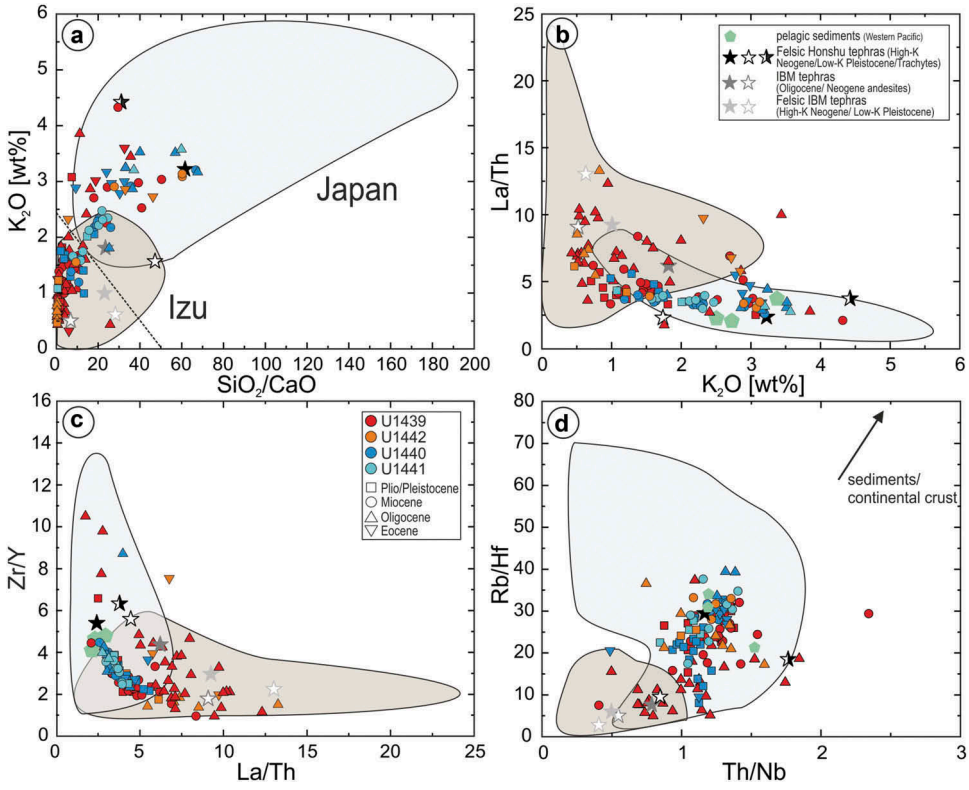

Figure 11. Selected binary plots of elements and elemental ratios, used as provenance indicators. (a) K_2O *versus* SiO_2/CaO; (b) La/Th *versus* K_2O; (c) Zr/Y *versus* La/Th; (d) Rb/Hf *versus* Th/Nb (see Hannah *et al*. 2002; Plank 2005; Bryant *et al*. 2003; Schindlbeck *et al*. 2017. for background information). For the new chemical data, the symbol shape is indicative of time slices and the colours of drill locations (as above). The typical ratios of Western Pacific pelagic sediments (green polygons; Lin 1992; Cousens *et al*. 1994), Chinese loess and tephras from several potential volcanic source areas are indicated for comparison. Correlation fields for the Honshu tephras are after Kimura *et al*. (2015) and references; IBM correlations (stars) are from Fryer *et al*. (1990), Hochstaedter *et al*. (1990), Hochstaedter *et al*. (2001), Tollstrup *et al*. (2010), Gill *et al*. (1992), Yokoyama *et al*. (2003, 2006), Kuritani *et al*. (2003), Tamura *et al*. (2005), Tamura *et al*. (2007, 2009), and Taylor and Nesbitt (1998). See Supplementary Table 3 for analytical data.

Plank *et al*. 2007) suggest contributions from different crustal types, lithological associations, or tectonic settings. The absolute values or ratios of trace element and REEs indicate the extent of reworking/recycling and the relative contributions of different possible sources, i.e. E-MORB, N-MORB, volcanic rocks of Japan, the Izu–Bonin arc, their related tephras (Kutterolf *et al*. in press), loess (Chauvel *et al*. 2014, Liang *et al*. 2009), upper continental crust (UCC) (McLennan *et al*. 1993), or pelagic sediments (Lin 1992; Cousens *et al*. 1994).

The Th/Sc *versus* Zr/Sc plot (Figure 12(a)) is suggestive of primary compositional variations rather than sediment recycling or mineral (e.g. zircon) enrichment in the Izu–Bonin forearc sediments because the Th/Sc ratios point to a relatively primitive source (e.g. Zimmermann and Bahlburg 2003). The La *versus* Th diagram (Figure 12(b)) suggests that the Oligocene–early Miocene sediments (Time Slice 1) were preferentially derived from an oceanic island arc setting (OIA), whereas the early Miocene–mid-Pliocene–Holocene sediments (Times Slice 2 and 3) appear to have a mostly continental island arc source. The youngest sediments are split between both of these fields. There is a tendency for implied oceanic sources to predominate in the upslope sites (U1439, U1442), whereas the downslope sites appear to contain relatively more abundant continental island arc source material.

The La/Th *versus* Hf diagram (Figure 12(c)) is indicative of an andesitic island arc source for most of the Oligocene–early Miocene sediments of the upslope sites (Time Slice 1). This is unexpected because the sediments have rhyodacitic bulk compositions that are typical of continental island arcs (Floyd and Leveridge l987; Bhatia l983; Bhatia and Crook l986; Plank *et al*. 2007). The relatively felsic compositions presumably reflect fractionation from parent andesitic island arc volcanoes (Tamura *et al*. 2009). In contrast, the downslope site sediments mainly plot in the 'mixed felsic and mafic sources'. Few of the sediments plot in the felsic island arc source area typical of continental island arcs, loess, or western Pacific pelagic sediments probably because of mixing with more mafic source material.

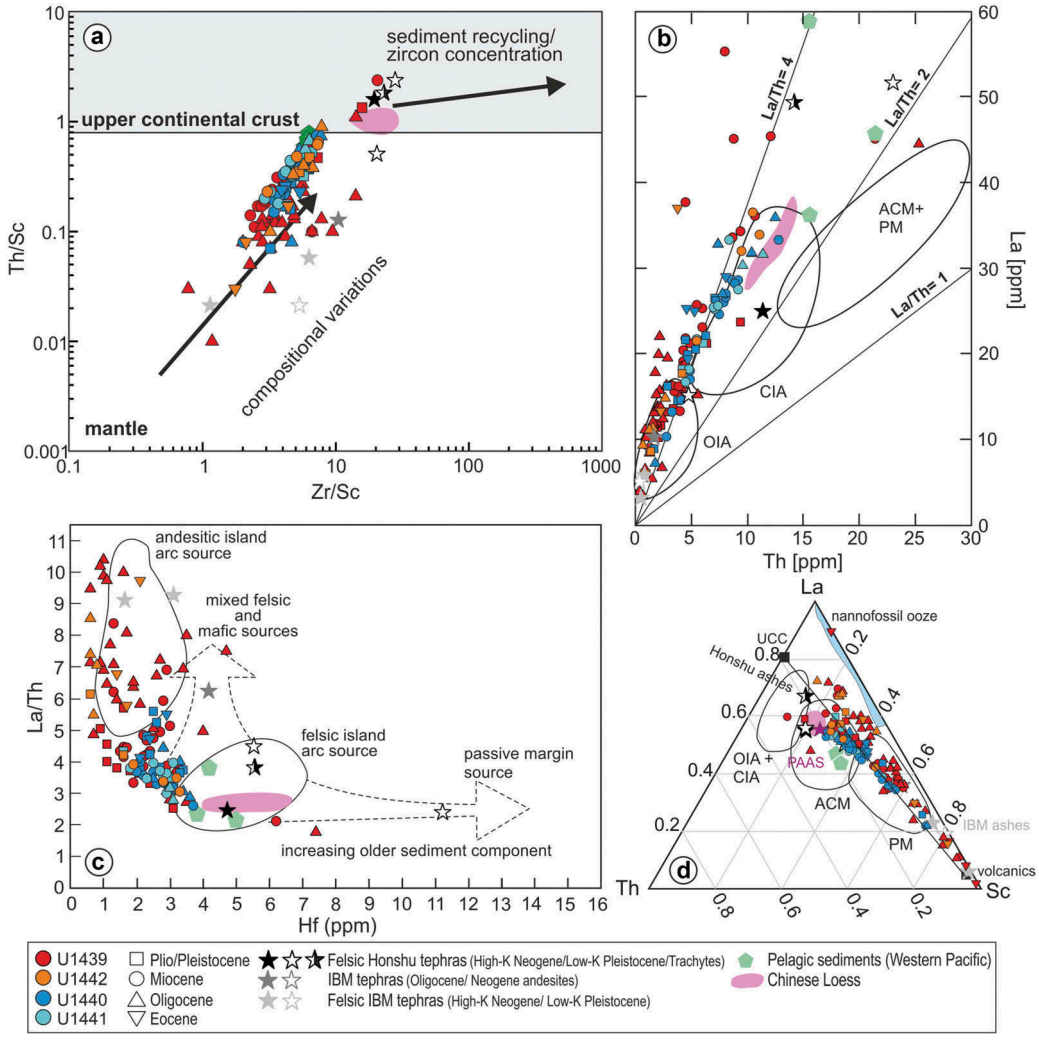

Figure 12. Discrimination diagrams utilizing selected trace elements. For the new chemical data, the symbol shape is again indicative of time slices and the colours of drill locations (as in previous chemical plots). (a) Th/Sc *versus* Zr/Sc (modified after McLennan *et al*. 1993). The diagram indicates chemical composition relative to mantle and upper continental crust (UCC) and the extent of sediment recycling (which results in Zr addition); also shown are the typical compositions of pelagic sediment (green polygons) and tephras (stars; see c); (b) La *versus* Th diagram showing fields of different tectonic settings (fields: ACM active continental margin, CIA Continental island arc, OIA Oceanic island arc, PM Passive margin; after Bhatia 1983); (c) Hf *versus* La/Th diagram indicating different source areas of clastic sediments (after Floyd and Leveridge 1987); see key to symbols; (d) La *versus* Th *versus* Sc diagram showing provenance fields (after Bhatia and Crook 1986) (see b). Additional fields in some of the diagrams indicate deep-sea carbonate sediments, after Ziegler *et al*. (2007) (cyan-coloured field), typical compositions of Western Pacific pelagic sediments (green polygons; Lin 1992; Cousens *et al*. 1994), tephra layer compositions at Expedition 352 sites (stars; Kutterolf *et al*. 2017), Chinese loess (purple field; Liang *et al*. 2009; Chauvel *et al*. 2014), and also average post-Archaean Australian shale (PAAS; purple star and labelling; Rollinson 1993) (See Supplementary Table 3 for analytical data).

The La *versus* Th *versus* Sc discrimination plot (Figure 12(d)) highlights the similarities of many of the Oligocene–early Miocene, generally up-slope sediments, with typical basalt–andesite compositions of the Izu–Bonin arc (e.g. Fryer *et al*. 1990; Hochstaedter *et al*. 1990, 2001; Gill *et al*. 1992; Taylor and Nesbitt 1998; Kuritani *et al*. 2003; Yokoyama *et al*. 2003, 2006; Tamura *et al*. 2005, 2007; Tollstrup *et al*. 2010). In contrast, the mid-Pliocene to Holocene downslope sediments are more similar to volcanic ash from Honshu (e.g. Kimura *et al*. 2015). These relationships are supported by comparison with the average compositions of the discrete tephra layers (Figure 12(d)) (see also Kutterolf *et al*. 2017).

The Th/La *versus* Sm/La diagram for the bulk sediments (Figure 13(a)) and also for the tephras (Figure 13(b)) supports an Izu–Bonin arc derivation for many of the Oligocene–early Miocene sediments (Time Slice 1), especially those of the upslope sites (U1439, U1440). This diagram also suggests an increased influence of an

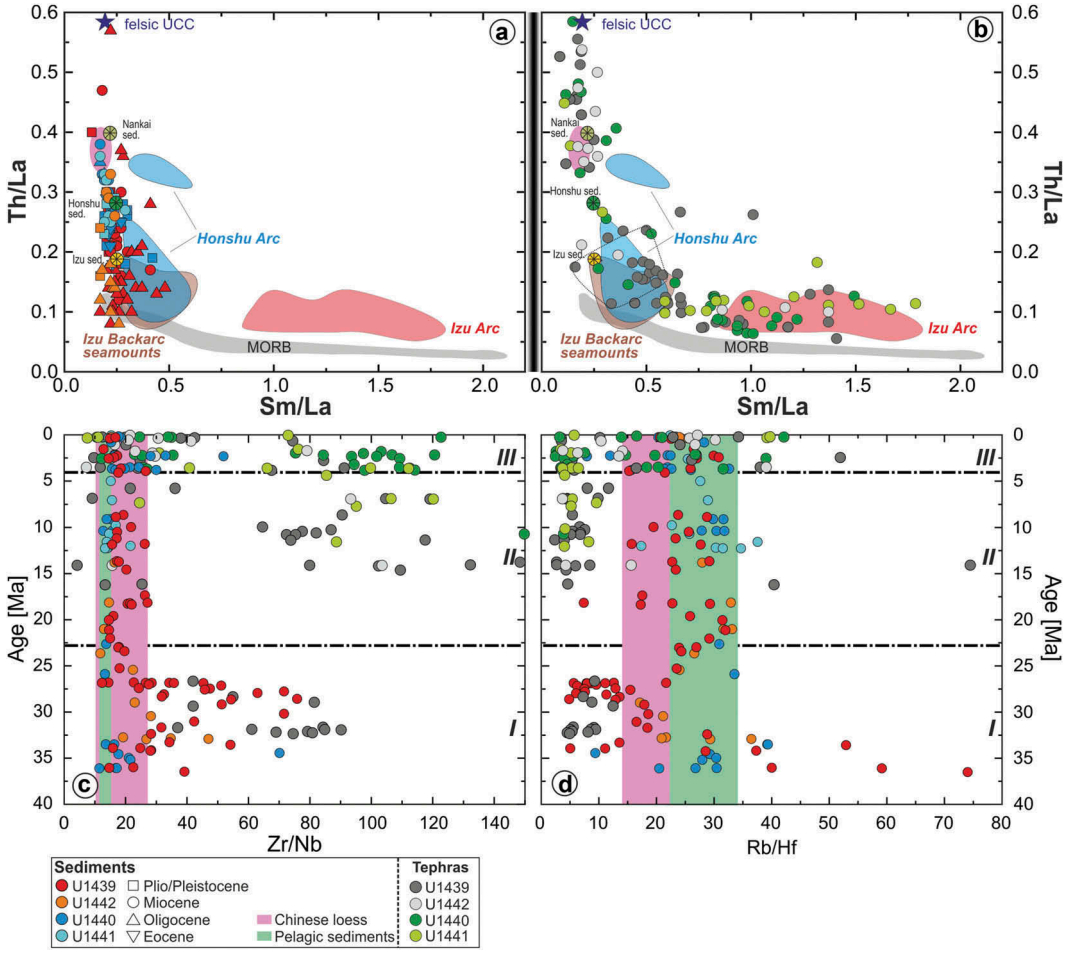

Figure 13. Binary plots comparing bulk sediment composition (this study) with tephra glass composition of the same sites based on Laser Ablation ICP MS (Kutterolf *et al*. 2017). (a) Th/La *versus* Sm/La diagram (modified after Plank *et al*. 2007) comparing the Expedition 352 whole-rock sediment data with sediments from different settings, in Plank *et al*. (2007), i.e. Nankai hemipelagic sediment (olive wheel symbol), Honshu hemipelagic sediments (green wheel symbol), Izu sediments (yellow wheel symbol), and felsic upper continental crust (dark star) (from Taylor and McLennan 1985). The symbol shape is indicative of three time slices, whereas sediment colours refers to drill locations as in previous chemical plots; (b) same diagram plotting but instead tephra analyses from single point La-ICPMS glass measurements (Kutterolf et al., 2017). The dotted field represents Oligiocene tephras from Hole U1439A; (c) age *versus* Zr/Nb plot; (D) age *versus* Rb/Hf plot. These two plots indicate changes in bulk sediment (a) and tephra glass composition (b) through time. (c) Age *versus* Zr/Nb plot; (d) age *versus* Rb/Hf plot. These two plots indicate changes in bulk sediment (a) and tephra composition (b) through time. See text for explanation.

upper continental and/or loess source within the early Miocene–Pleistocene sediments of the lower slope sites.

The Oligocene–Holocene bulk sediment composition is compared with equivalent compositional glass data for associated tephras in Figure 13(b) (Kutterolf *et al*. 2017). There is a generally good match between the continentally influenced early Miocene and younger sediments and the associated tephras, both of which show a trend towards an UCC composition, especially for the lower slope sites (U1440, U1441). However, many of the tephras of various ages from the different sites plot within, or near, the Izu arc field, in contrast to the interbedded fine-grained sediments. Possible explanations are either that the older sediments represent a mixture of Izu arc-related and/or MORB sources or that the sediments contain variable amounts of components such as loess and/or pelagic sediment (itself a mixture of different source materials). The age *versus* Zr/Nb plot (Figure 13(c)) indicates overlapping compositions of the bulk sediment and tephra for the Oligocene–Miocene interval (Time Slice 1) suggesting that the bulk sediment and tephra compositions co-vary especially at the upslope sites (U1439, U1442). In contrast, bulk sediment compositions deviate strongly from associated tephra during Pliocene–Pleistocene, suggesting an important additional source during this time interval. Some of the Japanese continental arc-derived tephra is chemically similar to some of the sediments on this diagram.

However, the abundant relatively Zr-rich tephra composition is not reflected in the sediment bulk composition. Many of the bulk sediments plot within the compositional range of loess or pelagic sediment, especially for the Miocene–Pleistocene (Time Slices 2 and 3) in the age *versus* Rb/Hf plot (Figure 13(d)). Some of the bulk sediments throughout the entire sequence are compositionally similar to pelagic sediment or loess. Loess contributes significantly to the bulk composition of pelagic sediment even in very distal open-ocean equatorial settings (e.g. Ziegler *et al*. 2007; Ferrat *et al*. 2011; Scudder *et al*. 2016). The contribution of Asian loess has specifically been demonstrated using multivariate statistical analysis of bulk marine sediments (ODP Site 1149; Scudder *et al*. 2014). Loess can contribute strongly in open-ocean settings that are isolated from terrestrial-derived input via gravity flows (turbidites and contourites), as for the Expedition 352 sites.

The probable explanation for the tendency of the lower slope site sediments (U1440, U1441; Figure 13(a)) to be more continentally influenced than the upper slope sites (i.e. Japan-derived field) is that IBM-derived eruptive products (gravity flows or fall-out deposits) were ponded in upslope basins. In contrast, continentally derived loess and tephra underwent long-distance wind transport and settled out over the entire IBM forearc area as elsewhere. This regional input was masked in the upper slope basins by much greater input directly from the IBM arc.

In summary, the main constraints from sediment chemistry are as follows: (1) The Oligocene–early Miocene sediments (Time Slice 1) that were mainly derived from fractionated oceanic arc volcanic products are correlated with the Izu–Bonin arc. (2) The late Miocene–Pleistocene sediments (Times slices 2 and 3) received an important contribution from a continental island arc, correlated with Japan. (3) Tephra input during the later Miocene and Plio-Pleistocene (upper part of time slices 2 and 3), as indicated by tephra analysis, was masked by a dominant input of Western Pacific-like hemipelagic sediment and, or Chinese loess, especially for the lower slope sites (U1440, U1441). This input is especially marked during the early Miocene.

Constraints from sediment magnetic properties

The magnetic hysteresis properties and first-order reversal curves (FORCs; Pike *et al*. 1999; Roberts *et al*. 2000) of sediment samples were measured to identify the composition and grain size of magnetic minerals, which provide clues to sediment input, provenance, and extent of alteration. Twenty samples of typical fine-grained hemipelagic sediments were analysed from the upper slope (Site U1439) and the lower slope (Site U1440) to test the inference from the sediment chemistry that the early Miocene (lower part of Time Slice 2) lacks significant tuffaceous input. To validate the test, tephras or tuffaceous material occurs within some of the sediments sampled (e.g. Unit I and the upper part of Unit II at Sites U1439 and U1440) but not in others (e.g. lowest part of Units II–IV, and the upper part of Unit V at Site U1439; and lower Unit II and the upper part of Unit III at Site U1440).

Shipboard palaeomagnetic data indicate that the magnetic carriers of the sediments generally have a median destructive field (MDF) of the natural remanent magnetization (NRM) that is <20 mT. Progressive thermal demagnetization of a few samples showed a gradual decay of remanence from ~100°C up to ~550–600° C (Reagan *et al*. 2015). These observations are consistent with titanomagnetite of variable grain size, degree of oxidation, and/or amount of titanium as the magnetic carrier, as is commonly found in marine sediments and tephra.

Postcruise magnetic hysteresis and FORC data give log-normal coercivity distributions that range from 0 mT to slightly above 200 mT and coercivities of remanence, which are equivalent to MDFs for fully magnetically saturated samples, are <50 mT (see Supplementary Table 9). These data are also consistent with a titanomagnetite magnetic carrier.

Magnetic grain size can be assessed for titanomagnetite on Day plots (Day *et al*. 1977; Dunlop 2002), where magnetic hysteresis data are compared with theoretical values calculated using known amounts of single-domain (SD, long-axis length ~0.03–1 μm), pseudo-single-domain (PSD, ~1–20 μm), multidomain (MD, >20 μm), and superparamagnetic (SP, <0.03 μm) magnetite/Ti–magnetite grains. Most seafloor sediments fall in the PSD field, even though actual grain sizes most likely comprise mixtures of SD, PSD, and MD grains, as well as SP grains in some lithologies.

Overall, the IBM forearc results are consistent with the SD–MD theoretical curves and indicate that the sediments are dominated by populations of PSD magnetic grains (Figure 14). Some of the data are offset towards the SD–SP curves, indicating contributions from very small SP magnetic grains. The SP contribution is present in Hole U1439A Unit I (Time Slice 3) and the upper part of Unit II (upper Time Slice 2) where there are abundant tephra layers/pods or tuffaceous mud. The SP contribution is absent, however, in the lower part of Unit II, Unit III, and the upper part of Unit IV (lower part of Time Slice 2), as well as the upper part of Unit V (upper part of Time Slice 1), where tephra layers are rare or absent.

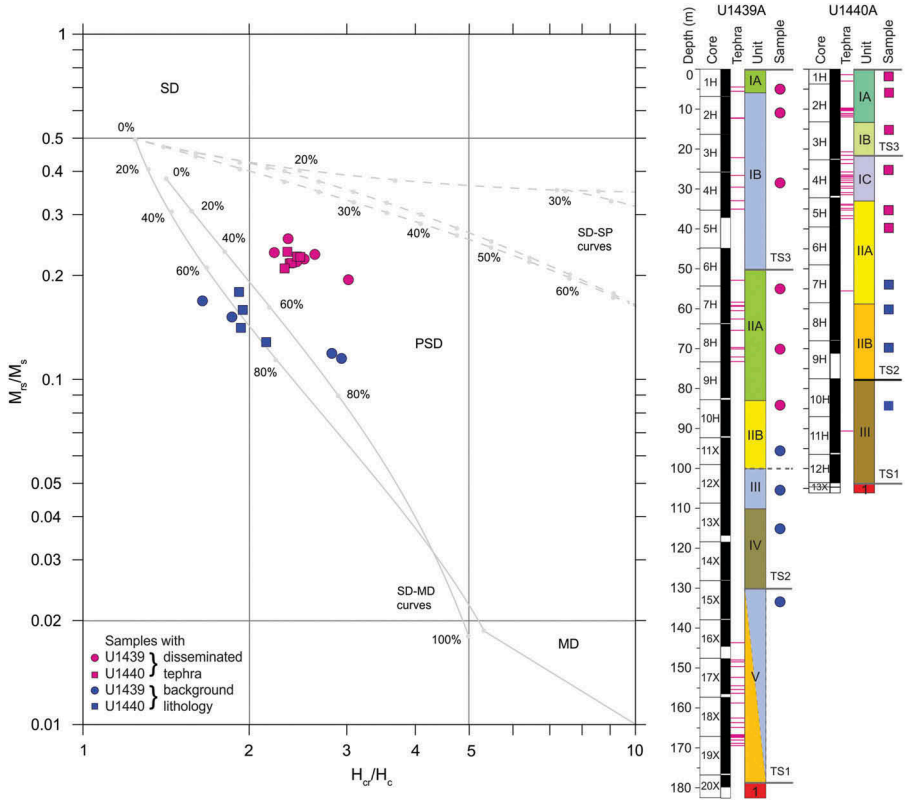

Figure 14. Day plot (Day *et al*. 1977) of magnetic hysteresis properties of sediments from Sites U1439 and U1440. Light grey mixing lines for samples with mixtures of single domain (SD), multi-domain (MD), and superparamagnetic (SP) particles are from Dunlop (2002). Samples from intervals that have numerous tephra layers plot towards mixing lines with SP grains and have higher M_{rs}/M_s values, indicating the presence of a finer grained magnetic carrier.

Similar observations are true for Time Slices 1–3 in Hole U1440A. Tephras are commonly fine-grained (e.g. Heider *et al*. 1993; Petronotis *et al*. 2015). Hence, the background sediment in the intervals with SP grains likely contains a disseminated tephra component.

The FORC distributions can also be divided into two distinct groups based mainly on the range of coercivities (the H_c axis in the FORC diagrams). Samples from stratigraphic intervals with tephra all have a population of grains with higher coercivity than those samples from intervals lacking in tephra (Figure 15). In intervals without tephra, the maximum coercivities are typically less than <75 mT, whereas in the intervals with tephra, the maximum coercivities typically are >150 mT, with some samples having coercivities >200 mT.

The magnetic interactions (the H_a axis in the FORC diagrams) for intervals with and without tephra are similar and suggest that magnetic grains are abundant and close enough to one another that strong interactions occur (Figure 15). Such behaviour is common in marine sediments with a significant terrigenous and/or volcanic source. This differs from deep marine sediments with a dominant biogenic magnetite component, which commonly have little or no magnetic interaction (e.g. Roberts *et al*. 2012).

Taken together, the discrete magnetic observations indicate that the hemipelagic sediment in the intervals with tephras (or tuffaceous material) also contain disseminated tephra, which contributes to the finer magnetic grain size and higher coercivity relative to intervals without observable tephras. These results therefore support the sediment chemical evidence that indicates a significant tephra contribution, except during the early Miocene (lower part of Time Slice 2) when metal-enriched hemiplegic sedimentation took place below the CCD.

Synthesis of forearc sedimentation and basin development

Our new biostratigraphical, chemical, and magnetic data are synthesized with the site-by-site shipboard descriptions (Reagan *et al*. 2015) in Figure 16. Shipboard data for the background fine-grained lithology, microfacies, associated sediments, and diagenesis

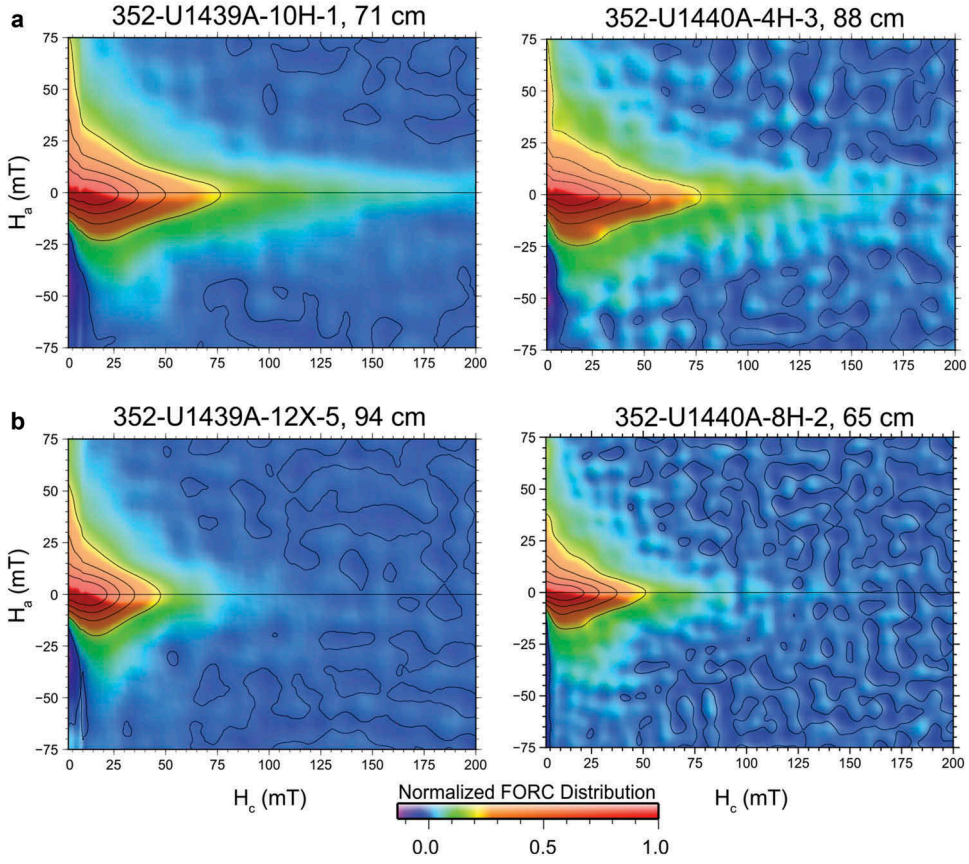

Figure 15. FORC diagrams of sediments from Sites U1439 and U1440 illustrating the coercivity distributions along the H_c axis and interactions between magnetic grains along the H_a axis. Samples from intervals with numerous tephra layers (a) contain higher magnetic coercivity minerals than intervals where tephra layers are rare or absent (b).

are summarized in Supplementary Tables 4–7 for Sites U1439, U1440, and U1442. In addition to the fine-grained sediments discussed above, relatively coarse-grained tuffaceous and epiclastic (erosionally derived) talus are taken into account. During the Eocene–Recent, the CCD is assumed to have a broadly similar depth to that inferred for the Pacific basin for the equivalent time intervals (Pälike *et al*. 2012).

Clastic sediments within and directly above the eruptive igneous basement

Dominantly Mg-rich boninitic basalts were recovered from the basement at the two upslope Sites U1439 and U1442 (Reagan *et al*. 2015). In Holes U1439A and U1439C, mafic dikes or sills are overlain by intercalations of pillow lava, massive sheet flows, breccia, and pyroclastic flow deposits, ranging from high-Mg andesite to primitive boninite in composition. The volcanic succession there is covered by a thin layer of epiclastic sediments made up of basaltic clasts in a matrix of gravel-sized lava fragments and altered glass (~1 m thick). The epiclastic material is interpreted as the result of erosion (mass wasting) on an irregular seafloor after volcanism ended. The volcanic sequence in nearby Hole U1442A begins with boninitic lava and hyaloclastite and is topped by a veneer (25 cm thick) of epiclastic breccia, with gravel-sized volcanic clasts in a sandy-granular matrix of altered glassy boninitic fragments. The clasts are subrounded, coated with metalliferous oxide (<3 mm thick), and occur within a matrix of pinkish, non-calcareous sandy, and silty clay. This thin basal clastic material is indicative of post-volcanic seafloor erosion and reworking. Basaltic rocks known as forearc basalt (FAB) were recovered from the basement at the two lower slope sites. In Hole U1440B, an inferred sheeted dike complex is followed upwards by volcanic rocks. Downhole resistivity measurements using the formation microscanner suggest that the succession is dominantly fragmental (e.g. hyaloclastite), with scarce intercalated pillow lava flows (Reagan *et al*. 2015; S. Morgan, unpublished data). The primary extrusive material culminates in volcanic breccia with lava fragments, including pillow lava in a matrix of mud (c. 1 m thick). Similar material was also recovered in Hole U1440A. In Hole U1441A, basaltic extrusive rocks,

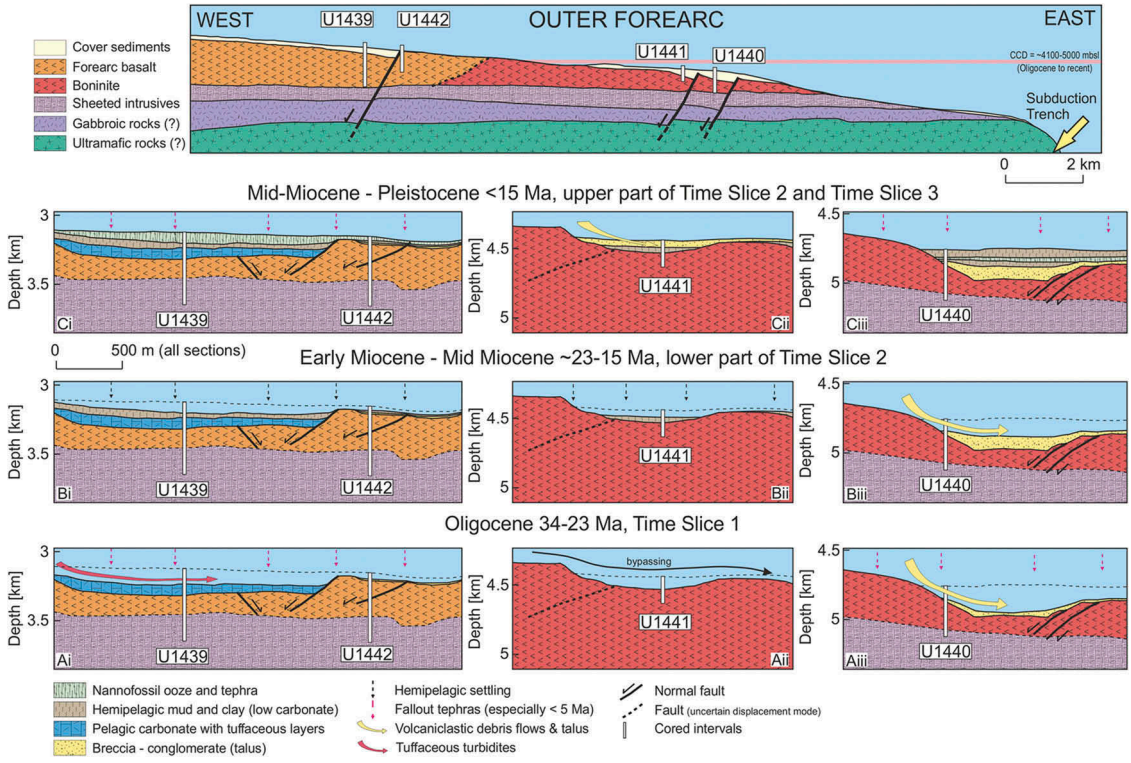

Figure 16. Line drawings of the setting of recovered sediments and igneous basement (a–c) in relation to the Izu–Bonin lower outer forearc (upper section; true scale). The basin morphology is based on seismic reflection data (Christeson *et al*. 2016) and shipboard information (Reagan *et al*. 2015). The diagrams highlight the dominant lithology, the importance of extensional faulting, and the modes of accumulation for the three time slices. See text for explanation.

similar to those recovered in Holes U1440A and U1440B, are overlain by monomict lava breccias (c. 80 m thick) with a matrix of coarse volcaniclastic sand. The clasts range from angular to subrounded, with the largest clasts (>10 cm in size) occurring near the top of the unit (Igneous Unit 1; Reagan *et al*. 2015; S. Morgan, unpublished data). There is no evidence that the breccias are primary eruptive products (Reagan *et al*. 2015; Figure 6). Alternative interpretations that the breccias represent either physical brecciation (tectonic or drilling induced) or reworked sedimentary talus were tested by postcruise palaeomagnetic study.

Palaeomagnetic evidence of basal talus breccias

Thirteen minicores with a diameter of 0.5 in were taken from pieces of volcanic rocks that were large and intact enough to be sampled from the uppermost part of the oceanic basement (igneous Unit 1) at Site U1441. Six samples were thermally demagnetized, and seven were demagnetized using the alternating field (AF) method. Magnetic remanence was measured using an AGICO JR-6 Spinner Magnetometer. Thermal demagnetizations were carried out in steps of 50°C from 150 to 450°C and 25°C from 450°C to 550° or 575°C. Because of very low coercivities, AF demagnetization steps were very small (0.5 or 1 mT) and began at very low fields. Most samples were almost completely demagnetized by 30 mT.

For the AF-demagnetized samples, NRMs drop sharply after demagnetization at 0.5 mT and then the NRM decay is univectorial. Principal component analysis (PCA) gives reliable direction values, with maximum angular deviation (MAD) values between 1° and 3°. Thermal demagnetization spectra generally show a first decay of the NRM until 350°C, then either a plateau or a small self-reversal, and finally unblocking of the characteristic remanent magnetization (ChRM) between 400 and 550–575°C. The ChRM directions given by PCA have a slightly more reliable MAD (between 2° and 7.5°) because samples broke after several heating steps and it was difficult to reposition them for further measurement.

The 13 inclinations obtained by PCA are inconsistent (see Supplementary Table 8). This contrasts with the directions obtained from initial shipboard demagnetization which were less scattered, with inclination values around the present-day geocentric axial dipole (Reagan *et al*. 2015). The random inclinations obtained here are consistent with igneous Unit 1 at Site U1441

representing a c. 80-m-thick pile of redeposited volcanic rock talus (see discussion of forearc development, below). The talus is likely to have been eroded from a nearby subaqueous fault scarp. The talus could have formed either soon after volcanism ended or later, prior to the accumulation of the oldest recovered deep-sea sediments at this site (early Miocene?).

Talus accumulation within the sedimentary sequences

Basalt-derived talus represents an important part of the recovery at the two lower slope sites, where it occurs within the Oligocene–Pliocene interval at Site U1440 and reappears as an undated (Pliocene?) interval at Site U1440 (Figures 4, 6 and 16).

At Site U1440, coarse clastic accumulation began during the Oligocene with silty mud containing volcanic gravel followed by muddy volcanic breccia/gravel with gravel (Figures 4 and 6). This material is a mixture of angular-to-subrounded clasts (up to several cm in size), mostly composed of highly altered basalt that includes orthopyroxene. The large volumes of mud, sand, and coarse talus (breccia–conglomerate) were emplaced by mass-flow processes (Lowe 1982; Pickering *et al*. 1986; Mulder and Alexander 2001; Pickering and Hiscott 2016). The talus was shed from the sloping western margin of the small sediment pond in which Site U1440 is located (Figure 16(a)iii). Orthopyroxene is characteristic of boninitic rocks recovered from the two upslope sites (U1439, U1442) (Reagan *et al*. 2015). This observation suggests that the orthopyroxene-bearing detritus at Site U1440 originated several kilometres upslope from its present position (assuming unknown boninites did not erupt more locally). The overlying Miocene(?) interval at Site U1440 includes scattered, subangular clasts (up to pebble-sized) of pumice and lithified ash, together with clasts of altered basalt. This suggests that some of the talus is a mixture of local basement-derived material and lower density, evolved arc products.

The early Pliocene(?) interval at Site U1440 includes decimetre-thick interbeds of matrix-supported, clast-rich breccia–conglomerate. This is made up of layers (several centimetres thick) with poorly consolidated clasts of pink non-calcareous siltstone, highly altered basalt, and isolated angular basalt clasts (up to 2.5 cm in size). Some coarse clastic layers are impregnated with dark-coloured metalliferous oxide-rich material which is interpreted as a diagenetic precipitate. This evidence indicates reworking of previously lithified non-calcareous siltstone. The poorly dated Miocene(?) or Pliocene(?) interval near the depocentre at Site U1441 includes a c. 10-m-thick interval of reddish-brown muddy, matrix-supported breccia–conglomerate (Figure 16(b)ii) and randomly distributed centimetre-sized, rounded-to-sub-angular pumice clasts (Reagan *et al*. 2015) confirming the importance of evolved arc-derived volcanic material.

Seismic reflection data (Christeson *et al*. 2016) indicate that three of the sediment ponds drilled are bordered by normal faults (Figures 3a–d; 16(a–c)). Comparable west-facing half-grabens, infilled with Oligocene sediments, have also been seismically imaged further north on Bonin Ridge (Taylor and Fujioka *et al*. 1992). Structural observations from Site U1439 show that the angle of bedding increases from sub-horizontal up to 17° within the Oligocene nannofossil ooze/chalk (below 155.0 mbsf). This was coupled with the development of very small-scale shear zones and normal faults with displacement of up to ~5 cm (Reagan *et al*. 2015). Comparison with seismic reflection data suggests that eastward tilting took place (Kurz *et al*. 2015), which is biostratigraphically constrained as between c. 32 and 27 Ma (Figure 4). There is also evidence of syn-sedimentary tectonics at the nearby upfaulted Site U1442 (Figure 3(a)), where Oligocene (c. 27–32 Ma) sediments dip at up to c. 35°, whereas the overlying sediments (above c. 74–75 mbsf) are sub-horizontal (Kurz *et al*. 2015; Reagan *et al*. 2015).

Comparable talus to that recovered from the Izu–Bonin lower slope sites is known from numerous deep-ocean settings affected by extensional faulting, for example associated with the axial grabens and flanks of spreading ridges (e.g. Ballard and Moore l977). Talus locally overlies extrusive rocks in the vicinity of extensional faults within supra-subduction zone ophiolites of similar origin to the Izu–Bonin forearc basement (e.g. Troodos ophiolite (Robertson l975). In contrast, the talus at Sites U1440 and U1441 relates to later-stage extensional faulting. Comparable igneous-derived talus has been recovered from above a major extensional fault which transects an older emplaced SSZ-type ophiolite in the late Cenozoic backarc Woodlark basin (Taylor *et al*. 1999).

In summary, the breccia–conglomerates and associated gravel are interpreted as reworked subaqueous talus that was generated by mass wasting of extensional fault scarps that actively dissected the outer Izu–Bonin forearc. Talus appeared earlier at Site U1440A (Oligocene–Miocene) than at Site U1441A (Miocene(?)–Pliocene(?)), consistent with the absence of dated pre-Miocene sediments in this depocentre.

Metalliferous oxide sediments overlying the volcanic basement

In Hole U1439A, the igneous basement is overlain by a thin (<3 cm), consolidated but unlithified black

metalliferous oxide-rich crust. XRD analysis of the lowermost ~30 cm of the succession revealed minor manganese oxide, a serpentine mineral, and muscovite (Reagan *et al*. 2015). In Hole U1442A, the uppermost igneous basement includes a >40-cm thick sedimentary layer with subrounded, altered extrusive igneous rock clasts that are coated with metalliferous oxide (<3 mm thick) within a matrix of pinkish, non-calcareous sandy and silty clay. At Site U1440, the highest recovered basaltic rock is coated by a film of metalliferous oxide. The chemical data suggest that the basal metalliferous oxide sediments originated as a variable mix of northwest Pacific pelagic sediment, hydrothermal oxide-sediment, and hydrogenous precipitates (see Figure 10). The composition of the basal sediments merges with that of siliceous and clay-rich sediments.

40Ar/39Ar ages on cores from Expedition 352 suggest igneous basement ages of around 50-51 Ma (D. Heaton and A. Koppers, pers. com. 2016). Since the oldest recorded age of the sediment cover is earliest Oligocene (~35 Ma) based on calcareous nannofossil dating (see Figure 4), a hiatus of up to 15 million years is implied between the end of igneous activity and the start of pelagic carbonate deposition. The metalliferous sediments formed at some time during this hiatus of up to 17 million years between ocean crust genesis and the first dated pelagic carbonate sedimentation. There is no evidence that an older Eocene–Oligocene sequence accumulated but was later eroded. A possible reason for the hiatus is that most sediment bypassed the outer forearc to accumulate in the subduction trench. Some parts of the Troodos ophiolite (Cyprus), which formed in a comparable forearc setting (Pearce and Robinson 2010), for example, remained free of deep-sea sediment for tens of millions of years (e.g. Robertson 1977).

Early Oligocene–early Miocene pelagic and tuffaceous sediments (Time Slice 1)

Pelagic carbonate began to accumulate more or less coevally at Sites U1439, U1442, and U1440 and could also have accumulated near Site U1441 where the basin depocentre was not drilled (Figure 16(a)). The Oligocene–early Miocene time interval (Time Slice 1) of the upslope Sites U1439 and U1442 (Figure 6) began with the deposition of nannofossil ooze in an oxidizing environment where burrowing organisms flourished. Minor basement-derived silty and sandy material was supplied to near-basal sediments, although the overlying sequence is free of coarse clastic material in contrast to the lower slope sites (see below). These sediments accumulated near the depocentre of a foreac basin sediment pond (Site U1439) and on an adjacent topographic high (U1442). The CCD is inferred to have deepened from the end of the early Oligocene to the end of the Oligocene. The deepening relates to the growth of ice sheets, a fall in sea level, and a shift of carbonate from shallow to deep waters. The CCD in the open Pacific is placed around 4.6 km during the Oligocene (Pälike *et al*. 2012).

Higher in the sequence at Site U1439, repeated beds (<20 cm thick) with sandy erosional bases, micro-cross lamination, obvious normal grading, and parallel lamination are interpreted as the partially developed Bouma sequences (i.e. mostly D–E and C–D–E divisions) of volcaniclastic and/or tuffaceous turbidites (Bouma, l962; Pickering and Hiscott 2016), by comparison with other modern and ancient arc-related sediments (Huang l980; Pickering *et al*. 1986; Peters *et al*. 2000; Scudder *et al*. 2009, 2014; Pickering *et al*. 2013; Schindlbeck *et al*. 2013; see also Pickering and Hiscott 2016). The sandy bases of the turbidites are variably rich in arc-derived material, especially quartz, colourless glass, feldspar, amphibole and some pyroxene, orthopyroxene, and titanomagnetite. A few sandstone–siltstone layers contain mixtures of glass, mineral grains, calcareous nannofossils, and rare planktonic foraminifers (Reagan *et al*. 2015). In contrast, similar tuffaceous sediments are effectively absent from the condensed sequence at adjacent Site U1442 and are restricted to rare (distorted) layers of silty volcaniclastic sand at Site U1440.

At both Sites U1439 and U1442 numerous thin (<3 cm), repeated interbeds and partings of fine-grained ash, have sharp bases, subtle normal grading, and bioturbation. These layers are interpreted as fallout deposits that were variably redeposited near and within the sediment ponds by local downslope reworking and bioturbation (cf. Scudder *et al*. 2009, 2014; Schindlbeck *et al*. 2013; Pickering and Hiscott 2016). The Oligocene tephra layers at Site U1439 have a distinctive chemical composition that was also recognized in fine-grained fallout material in the coeval sediments at Site U1442 (Figure 13(a,b)). The tuffaceous turbidites were derived from the Izu–Bonin arc, either directly via eruption or via coarse proximal fallout that was reworked into lower slope sediment ponds, as at Site U1439. The source volcanoes within the Izu–Bonin arc are estimated as c. 150 km away based on tephra composition (Kutterolf *et al*. 2017) (Figures 11–13).

Time-equivalent near-basal mudstones on the lower slope (Site U1440) (Figure 6) include abundant altered volcanic glass, reworked pyroxene, sparse plagioclase, and serpentinite (Reagan *et al*. 2015), all derived from the igneous basement. Above this, the sequence is

dominated by c. 15 m of mud-supported, granule-grade breccia/conglomerate, which continues for c. 65 m upwards through the early Miocene-to-mid-Pliocene interval (Time Slice 2; Figure 6). Similar coarse volcaniclastic material was recovered from the mid-Pliocene-to-Pleistocene interval (Time Slice 3).

Sediments of the more proximal (westerly) Izu–Bonin forearc were drilled further north during ODP Leg 126 (Figure 1(b)) where a depocentre (Sites 792 and 793) is infilled by proximal volcanogenic turbidites and debris-flow deposits (up to 15 m thick individually) with mudstone interbeds. Sediment was supplied axially from the north in this area (Hiscott *et al*. 1992), together with sparse shallow-water to non-marine material from nearby frontal arc highs. Thick and coarse volcanic products, therefore, formed near the IBM arc, whereas topographical barriers (e.g. Bonin Ridge) and any proximal fault-bounded basins restricted sediment supply to the Expedition 352 distal forearc sites.

Early Miocene–early Pliocene low-carbonate sediments (Time Slice 2)

Early Miocene to early Pliocene (Time Slice 2; c. 23–4 Ma) was dominated by low-carbonate hemipelagic sedimentation near or below the CCD, as recovered at Sites U1439, U1442, and U1441 (Figure 16(b)i–iii). Reddish coloured clay/claystone with metalliferous oxide enrichment (Figures 7, 9, and 10) characterizes the early Miocene (lower interval of Time Slice 2), followed by brownish muds (with some carbonate-rich intervals) during the early Miocene-to-early Pliocene time (upper interval of Time Slice 2) (Figures 3 and 4).

The sharp reduction in calcium carbonate preservation at around 23 Ma (earliest Miocene) approximates to the 'carbonate crash' and resulting 'carbonate famine' (Lyle *et al*. 1995) across the entire Pacific Ocean. Recent work suggests that 600 m of shoaling occurred at 18.5 Ma and lasted for c. 2.5 Ma (Pälike *et al*. 2012). The 'crash' corresponds to rising seawater temperature and a small rise in eustatic sea level, which together resulted in overall shallowing of the CCD (Lyle 2003). Increased amounts of calcium carbonate are likely to have been retained in shallow-water settings allowing the oceanic CCD to rise. The relatively short period of warming relates to ice sheet decay within a cycle of longer term cooling and overall ice advance (Lyle 2003).

The period of low-carbonate clay-rich accumulation on the Izu–Bonin outer forearc (c. 8 million years) partially corresponds to the period of CCD shoaling that lasted until c. 16 Ma (Pälike *et al*. 2002). However, some low-carbonate accumulation (mostly muds) continued for a further c. 10 Ma (until 4 Ma; upper limit of Time Slice 2). The low-carbonate clay-rich deposition overlaps with rifting and spreading of the Shikoku Basin and the Ogasawara Trough from c. 25 to 20 Ma (Ishizuka *et al*. 2011a). The rifting was probably triggered by rollback of the Pacific plate which caused subsidence of the Izu–Bonin forearc as a whole. Global palaeoceanography and regional tectonics therefore both played a role in the early Miocene-to-early Pliocene low-carbonate deposition.

The early Miocene (lower part of Time Slice 2) lacks airfall tephra input to the Expedition 352 sites (Figures 13(a), 14, and 15). Other types of fine-grained sediment relatively increased, notably pelagic sediment, loess, and metalliferous oxide precipitates.

During mid-Miocene-to-early Pliocene (upper interval of Time Slice 2) nannofossil-bearing, pinkish grey silty clay accumulated periodically, together with pinkish nannofossil ooze at Sites U1439 and Site U1442. Siliceous sponge spicules are common together with sparse radiolarians, common zeolite, and mixed-layer clays (Reagan *et al*. 2015). Thin interbeds of fine-to-medium-grained tuffaceous siltstone–sandstone (mostly felsic but occasionally mafic) and ash layers occur with quartz, plagioclase, pyroxene, amphibole, and felsic glass. Metalliferous oxides continued to be enriched within hemipelagic mud.

Radiolarians, diatoms, and siliceous sponge spicules are relatively abundant at both downslope sites. The early Miocene(?) interval at Site U1440 includes scattered, subangular clasts (up to pebble-sized) of pumice and lithified ash, together with clasts of altered basalt which is explained by reworking of pre-existing sedimentary material. Beginning around the mid-Miocene (c. 15 Ma), there was a gradual return to calcareous sediment, accompanied by some air-fall tephra and tuffaceous sediments, similar to the two upslope sites.

Proximal forearc basin sediments were previously recovered further north on the Izu–Bonin Ridge during ODP Leg 126 at Sites 787, 792, and 793, where incomplete Miocene sequences comprise bioturbated sandy mudstone and sandy mudstone rich in nannofossils, and both felsic and mafic volcanic grains (Taylor and Fujioka *et al*. 1992). Miocene sediments were also recovered during ODP Leg 125 at Site 782 comprising nannofossil marls, clay, and volcanogenic sand (early Pleistocene–mid-Miocene) (Fryer *et al*. 1990). These results emphasize the differences between the calcareous sedimentation in the proximal forearc basin *versus* the generally low-carbonate accumulation on the distal forearc drilled during Expedition 352.

Early Pliocene-to-Holocene pelagic carbonate and tephra (Time Slice 3)

Weakly calcareous clay/claystone/mudstone and nannofossil ooze accumulated during early Pliocene-to-

Recent time at both of the upslope sites (U1439, U1442) (Figure 16(c)i–iii). In contrast, weakly calcareous mud was deposited at both of the downslope sites (U1440, U1441), with occasional thin interbeds of nannofossil ooze. At Site U1439, the nannofossil ooze is interbedded with calcareous mud and muddy, sandy, and clayey nannofossil ooze. Holocene background sediments are characterized by relatively pure nannofossil ooze with abundant planktic foraminifers. The nannofossil ooze is commonly silty with quartz and plagioclase, together with variably abundant planktonic foraminifers, radiolarians, diatoms, sponge spicules, and rare silicoflagellates. Felsic glass, volcanic and sedimentary rock fragments, and also mineral grains (e.g. clinopyroxene) occur in a few samples. Plio-Pleistocene sediments recovered on the proximal forearc during Legs 125 (Fryer *et al*. 1990) and 126 (Taylor and Fujioka *et al*. 1992) are similarly dominated by nannofossil-rich pelagic and hemipelagic sediments, with variable tuffaceous input including pumice.

The return to high-carbonate accumulation on the Izu–Bonin forearc corresponds to an increase in carbonate in the Indo-Pacific ('biogenic bloom'), as reported in the Western Equatorial Pacific (Nathan and Leckie 2009; see also Pälike *et al*. 2002). Maxima in carbonate accumulation rates correspond to glaciation-controlled Neogene cooling (Lyle 2003). The increased productivity also reflects increased nutrient supply from rapidly eroding land areas, notably the Himalayas and the Andes. The deepwater circulation that channelled the nutrients was further influenced by developing regional tectonics (e.g. Indonesian Seaway; Hall 2012).

The Pleistocene upper part of the succession at Site U1439 includes numerous tephra layers (10–20 cm thick) and one discrete tuffaceous interval (Reagan *et al*. 2015). Similar facies are present at the adjacent Site U1442, where relatively muddy nannofossil ooze contains rare transparent and coloured glass, together with minor basaltic fragments, quartz, plagioclase, and ferromagnesian minerals. Ten discrete ash layers and seven tuffaceous intervals were recognized at this site (Kutterolf *et al*. sub.). In contrast, the fine-grained sediments at the downslope Site U1440 are dominated by weakly burrowed calcareous mud (variably mixed with ash) and interbedded ash layers (as cm-thick normal-graded beds). The tuffaceous layers contain abundant colourless glass, together with rare quartz and feldspar, and also trace amounts of biotite, pyroxene, amphibole, apatite, nannofossil ooze, silt, and siliceous microfossils (mostly radiolarians). Shipboard XRD of muddy nannofossil ooze revealed quartz, calcite, illite, mixed-layer clays, chlorite, phillipsite and manganese oxide, and serpentinite (Reagan *et al*. 2015). Siliceous microfossils are spasmodically abundant. Ash of similar composition was also recovered from the Pleistocene interval at Site U1441. These sediments record felsic fallout ash that was modified by local redeposition and bioturbation, as inferred for the Oligocene–early Miocene ash layers. The tephra mainly originated from the Honshu arc, coupled with further input from the Izu–Bonin arc (Figure 13(b); Kutterolf *et al*. 2017). The IBM arc as a whole was highly active during the Pleistocene (Taylor and Fujioka *et al*. 1992; Straub and Schmincke 1998; Straub 2003), as was the Japanese continental margin arc (Machida and Arai 1983; Taylor and Fujioka *et al*. 1992; Mahony *et al*. 2011), possibly reflecting a global increase in explosive volcanism (Kennett and Thunnel 1975; Prueher and Rea 2001; Cambray *et al*. 1993; Kutterolf *et al*. 2013).

Comparison with the most proximal forearc

Eocene–Oligocene arc-derived sediments were recovered from the Amami Sankaku Basin (Site U1438) during IODP Expedition 351 (Arculus *et al*. 2015c; Johnson *et al*. 2017; Figure 1(b)). The depositional setting is inferred to have been a distal volcaniclastic apron or submarine fan that was located c. 50 km oceanwards of the arc front (now represented by the Palau-Kyushu remnant arc). The oldest recovered sediments at Site U1438, within 50 m of the drilled igneous basement, are a mixture of fine-to-very coarse-grained tuffaceous and volcaniclastic sediments, together with some basaltic andesite (Barth *et al*. 2014; Marsaglia *et al*. 2014; Arculus *et al*. 2015c). In contrast, Eocene sediment is absent from the Expedition 352 drill sites. Possible reasons are because of topographic barriers (i.e. fault-bounded basins) or sediment bypassing to the trench. Even today, the IBM forearc in the vicinity of the Expedition 352 drill sites is largely devoid of a sedimentary cover (Reagan *et al*. 2015; Figure 3(a–d)).

Within the Amami Sankaku Basin, at around 25 Ma (late Oligocene), there was a marked decrease in grain size and the deposition of c. 50 m of reddish-brown, radiolarian-bearing hemipelagic mudstone with thin volcaniclastic siltstone to sandstone beds (at 160 mbsf) (Marsaglia *et al*. 2014; Arculus *et al*. 2015c; Johnson *et al*. 2017). The distinctive colour prompts comparison with the reddish fine-grained intervals at the Expedition 352 sites although these may be mostly younger (i.e. early Miocene). Above this, the Neogene–Recent succession is dominated by tuffaceous mud, ash-bearing mud, mud, clay, and ash with minor foraminifer- and radiolarian-rich pelagic and hemipelagic sediments. The Expedition 351 results (Arculus *et al*. 2015c) emphasize the dominance of volcanic ash input throughout Miocene-to-Recent time in the

proximal forearc in contrast to the more varied hemipelagic and distal tuffaceous accumulation in the Expedition 352 outer forearc sites.

Regional development of the Izu–Bonin forearc

The synthesis takes account of the results of previous scientific drilling in the northwest Pacific region (Figure 1(a,b)), including the Izu–Bonin forearc (e.g. Fryer *et al*. 1992; Hiscott *et al*. 1992; Pearce *et al*. 1992), the Mariana forearc (e.g. Natland and Tarney 1982; Lee *et al*. 1995), the West Philippine Sea backarc basin (deVries Klein *et al*. 1980; Taylor and Fujioka *et al*. 1992), the Pacific plate (Plank *et al*. 2007), and the wider region, especially Honshu, and also IODP Expedition 351 drilling (Arculus *et al*. 2015c; Figure 1(b)).

Eocene forearc genesis

The Izu–Bonin forearc was initiated around 50 Ma (Reagan *et al*. 2015, 2017). Basalts and gabbros from the IBM forearc, trench, and islands on the IBM Ridge (Guam) have ages going back to 51-52 Ma for the trench slope (Reagan *et al*. 2010; Ishizuka *et al*. 2011a) and for the Mariana forearc (Cosca *et al*. 1998; Reagan *et al*. 2013). Transitional high-Mg andesites are dated at c. 43–44 Ma on Guam and in the Bonin islands (Reagan *et al*. 2010). $^{40}Ar/^{39}Ar$ and U–Pb zircon ages of basalt from the forearc slope east of the Bonin Ridge and south of Guam imply forearc volcanism around 50–52 Ma. This was followed by low-Ca boninite volcanism on Chichijim around 48–46 Ma (Ishizuka *et al*. 2006). $^{40}Ar/^{39}Ar$ ages of the Expedition 352 igneous basement indicate magmatism around 50–51 Ma (D. Heaton and A. Koppers, pers. com. 2016). Widespread FAB volcanism also took place within the Amami Sankaku Basin, c. 250 km to the west of the Expedition 352 sites (pre-Shikoku Basin opening), as drilled at Site U1438 during IODP Expedition 351 (Arculus *et al*. 2015c). A late Palaeocene-early Eocene age for this volcanism is possible based on radiolarians and other evidence (Arculus *et al*. 2015c; Ishizuka *et al*. 2016; Brandl *et al*. 2017). The 52–48-Ma age range of volcanic rocks recovered from the Bonin forearc (Ishizuka *et al*. 2011a; Reagan *et al*. 2017) is comparable to the basaltic basement of the Amami Sankaku Basin drilled at Site U1438 (Arculus *et al*. 2015c, 2015a, 2015b; Reagan *et al*. 2017). FAB overlies dolerite based on Expedition 352 drilling (Reagan *et al*. 2017). Also, nearby Shinkai 6500 diving shows that diabase is underlain by gabbro (Reagan *et al*. 2010). One interpretation is that FAB exclusively erupted during subduction initiation. An alternative (Lallemand 2016) is that the Amami Sankaku Basin basalt relates to early-stage backarc rifting of the Western Philippine Basin (at a high angle with respect to the IMB forearc). The rift magmatism could have been influenced by the Manus plume (Ishizuka *et al*. 2013; see also Hickey-Vargas 2005; Savov *et al*. 2006; Fletcher and Wyman 2015; Wu *et al*. 2016).

Subduction-initiation process

Models of subduction zone initiation and related crustal spreading (e.g. Stern 2004) commonly infer an open-ocean setting (Uyeda and Ben-Avraham 1972; Casey and Dewey 1984; Stern and Bloomer 1992; Stern 2004). In the popular oceanic transform model, the Pacific plate subducted northwards, offset by very long c. N–S transform faults (Hilde *et al*. 1977; Hussong and Uyeda 1981; Stern and Bloomer 1992; Figure 17(a)). Passive sinking of the Pacific plate initiated subduction and a change in Pacific plate motion around 50 Ma (Stern and Bloomer 1992). The leading edge of the subducting plate retreated oceanwards initiating decompression melting and boninitic magmatism, followed by the onset of 'normal' arc volcanism (up to 10 million years later). Several lines of evidence question the oceanic transform-initiation model: (1) Although Pacific plate subduction was generally northward on a very large scale including the Sunda arc and the northwest Pacific region, recent reconstructions of the Izu–Bonin region involve several plates and even phases of southward as well as northward subduction (Hall 2002, 2012; Deschamps and Lallemand 2002; Wu *et al*. 2016). (2) Direct evidence of a pre-Eocene precursor oceanic fracture zone is lacking (although preservation is unlikely). (3) The implied existence of a fracture zone >3500 km long may be improbable by comparison with modern oceanic settings. (4) The incipient Izu–Bonin magmatism restores to a position close to a late Mesozoic volcanic arc (Daito Ridge Group) rather than an open-ocean setting (Arculus *et al*. 2015a, 2015b, 2015c). The crust directly west of the IBM system was probably composed of late Mesozoic arc-type material, as preserved to the north of the West Philippine Basin (e.g. Daito Ridge Group; see Arculus *et al*. 2015a) and implied conjugates to the south (Hall *et al*. 1991; Hall 2002). An alternative reconstruction suggested here (Figure 17(b)) precludes tectonic models in which at ~50 Ma, the IBM was bordered on both sides by oceanic crust, with important implications for genesis of the Izu–Bonin forearc and its sediment cover (and supra-subduction ophiolites generally).

A comparison of the preliminary Expedition 351 and 352 basalt chemical data (Arculus *et al*. 2015a; Reagan

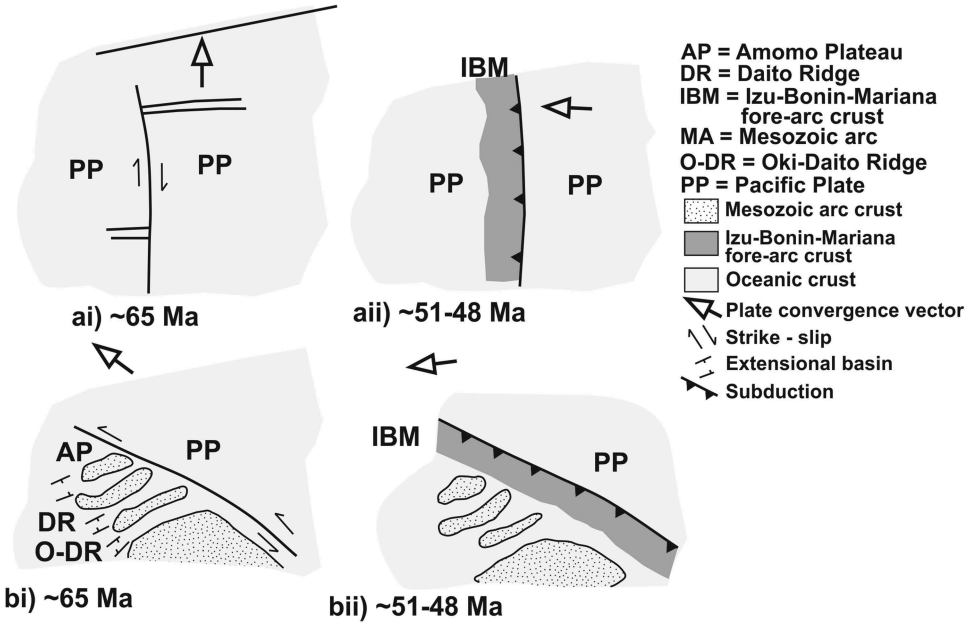

Figure 17. Alterative tectonic models for the genesis of the Izu–Bonin–Mariana forearc crust related to subduction initiation. (ai,aii) Oceanic fracture zone converted into a subduction zone when plate convergence direction greatly changed (simplified from Stern and Bloomer 1992); (bi,bii) pre-existing Mesozoic arc rifted adjacent to a continent–ocean transform plate boundary (possibly related to transtension). Changed plate convergence vector then resulted in subduction initiation as in (ai). Spreading of the West Philippine Sea follows immediately (51–45 Ma), possibly plume influenced. Reconstruction based on palaeomagnetic data (interpolated back to c. 50 Ma) and subaqueous regional geology (e.g. Arculus *et al*. 2015a, 2015b). Model (b) is preferred here.

et al. 2017) suggests that the former are relatively fertile, consistent with an incipient backarc setting. If correct, more depleted subduction-initiation crust, as drilled in the Izu–Bonin Ridge at the Expedition 352 sites also existed oceanwards of the restored Amami Sankaku Basin but was removed by subduction erosion (Reagan *et al*. 2107). South of the Expedition 352 sites (c. 200 km) the Ogasawara Plateau ('Ogasawara palaeoland'; Ishii *et al*. 1985; Figure 1(b)) is interpreted as accreting Pacific Ocean seamount crust (Kaiho *et al*. 2007; Kodeira *et al*. 2010; Ohara *et al*. 2015). There are hints of compressional and strike-slip deformation in the Expedition 352 cores (Kurz *et al*. 2015; Reagan *et al*. 2015). Seamount collision and related subduction erosion could have affected the Izu–Bonin forearc over wide regions.

Subduction might have initiated spontaneously (spontaneous subduction model: Leng and Gurnis 2015) as suggested for the Amami Sankaku Basin (Arculus *et al*. 2015a, 2015b). The coring and reflection seismic evidence from the Amami Sankaku Basin (Arculus *et al*. 2015a, 2015b) does not reveal evidence of thrusting, uplift, or sedimentary reworking as expected for compression-related subduction initiation. However, the site could be too far away from the restored locus of subduction initiation (>100 km) to show obvious evidence of convergence (e.g. uplift and mass wasting). The evidence is equivocal (Keenan and Encarnación 2016) because the link between the MORB-basement and subduction initiation is uncertain. Modelling suggests that subduction initiation along a convergent boundary between oceanic crust and older arc crust is plausible where crust of markedly differing buoyancy is juxtaposed. The late Mesozoic arc crust (Daito Ridge Group) could have become relatively buoyant and elevated as a result of crustal extension, and the associated thermal heating then promoted rifting of the Amami Plateau and the Daito Ridge to form the Amami Sankaku Basin. The effective crustal age of the overriding plate was thereby reduced to c. 0–7 Ma in contrast to a 50–70-Ma age of the subducting Pacific oceanic crust (Leng and Gurnis 2015).

Subduction initiation along the IBM forearc (52–48 Ma) corresponds to a time of regional to global plate reorganization. In the spontaneous subduction model, the initiation of the Bonin-Mariana/Tonga-Kermadec convergent system might itself have triggered such a global reorganization, which is seen as far afield as Hawaiian-Emperor seamount chain bend (53.3–43.8 Ma) (Whittaker *et al*. 2007). The reconstructed Pacific plate motion direction changed from northwesterly during 60–50 Ma to more westerly during 50–40 Ma (Whittaker *et al*. 2007).

An alternative is that the IBM subduction initiation was forced, possibly by India–Asia collision in the

Himalaya–Tibet region (Reagan *et al*. 2013). Collision is commonly put at 60–50 Ma, although later collision has its advocates (see Najman *et al*. 2010). It is unclear how long the effects of Himalaya–Tibet collision would take to propagate to the northwest Pacific region. However, accepting collision around 60–50 Ma, a related triggering of subduction in the IBM forearc is plausible.

In summary, prior to 50 Ma, pre-existing Mesozoic arc crust is likely to have been bounded by a transform fault (c. WSW–ESE trending) which was then transformed to a convergent plate boundary. The likely cause was a switch from strike-slip to transpression/convergence (i.e. forced subduction).

Eocene–Recent development of the Izu–Bonin arc

Early Eocene magmatism (c. 52–50 Ma) was followed by tholeiitic to calc-alkaline volcanism (e.g. on the Bonin Ridge) to create an Eocene volcanic arc to the west of the subduction-initiation crust. This started at about 44 Ma (e.g. on Chichijima, Hahajima and Saipan) (Ishizuka *et al*. 2006; Reagan *et al*. 2008), as also documented during Expedition 351 (Brandl *et al*. 2017). From 42 to 25 Ma, the front of the active magmatism was located ~20 km east of the present arc (Taylor and Fujioka *et al*. 1992; Ishizuka *et al*. 2006). The volcanism continued along this arc lineament until 29 Ma for the Mariana segment, 27 Ma for the Izu–Bonin segment and 25 Ma for the Kyushu-Palau Ridge (Ishizuka *et al*. 2011b), which is consistent with the abundance of arc-derived ash layers at the Expedition 352 sites. The arc volcanism was coupled with near-orthogonal spreading of the West Philippine Basin (Fujioka *et al*. 1999; Deschamps and Lallemand 2002; Taylor and Goodliffe 2004; Sasaki *et al*. 2014).

During ongoing Pacific Ocean subduction, the IBM arc rifted during the late Oligocene (c. 26–25 Ma), followed by early Miocene spreading to form the Shikoku Basin in the north, the Parece Vela Basin further south and related basins and highs (e.g. Ogasawara and Nishinoshima Troughs), all bounded by major normal faults (Taylor and Fujioka *et al*. 1992; Ishizuka *et al*. 2006, 2011b; Takahashi *et al*. 2009; see also Sibuet *et al*. 1987; Figure 1(a)).

A magmatic minimum in the Izu–Bonin arc magmatism is inferred to exist from c. 25 to 15 Ma (Taylor and Fujioka *et al*. 1992). This encompasses the overall timing of deposition of the unusual reddish coloured, well-oxidized sediments, as recorded at both the Expedition 351 and 352 sites (Reagan *et al*. 2015; Arculus *et al*. 2015c). Backarc spreading finally ceased at ~15 Ma, around the time that the Japan Sea began to open.

After 15 Ma, the Neogene IBM arc relocated to near its present position (Taylor and Fujioka *et al*. 1992; Hall *et al*. 1995; Yamazaki *et al*. 2010; Mahony *et al*. 2011), during which there was copious supply of tuffaceous sediment from the Izu–Bonin forearc, as drilled during Expedition 352 (Reagan *et al*. 2015) and elsewhere (e.g. Amami Sankaku Basin; Arculus *et al*. 2015c). Volcanism became active along rear-arc seamount chains and isolated seamounts from c. 17 to 3 Ma (Ishizuka *et al*. 1998, 2003; Tamura *et al*. 2014, 2015; Busby *et al*. 2017). During this time, the IBM arc moved northwards to its current position.

The sedimentary history of the Expedition 352 sites and the Izu–Bonin arc as a whole reflects northward motion from a near equatorial palaeolatitude, followed by amalgamation with the Japan continental margin arc. There are several different interpretations of how this took place (Figure 18), which may be constrained by sedimentary evidence from the Expedition 352 forearc sites.

First, the 'retreating slab' model which is based on palaeomagnetic data indicates substantial northward drift of the Izu–Bonin arc from near the equator, coupled with major clockwise rotation since c. 50 Ma (Shih 1980; Haston and Fuller 1991; Hall *et al*. 1995; Hall 2002; Yamazaki *et al*. 2010; Figure 18(a)). Based largely on land palaeomagentic evidence from Palau, Guam, Saipan Chicijima, and Anijima, the Philippine Sea plate rotated 84° clockwise (Hall *et al*. 1995; Deschamps and Lallemand 2002; Hall 2002). An initial 50° of rotation took place between 55 and 45 Ma (around a pole at 10° N), followed by 34° of continuous rotation between 25 and 5 Ma (around a Euler pole at 15°N, 160°E) (Hall 2002). As a result, the Izu–Bonin arc swept around like a windscreen wiper from an initial c. NW–SE trend to its present c. NNW–ESE trend. The resulting tectonic reconstruction implies >2000 km of rollback of the downgoing Pacific plate, a low-angle 'soft collision' of the Philippine Sea plate with the Eurasian plate, and the arrival of the Izu–Bonin arc at southernmost Honshu by early Miocene (20 Ma). Palaeomagnetic data from drill and gravity cores from the West Philippine Basin (Sdrolias *et al*. 2004; Yamazaki *et al*. 2010), from Leg 195 (Richter and Ali 2015), and from Expedition 352 (Reagan *et al*. 2015; Sager *et al*. 2017), combined with the known seafloor spreading fabric (Hilde and Lee 1984) confirm that this area was located close to the equator at 50 Ma. Major northward movement took place from 50 to 25 Ma but apparently little movement after 15 Ma, according to Yamazaki *et al*. (2010). The marine magnetic data support up to c. 84° of the clockwise motion occurred between 50 and 15 Ma. However, there is an apparent discrepancy between the land and

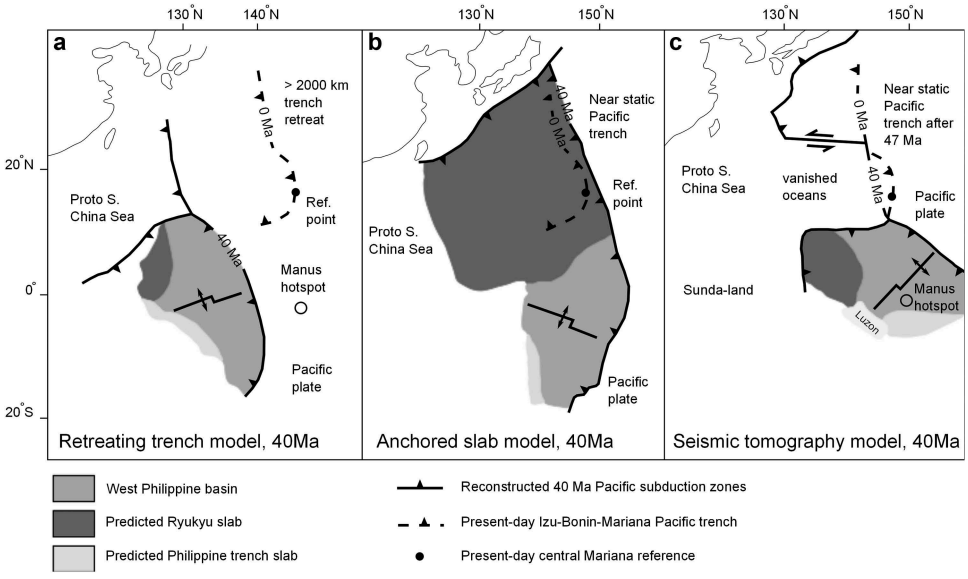

Figure 18. Alternative tectonic models of the northwest Pacific region. Modified after Wu *et al*. (2016). a, 'Retreating trench' model; (b) 'anchored slab' model; (c) 'seismic tomography' model. Each of these (and variants) have pros and cons as discussed in the text. The retreating trench models fits the geophysical and geological evidence better than the other two, as discussed in the text.

marine palaeomagnetic evidence during 15–5 million years concerning the presence or absence of continuing rotation and northward drift. Palaeomagnetic-based reconstructions have however been criticized on several grounds: (1) Palaeomagnetic data from the land outcrops could be of only local significance. (2) Land palaeomagnetic data are sparse, without many data that pass strict statistical significance criteria. (3) Data from Indonesia and elsewhere could come from tectonically decoupled areas. (4) The required Pacific slab rollback of >2000 km may be improbable.

The second type of model (Figure 18) assumes a nearly static Pacific trench in a hotspot mantle reference frame ('anchored slab model'), with little change in plate geometry since around 50 Ma. As a result, the Izu–Bonin arc system is shown as generally NW–SE trending (Seno and Maruyama 1984; Ishizuka *et al*. 2011a, 2011b, 2013; Xu *et al*. 2014; Zahirovic *et al*. 2014; Leng and Gurnis 2015). Such interpretations are questionable: (1) Palaeomagnetic data indicate major rotations on land and under the sea in the Philippine Sea region (e.g. Indonesia). (2) Absence of geological evidence from Honshu that the Izu–Bonin arc was located near its present position until the Miocene. (3) Evidence from other regions where slab rollback is well documented as playing an important role (e.g. Mediterranean Sea; Pannonian Basin; see below).

The third type of model is based on seismic tomographic evidence ('tomographic model)'. Palaeotrench analysis suggests that at least the north-central portion of the IBM subduction zone has moved no more than 200 km since c. 48 million years (Wu *et al*. 2016; Figure 18). The Philippine Sea plate began as a small microplate near the equator (possibly above the Manus plume), bordered by now-subducted, large oceanic tracts to the northwest, west, and southwest. The microplate expanded by seafloor spreading and drifted northwards to collide with southern Honshu by early Miocene (20 Ma). Problems with this interpretation include: (1) The need to invoke huge vanished east Asian oceans for which there is little or no supporting geological evidence. (2) The requirement to invoke complex strike-slip and convergent boundaries on several plates in order to juxtapose the IBM arc with Honshu by 20 Ma. (3) The difficulties inherent in resolving complex microplate interactions in areas such as Indonesia (e.g. Hall 2002). (4) Apparent inconsistencies with the geological evidence, for example the existence of a passive margin along the northern margin of the Australian plate (e.g. Hall 2002). (5) Non-slab rollback since c. 48 Ma is questionable in view of geophysical and geological evidence of long-distance (hundreds of kilometres) and long-term (10 s of Ma) rollback elsewhere, including southeast Asia (Hall and Spakman 2015) and the Mediterranean region (e.g. Wortel and Spakman 2000).

The sedimentary evidence from Expedition 352 is consistent with models 1 and 3, which both involve migration of Izu–Bonin–Mariana arc from near the equator to collide with Honshu. However, the sedimentary evidence is inconsistent with model 2. If the Izu–Bonin–Mariana arc was always near the Eurasian active

continental margin, the sediments should contain continental-arc-derived tephra throughout, whereas, instead, Japan arc-derived tephras appear only after the early Miocene (Figure 13(a–d); Kutterolf et al., sub).

Constraints from the geology of Honshu

Today, the Izu–Bonin–Mariana arc system is in collision with Honshu directly northwest of the Boso triple junction of the Eurasian plate, the Pacific plate, and the Philippine Sea plate (Figure 19(c)). Similar lithologies to those drilled during Expedition 352 are exposed in the Boso Peninsula (Ogawa *et al.*, 1985). The Boso Peninsula was established by around 15 Ma (Figure 19 (b)). During the mid-to-late Miocene (15–6 Ma), the triple junction area (Kanto syntaxis) experienced clockwise rotation of >90° (Figure 19(c)). About half of the rotation is interpreted to relate to the opening of the Japan Sea and the remainder (mainly late Miocene) to collision of the Izu–Bonin arc (Takahashi and Saito 1997).

During Pliocene–Pleistocene time, the NW–SE trending segment of the Pacific active margin in the Boso and Miura Peninsula areas experienced near-orthogonal convergence. This was associated with thrusting, accretion, trench-forearc sedimentation, exhumation of felsic mid-crustal rocks (mostly tonalite), coupled with related local tectonic rotations (Figure 19(c)). The overall driving force was attempted subduction of the Izu–Bonin arc system during Plio-Pleistocene-to-Recent (Ogawa *et al.* 1985; Koyama and Kitazato 1988; Soh *et al.* 1998; Yamamoto and Kawakami 2005; Yamamoto *et al.* 2007; Ogawa *et al.* 2008). The Izu–Bonin–Mariana arc indented the pre-existing active margin of the Eurasian plate, which would be expect to result in right-lateral (tectonic escape) structures along the northwest margin of the indentor (Koyama and Kitazato 1988; Figure 19(c)). Field evidence indicates that right-lateral strike-slip/transpression, exemplified by Riedel shear fabrics, did indeed dominate the Miocene-recent structural development of pre-existing accretionary melange (Mineoka melange) (Ogawa and Takahashi 2004; Mori and Ogawa 2005; Mori *et al.* 2011).

In an alternative plate-kinematic model, the Izu–Bonin arc collided with central Honshu during the Pliocene (Ali and Moss 1999), specifically 2–5 Ma (Mahony *et al.* 2011). If correct, the Pliocene-recent indentation could relate to orthogonal northward collision, as in the 'anchored slab model' (Figure 18). However, geological evidence indicates that Honshu and the IBM amalgamated during the Miocene. The Eurasian plate active margin including older accretionary mélange (Mineoka mélange) and forearc basin sediments (Shimanto Group) was covered by heterogeneous clastic sediments (Sakuma Group)

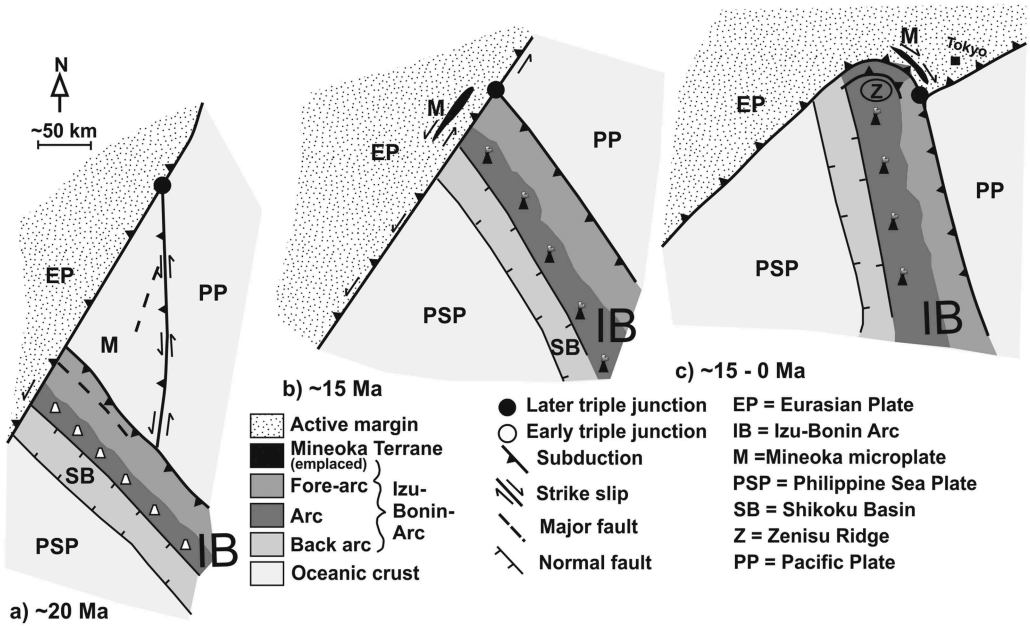

Figure 19. Simplified plate tectonic sketch showing the amalgamation of the Izu–Bonin arc with the active continental margin of Honshu (Japan). Reconstruction of the Eurasian, Pacific, and Philippine plate boundary is mainly based on Hall *et al.* (1995), Takahashi and Saito (l997), Kawate and Arima (1998), Hall (2002), and Yamazaki *et al.* (2010). The Mineoka plate as shown in (a) is based on Mori *et al.* (2011). The Izu–Bonin arc amalgamated with Honshu by 20 Ma and underwest northeastward translation later during the Miocene (c. 15 Ma) and later indentation. Honshu-derived felsic tuff reached the Expedition 352 sites from c. 15 Ma.

during the mid-Miocene (c. 15 Ma), as indicated by the presence of the large foraminifer, *Lepidocyclina* sp. (Mori and Ogawa 2005; Ogawa and Sashida 2005; Ogawa *et al*. 2008). Basic tuffaceous rocks that are interpreted to have been derived from the Izu–Bonin arc first appear in the Honshu forearc basin in the Boso Peninsula (Amatsu Formation) during the early late Miocene (13–12 Ma) (Takahashi and Saito 1997, 1999). Some palaeomagnetic data for mid-Miocene time suggest that amalgamation of the Izu–Bonin arc with Honshu began before 15 million years (Hoshi and Sano 2013).

The three alternative tectonic reconstructions of the Oligocene–Miocene tectonic-volcanic development of the Izu–Bonin arc (Figure 18) can also be tested by the evidence from Honshu, with implications for regional sedimentation. In the 'retreating slab' model (Seno and Maruyama 1984; Hall *et al*. 1995; Hall 2002; Sdrolias *et al*. 2004; Figure 18; Yamazaki *et al*. 2010), the Izu–Bonin arc impinged on the Japanese active continental margin (Eurasian plate) at a low angle favouring strike-slip/transpression. In the 'anchored slab' model (Matsuda 1978; Seno and Maruyama 1984; Ishizuka *et al*. 2011a, 2013; Xu *et al*. 2014; Zahirovic *et al*. 2014), the initial collision with Honshu took place at a high angle, resulting in near-orthogonal collision/accretion. In the 'tomographic model' (Whittaker *et al*. 2007; Wu *et al*. 2016), both the Pacific Plate and the Philippine Sea Plate underwent orthogonal subduction beneath the Eurasian Plate from 50 Ma to recent. In a variant (Wu *et al*. 2016), the Philippine Sea Plate near southern Japan subducted southeastwards at c. 20 Ma while a remnant of the Pacific Plate subducted northwestwards. This 'double subduction' culminated in near-orthogonal accretion/collision prior to 10 Ma.

Prior to the collision of the Izu–Bonin arc with the active margin of the Eurasian plate in Honshu, accretionary melange developed related to subduction of the Pacific Plate and/or the Philippine Sea Plate to form the Shimanto accretionary prism (Taira *et al*. 1982, 1989; Taira 2001). The northward drift of the Izu–Bonin arc is believed to have been associated with isolation of a crustal sliver (Mineoka microplate) between the Eurasian Plate, the Pacific Plate, and the Izu–Bonin arc prior to, or during, early Miocene time (Ogawa *et al*. l983; Mori *et al*. 2011; Figure 19(a)). The inferred Mineoka microplate might have a counterpart in a now-subducted (putative) North New-Guinea Plate (Ogawa *et al*. 1985). The Mineoka microplate is mostly harzburgitic serpentinite mélange with blocks of limestone, radiolarian chert, basalts of mid-ocean ridge, island arc tholeiitic and within-plate types, plutonic rocks (e.g. gabbro and tonalite of island arc affinity), and some metamorphic rocks (Ogawa and Taniguchi 1989; Mori *et al*. 2011). The mélange blocks are dated at c. 41 24 Ma (Hirano *et al*. 2003; Mori *et al*. 2011). The mélange is restored as oceanic crust (Mineoka ophiolite) that accreted around mid-Miocene time (18–15 Ma).

Both the 'retreating trench' model and the 'tomographic' model explain the juxtaposition of the Izu–Bonin arc with Honshu during the Miocene, the former implying strike-slip/transpression and the latter orthogonal collision (Figure 18). Both models infer collision of the Izu–Bonin arc by c. 20 Ma (early Miocene), considerably earlier than the first sedimentary evidence of juxtaposition (c. 15 Ma). However, a hiatus could exist between the collision and the initial cover deposition. In the 'retreating plate' model, the Izu–Bonin arc approached southernmost Honshu several million years before reaching the Bozo Peninsula area (near Tokyo) where the sedimentary age evidence comes from.

Summary of tectonic development

The 'retreating trench' model is consistent with most of the regional geological and geophysical evidence (Figure 20). In this scenario, after genesis of the IBM forearc at c. 50 Ma and formation of the early IBM arc and the West Philippine Basin, the Shikoku Basin rifted around 25–20 Ma (Ishizuka *et al*. 2011b), followed by amalgamation with southern Honshu around 20 Ma. The geological evidence from Honshu is compatible with oblique subduction/collision of the Izu–Bonin crust during the Miocene, followed by near-orthogonal subduction/collision during Pliocene–Pleistocene. Izu–Bonin arc volcanism paused during backarc rifting as the Pacific plate retreated oceanward, as documented by the absence of Izu–Bonin arc-derived tephra from c. 26 to 15 Ma. After the Izu–Bonin arc migrated northward and indented with central Honshu (Bozo Peninsula), subduction of the Philippine Sea plate reactivated the input of Honshu-derived tephra beginning at c. 18 Ma and becoming abundant from c. 8 Ma, as documented from the Expedition 352 cores. It thus took an additional c. 3 Ma for ash input to resume from the Honshu arc compared to the Izu–Bonin arc after the c. 26–15 Ma switch off. The later resumption of ash input from Honshu may reflect the time needed for the Izu–Bonin arc to move sufficiently northward for subduction to resume.

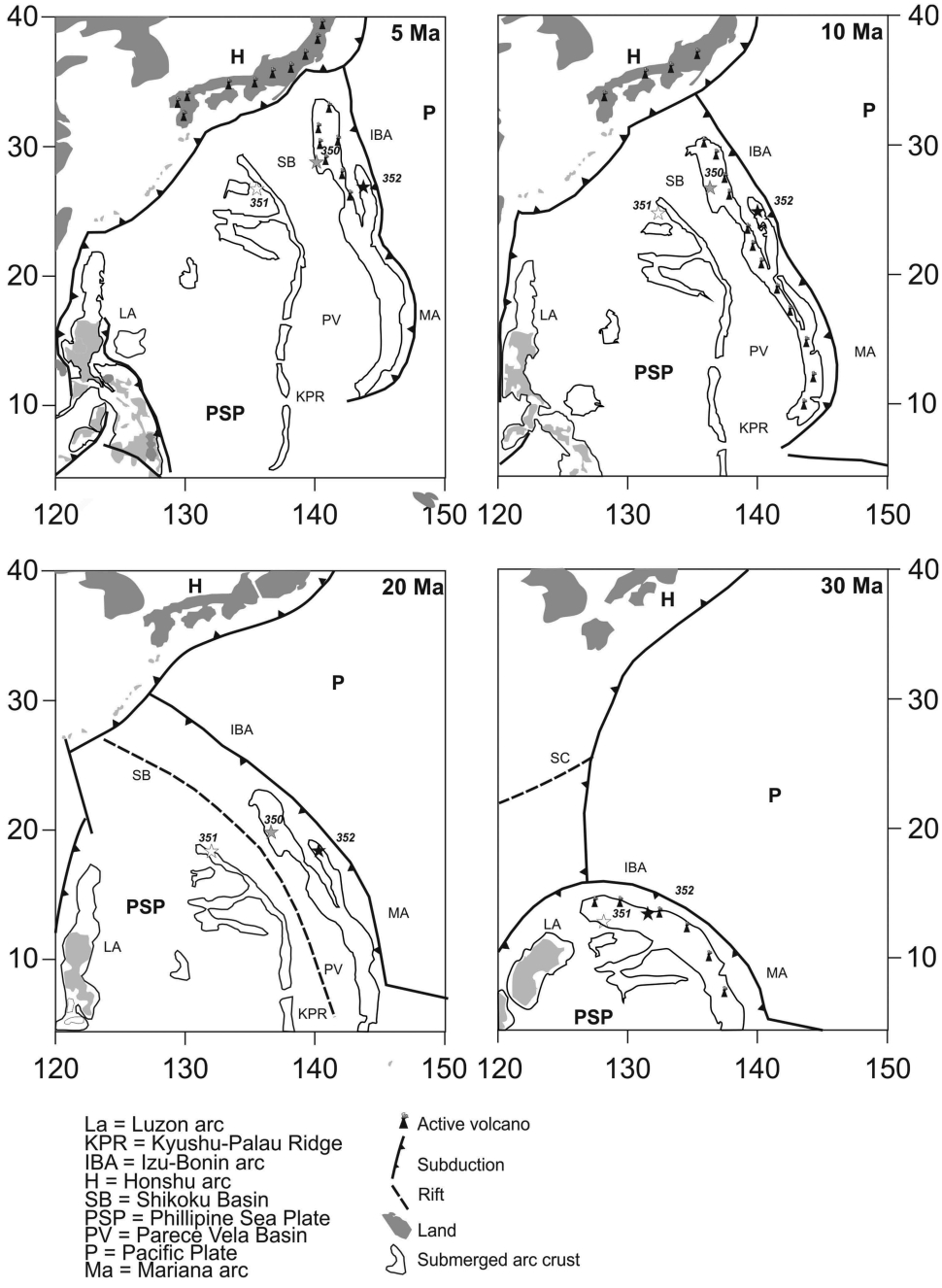

Figure 20. Preferred Oligocene–Pliocene development of Izu–Bonin arc, based on the 'retreating slab' model (see Figure 18(a); Hall 2002). Note the locations of the Expedition 350, 351, and 352 drilling areas (different density stars). Inferred sources of the tuffaceous sediments in the Izu–Bonin oceanic arc and the Honshu continental margin.

Conclusions

(1) The four Expedition 352 drill sites, two on the upper slope (Sites U1439 and U1442) and two on the lower slope (Sites U1440 and U1441), document the sedimentary, tectonic, magmatic, and palaeoceanographic development of the Izu–Bonin forearc from Eocene–Recent time, including its amalgamation with southern Japan (Honshu).

(2) Early Eocene (c. 51–52 Ma) supra-subduction spreading of the igneous basement was followed by an up to c. 15 Ma hiatus. Seafloor erosion and reworking locally produced basaltic talus (c. 80 m thick) on the lower forearc slope, as supported by palaeomagnetic evidence.

(3) Based on sediment chemistry, basal iron-rich metalliferous oxide-deposits at several sites represent a mixture of distal hydrothermal precipitates and Pacific hemipelagic sediment that

accumulated over an extended time interval, consistent with the biostratigraphically determined hiatus.

(4) During the Oligocene (c. 34–23 Ma), pelagic carbonate accumulated above the CCD, with copious input of volcanic ash of largely felsic composition, mainly derived from the Izu–Bonin arc.

(5) Early Miocene–early Pliocene (c. 23–4 Ma) was dominated by carbonate-poor hemipelagic clay and mud deposition near or beneath the CCD, together with hydrogenous metal enrichment (but with considerable variation after 15 Ma). The low-carbonate relates to the global carbonate 'crash' (23–20 Ma), coupled with forearc subsidence during rifting of the backarc Shikoku Basin (25–20 Ma).

(6) The early Miocene (c. 23–18 Ma) was virtually free of tuffaceous input, as indicated by chemical and sediment magnetic property data.

(7) Mid-Miocene to mid-Pliocene (c. 15–4 Ma) tephras were mainly derived from the Izu–Bonin arc. Tephras of mid-Pliocene to Pleistocene age came from both the Izu–Bonin arc and from the Japanese continental margin arc (Honshu) based on the tephra chemical evidence.

(8) Loess contributed to the hemipelagic sediments throughout the entire sedimentary history, especially from the early Miocene onwards (c. 23 Ma) after collision with Honshu.

(9) The hemipelagic sediments became increasingly calcareous during mid-Miocene to early-Pliocene (c. 16–4 Ma) related to global increase in carbonate production. The lowered CCD allowed nannofossil ooze to accumulate on the upper slope sites whereas low-carbonate accumulation persisted on the lower slope sites.

(10) Productive nannofossil chalk accumulated at the upper slope sites during the later Pliocene and Pleistocene (<4 Ma), while near or sub-CCD accumulation continued at the lower slope sites.

(11) Extensional faulting created outer forearc small basins and was active in generating large volumes of basaltic talus by mass wasting and debris-flow processes during Oligocene–Pliocene(?). Hemipelagic and pelagic sedimentation accumulated on a fault-influenced topographic high between two fault-bounded basins.

(12) Compositionally different tuffaceous sediment accumulated at the upper slope *versus* the lower slope sites. The upper slope sites received turbiditic input from the Izu–Bonin arc, whereas the topographically isolated lower slope sites preferentially accumulated distal continental margin fallout (continental margin arc tephra, loess, and pelagic sediment).

(13) Sediment chemistry and magnetic data suggest that Izu–Bonin arc volcanism switched off during opening of the Shikoku backarc basin.

(14) Amalgamation of the Izu–Bonin arc with Japan during the Miocene (c. prior to c. 15 Ma) and its later northward translation and indentation (Plio-Pleistocene) allowed Honshu-derived tephra to reach the Izu–Bonin forearc after c. 15 Ma. The Izu–Bonin arc reactivated allowing resumed input of tephra to the Izu–Bonin outer forearc (15 Ma–Recent).

(15) The Izu–Bonin outer forearc sedimentation history combined with evidence from Honshu is most consistent with the 'retreating slab' model for the Oligocene–Miocene tectonic–magmatic development of the IBM arc.

Acknowledgements

This research used data and samples provided by the International Ocean Discovery Program (IODP). We thank the captain and crew of the *JOIDES Resolution* for helping to make Expedition 352 such a success, and our shipboard colleagues for on-going scientific discussions. We also thank the Paleomagnetism Lab at the University of California at Davis. Our understanding of the regional setting benefited considerably from discussions with Mark Reagan, Julian Pearce, Robert Hall, and Yujiro Ogawa. Mark Reagan kindly commented on several scientific aspects of the pre-submission manuscript. The submitted manuscript benefitted from insightful comments and suggestions by Cathy Busby and Kathy Marsaglia.

Disclosure statement

No potential conflict of interest was reported by the authors.

Funding

The first author acknowledges a research grant from the UK Natural Environmental Research Council, SF/USSSP postcruise: [Grant Number COL-T352A13]. Steffen Kutterolf and Julie Schindlbeck were supported by the German Research Foundation (DFG): [Grant Numbers KU2685/4-1 and SCHI1349/1-1]. Katerina Petronotis was supported by the IODP-JRSO and NSF/USSSP postcruise grant: [Grant Number COL-T352A13]. Funding for Alan Baxter was through an Australian-New Zealand IODP Consortium (ANZIC) IODP: [Grant Number ARC-LE0882854].

References

Ali, J.R., and Moss, S.J., 1999, Miocene intra-arc bending at an arc-arc collision zone, central Japan: Comment: Island Arc, v. 8, p. 114–123. doi:10.1046/j.1440-1738.1999.00218.x

Arculus, R.J., Ishizuka, O., and Bogus, K., and the Expedition 351 Scientists, 2015c. Proceedings of the International Ocean Discovery Program, Expedition 351: Izu-Bonin-Mariana Arc Origins: College Station, TX (International Ocean Discovery Program). 10.14379/iodp.proc.351.2015

Arculus, R.J., Ishizuka, O., Bogus, K.A., Gurnis, M., Hickey-Vargas, R., Aljahdali, M.H., Bandini-Maeder, A.N., Barth, A. P., Brandl, P.A., Drab, L., Do Monte Guerra, R., Hamada, M., Jiang, F., Kanayama, K., Kender, S., Kusano, Y., Li, H., Loudin, L.C., Maffione, M., Marsaglia, K.M., McCarthy, A., Meffre, S., Morris, A., Neuhaus, M., Savov, I.P., Sena, C., Tepley, F.J., Van Der Land, C., Yogodzinski, G.M., and Zhang, Z., 2015b, Reply to 'Unclear causes for subduction': Nature Geoscience, v. 9, p. 338–339. doi:10.1038/ngeo2704

Arculus, R.J., Ishizuka, O., Bogus, K.A., Gurnis, M., Hickey-Vargas, R., Aljahdali, M.H., Bandini-Maeder, A.N., Barth, A. P., Brandl, P.A., Drab, L., Do Monte Guerra, R., Hamada, M., Jiang, F., Kanayama, K., Kender, S., Kusano, Y., Li, H., Loudin, L.C., Maffione, M., Marsaglia, K.M., McCarthy, A., Meffre, S., Morris, A., Neuhaus, M., Savov, I.P., Sena, C., Tepley III, F.J., Van Der Land, C., Yogodzinski, G.M., and Zhang, Z., 2015a, A record of spontaneous subduction initiation in the Izu–Bonin–Mariana arc: Nature Geoscience, v. 8, p. 728–733. doi:10.1038/ngeo2515

Asiedu, D.K., Suzuki, S., Nogami, K., and Shibata, T., 2000, Geochemistry of Lower Cretaceous sediments, inner zone of southwest Japan: Constraints on provenance and tectonic environment: Journal of Geochemistry, v. 34, p. 155–173.

Bahlburg, H., and Dobrzinski, N., 2011, A review of the Chemical Index of Alteration (CIA) and its application to the study of Neoproterozoic glacial deposits and climate transitions, *in* Arnaud, E., Halverson, G.P., and Shields-Zhou, G.A., eds., The geological record of neoproterozoic glaciations, Vol. 36: Memoir, Geological Society, London, p. 81–92.

Ballard, R.D., and Moore, J.G., 1977, Atlas of the mid-Atlantic rift valley: New York, Springer-Verlag, 114.

Barth, A.P., Brandl, P.A., Hickey-Vargas, R., Jiang, F., Kanayama, K., Kusano, Y., Marsaglia, K.M., McCarthy, A., Meffre, S., Savov, I.P., Tepley, F.J.I., and Yogodzinski, G.M. 2014, IODP expedition 351 lithostratigraphy: Volcaniclastic record of izu-bonin-mariana (IBM) arc initiation. American Geophysical Union Meeting, San Francisco, California, Abstract T53A-4642.

Bhatia, M.R., 1983, Plate tectonics and geochemical composition of sandstones: Journal of Geology, v. 91, p. 611–627. doi:10.1086/628815

Bhatia, M.R., 1985, Rare earth element geochemistry of Australian Paleozoic graywackes and mudrocks: Provenance and tectonic control: Sedimentary Geology, v. 45, p. 97–113. doi:10.1016/0037-0738(85)90025-9

Bhatia, M.R., and Crook, K.A.W., 1986, Trace element characteristics of graywackes and tectonic setting discrimination of sedimentary basins: Contributions to Mineralogy and Petrology, v. 92, p. 181–193. doi:10.1007/BF00375292

Bonatti, E., Kraemer, T., and Rydell, H.S., 1972, Classification and genesis of submarine iron-manganese deposits, *in* Horn, D.R., ed., Ferromanganese deposits on the ocean floor: Washington, D.C., National Science Foundation, p. 149–167.

Boström, K., Peterson, M.N.A., Joensuu, O., and Fisher, D.E., 1969, Aluminum-poor ferromanganoan sediments on active oceanic ridges: Journal of Geophysical Research, v. 74, p. 3261–3270. doi:10.1029/JB074i012p03261

Bouma, A.H., 1962, Sedimentology of some flysch deposits: A graphic approach to facies interpretation: Amsterdam, Elsevier.

Brandl, P.A., Hamada, M., Arculus, R.J., Johnson, K., Marsaglia, K.M., Savov, I.P., Ishizuka, O., and Li, H., 2017, The arc arises: The links between volcanic output, arc evolution and melt composition: Earth and Planetary Science Letters, v. 461, p. 73–84. doi:10.1016/j.epsl.2016.12.027

Bryant, C.J., Arculus, R.J., and Eggins, S.M., 2003, The geochemical evolution of the Izu-Bonin arc system: A perspective from tephras recovered by deep-sea drilling: Geochemistry, Geophysics, Geosystems, v. 4, p. 1094. doi:10.1029/2002GC000427

Busby, C.J.,Tamura, Y., Blum, P., Guèrin, G., Andrews, G.D.M., Barker, A.K., Berger, J.L.R., Bongiolo, E.M., Bordiga, M., DeBari, S.M., Gill, J.B., Hamelin, C., Jia, J., John, E.H., Jonas, A.S., Jutzeler, M., Kars, M.A.C., Kita, Z.A., Konrad, K., Mahony, S.H., Martini, M., Miyazaki, T., Musgrave, R.J., Nascimento, D. B., Nichols, A.R.L., Ribeiro, J.M., Sato, T., Schindlbeck, J.C., Schmitt, A.K., Straub, S.M., Vautravers, M.J., and Yang, Y., 2017, The missing half of the subduction factory: Shipboard results from the Izu rear arc, IODP expedition 350: International Geology Review, p. 1–32. doi:10.1080/00206814.2017.1292469

Cambray, H., Cadet, J.-P., and Pouclet, A., 1993, Ash layers in deep-sea sediments as tracers of arc volcanic activity: Japan and Central America as case studies: Island Arc, v. 2, p. 72–86. doi:10.1111/j.1440-1738.1993.tb00075.x

Cambray, H., Pubellier, M., Jolivet, L., and Pouclet, A., 1995, Volcanic activity recorded in deep-sea sediments and the geodynamic evolution of western Pacific island arcs, *in* Taylor, B., and Natland, J., eds, Active margins and marginal basins of the western Pacific: Geophysical monograph: Washington, DC, American Geophysical Union, p. 97–124.

Casey, J.F., and Dewey, J.F., 1984, Initiation of subduction zones along transform and accreting plate boundaries, triple-junction evolution and fore-arc spreading centres—Implications for ophiolitic geology and obduction: Geological Society, London, Special Publications, v. 13, p. 269–290. doi:10.1144/GSL.SP.1984.013.01.22

Chauvel, C., Garçon, M., Bureau, S., Besnault, A., Jahn, B.-M., and Ding, Z., 2014, Constraints from loess on the Hf–Nd isotopic composition of the upper continental crust: Earth and Planetary Science Letters, v. 388, p. 48–58. doi:10.1016/j.epsl.2013.11.045

Christeson, G.L.S., Morgan, S., Kodaira, S., Yamashita, M., Almeev, R.R., MIchibayashi, K., Sakuyama, T., Ferré, E.C., and Kurz, W., 2016, Physical properties and seismic structure of Izu-Bonin-Mariana fore-arc crust: Results from IODP Expedition 352 and comparison with oceanic crust: Geochemistry, Geophysics, Geosystems, v. 17, p. 4973–4991. doi:10.1002/2016GC006638

Cosca, M., Arculus, R.J., Pearce, J., and Mitchell, J., 1998, 40Ar/39Ar and K–Ar geochronological age constraints for the inception and early evolution of the Izu–Bonin–Mariana

arc system: Island Arc, v. 7, p. 579–595. doi:10.1111/j.1440-1738.1998.00211.x

Cousens, B.L., Allan, J.F., and Gorton, M.P., 1994, Subduction-modified pelagic sediments as the enriched component in back-arc basalts from the Japan Sea: Ocean drilling program sites 797 and 794: Contributions to Mineralogy and Petrology, v. 117, p. 421–434. doi:10.1007/BF00307275

Cronan, D.S., 1976, Manganese nodules, and other ferro-manganese oxide deposits, in Riley, J.P. and Chester, R., eds., Chemical Oceanography (second edition), Volume 5: London, Academic Press, p. 217–263.

Day, R., Fuller, M., and Schmidt, V.A., 1977, Hysteresis properties of titanomagnetites: Grain-size and compositional dependence: Physics of the Earth and Planetary Interiors, v. 13, p. 260–267. doi:10.1016/0031-9201(77)90108-X

Deschamps, A., and Lallemand, S., 2002, The West Philippine Basin: An Eocene to early Oligocene back arc basin opened between two opposed subduction zones: Journal of Geophysical Research, v. 107, p. 2322. doi:10.1029/2001JB001706

deVries Klein, G., Kobayashi, K., White, S.M., et al., 1980, Proc. DSDP, Sci. Reports, 58: College Station, TX, Ocean Drilling Program. doi:10.2973/dsdp.proc.58.101.1980.

Dunlop, D.J., 2002, Theory and application of the Day plot (Mrs/Ms versus Hcr/Hc), 1. Theoretical curves and tests using titanomagnetite data: Journal of Geophysical Research, v. 107, p. 2056. doi:10.1029/2001JB000486

Ferrat, M., Wiss, D.J., Strekopytov, S., Dong, S., Chen, H., Najorka, J.Y.S., Gupta, S., Tada, R., and Sinha, R., 2011, Improved provenance tracing of Asian dust sources using rare earth elements and selected trace elements for palaeomonsoon studies on the eastern Tibetan Plateau: Geochimica Et Cosmochimica Acta, v. 75, p. 6374–6399. doi:10.1016/j.gca.2011.08.025

Fletcher, M., and Wyman, D.A., 2015, Mantle plume–subduction zone interactions over the past 60 Ma: Lithos, v. 233, p. 162–173. doi:10.1016/j.lithos.2015.06.026

Floyd, P.A., and Leveridge, B.E., 1987, Tectonic environment of the Devonian Gramscatho basin, south Cornwall: Framework mode and geochemical evidence from turbiditic sandstones: Journal of the Geological Society of Japan, v. 144, p. 531–542. doi:10.1144/gsjgs.144.4.0531

Floyd, P.A., Shail, R., Leveridge, B.E., and Franke, W., 1991, Geochemistry and provenance of Rhenoherzynian synorogenic sandstones: Implications for tectonic environment discrimination, *in* Morton, A.C., Todd, S.P., and Haughton, P.D.W., eds., Developments in sedimentary provenance studies, Geological Society of London Special Publications, V. 57, p. 611–626.

Fryer, P., Pearce, J.A., Stokking, L.B., et al., 1992, Proc. ODP, Sci. Results, 125: College Station, TX, Ocean Drilling Program. doi:10.2973/odp.proc.sr.125.1992.

Fryer, P., Taylor, B., Langmuir, C.H., and Hochstaedter, A.G., 1990, Petrology and geochemistry of lavas from the Sumisu and Torishima backarc rifts: Earth and Planetary Science Letters, v. 100, p. 161–178. doi:10.1016/0012-821X(90)90183-X

Fujioka, K., Okino, K., Kanamatsu, T., Ohara, Y., Ishizuka, O., Haraguchi, S., and Ishii, T., 1999, Enigmatic extinct spreading center in the west Philippine backarc basin unveiled: Geology, v. 27, p. 1135–1138. doi:10.1130/0091-7613(1999)027<1135:EESCIT>2.3.CO;2

Gill, J., Seales, C., Thompson, P., Hochstaedter, A., and Dunlap, C. 1992, Petrology and geochemistry of Pliocene-Pleistocene volcanic rocks from the Izu Arc, Leg 126: Paper presented at Proceedings of the Ocean Drilling Program, Scientific Results, Ocean Drilling Program College Station, TX. P. 383–404

Gradstein, F.M., Ogg, J.G., Schmitz, M., and Ogg, G., 2012, The geologic time scale 2012: Amsterdam, Elsevier.

Hall, R., 2002, Cenozoic geological and plate tectonic evolution of SE Asia and the SW Pacific: Computer-based reconstructions, model and animations: Journal of Asian Earth Sciences, v. 20, p. 353–431. doi:10.1016/S1367-9120(01)00069-4

Hall, R., 2012, Late Jurassic–Cenozoic reconstructions of the Indonesian region and the Indian Ocean: Tectonophysics, v. 570-571, p. 1–41. doi:10.1016/j.tecto.2012.04.021

Hall, R., Ali, J.R., Anderson, C.D., and Baker, S.J., 1995, Origin and motion history of the Philippine sea plate.: Tectonophysics, v. 251, p. 229–250. doi:10.1016/0040-1951(95)00038-0

Hall, R., Nichols, G., Ballantyne, P., Charlton, T., and Ali, J., 1991, The character and significance of basement rocks of the southern Molucca Sea region: Journal of Southeast Asian Earth Sciences, v. 6, p. 249–258. doi:10.1016/0743-9547(91)90071-5

Hall, R., and Spakman, W., 2015, Mantle structure and tectonic history of SE Asia: Tectonophysics, v. 658, p. 14–45. doi:10.1016/j.tecto.2015.07.003

Hannah, R.S., Vogel, T.A., Patino, L.C., Alvarado, G.E., Perez, W., and Smith, D.R., 2002, Origin of silicic volcanic rocks in central Costa Rica: A study of a chemically variable ash-flow sheet in the Tiribi Tuff: Bulletin of Volcanology, v. 64, p. 117–133. doi:10.1007/s00445-001-0188-8

Haston, R.B., and Fuller, M., 1991, Paleomagnetic data from the Philippine sea plate and their tectonic significance: Journal of Geophysical Research, v. 96, p. 6073–6098. doi:10.1029/90JB02700

Heider, F., Ko¨Rner, U., and Bitschene, P., 1993, Volcanic ash particles as carriers of remanent magnetization in deep-sea sediments from the Kerguelen Plateau: Earth and Planetary Science Letters, v. 118, p. 121–134. doi:10.1016/0012-821X(93)90163-4

Hickey-Vargas, R., 2005, Basalt and tonalite from the Amami Plateau, northern West Philippine Basin: New early cretaceous ages and geochemical results, and their petrologic and tectonic implications.: Island Arc, v. 14, p. 653–665. doi:10.1111/j.1440-1738.2005.00474.x

Hilde, T.W.C., and Lee, C.-S., 1984, Origin and evolution of the West Philippine Basin: A new interpretation: Tectonophysics, v. 102, p. 85–104. doi:10.1016/0040-1951(84)90009-X

Hilde, T.W.C., Uyeda, S., and Kroenke, L., 1977, Evolution of the western Pacific and its margin: Tectonophysics, v. 38, p. 145–165. doi:10.1016/0040-1951(77)90205-0

Hirano, N., Ogawa, Y., Saito, K., and Taniguichi, H., 2003, Multistage evolution of the Tertiary Mineoka ophiolite, Japan: New geochemical and age constraints, *in* Dilek, Y., and Robinson, P.T., eds., Ophiolites in Earth History: Geological Society of London Special Publications, v. 218, p. 279–298.

Hiscott, R.N., Colella, A., Pezard, P., Lovell, M.A., and Malinverno, A., 1992, Sedimentology of deep-water volcaniclastics, Oligocene Izu-Bonin forearc basin, based on formation micro scanner images, *in* Taylor, B., Fujioka, K., et al.,

eds, Proceedings ODP, scientific results, leg 126: College Station, TX, Ocean Drilling Program, p. 75–96.

Hochstaedter, A., Gill, J., Peters, R., Broughton, P., Holden, P., and Taylor, B., 2001, Across-arc geochemical trends in the Izu-Bonin arc: Contributions from the Subducting Slab, Geochemistry, Geophysics, Geosystems, v. 2, no. 7. doi:10.1029/2000GC000105.

Hochstaedter, A.G., Gill, J.B., Kusakabe, M., Newman, S., Pringle, M., Taylor, B., and Fryer, P., 1990, Volcanism in the Sumisu Rift, I. Major element, volatile, and stable isotope geochemistry: Earth and Planetary Science Letters, v. 100, no. 1–3, p. 179–194. doi:10.1016/0012-821X(90)90184-Y

Hoshi, H., and Sano, M., 2013, Paleomagnetic constraints on Miocene rotation in the central Japan Arc: Island Arc, v. 22, p. 197–213. doi:10.1111/iar.12022

Huang, T.C., 1980, A volcanic sedimentation model: Implications of processes and responses of deep-sea ashes: Marine Geology, v. 38, p. 103–122. doi:10.1016/0025-3227(80)90054-7

Huang, T.C., Watkins, N.D., Shaw, D.M., and Kennett, J.P., 1973, Atmospherically transported volcanic dust in South Pacific deep sea sedimentary cores at distances over 3000 km from the eruptive source: Earth and Planetary Science Letters, v. 20, p. 119–124. doi:10.1016/0012-821X(73)90148-9

Hussong, D.M., and Uyeda, S., 1981, Tectonic processes and the history of the Mariana arc: A synthesis of the results of deep sea drilling project leg 60, *in* Hussong, D.M., Uyeda, S., et al., eds., Initial reports of the deep sea drilling project, Volume. 60: Washington, D.C., U.S. Government Printing Office, p. 909–929.

Ishii, T., 1985, Dredged samples from the Ogasawara fore-arc seamount or "Ogasawara paleoland"—"Forearc ophiolite", *in* Nasu, N., Kushiro, I., et al., eds., Formation of active ocean margins: Terra, Adv. Earth Planetary Science, p. 307–342.

Ishizuka, O., Kimura, J.-I., Li, Y.B., Stern, R.J., Reagan, M.K., Taylor, R.N., Ohara, Y., Bloomer, S.H., Ishii, T., Hargrove, U. S., III, and Haraguchi, S., 2006, Early stages in the evolution of Izu–Bonin arc volcanism: New age, chemical, and isotopic constraints: Earth and Planetary Science Letters, v. 250, p. 385–401. doi:10.1016/j.epsl.2006.08.007

Ishizuka, O., Tani, K., Harigane, Y., Umino, S., Stern, R.J., Reagan, M.K., Hickey-Vargas, R., Yogodzinski, G.M., Kusano, Y., and Arculus, R.J., 2016, Tectonics of the Philippine Sea Plate before and after ~52 Ma subduction initiation to form the Izu-Bonin-Mariana arc: American Geophysical Union, Fall General Assembly 2016, abstract #V11E-02.

Ishizuka, O., Tani, K., Reagan, M.K., Kanayama, K., Umino, S., Harigane, Y., Sakamoto, I., Miyajima, Y., Yuasa, M., and Dunkley, D.J., 2011a, The timescales of subduction initiation and subsequent evolution of an oceanic island arc: Earth and Planetary Science Letters, v. 306, p. 229–240. doi:10.1016/j.epsl.2011.04.006

Ishizuka, O., Taylor, R.N., Ohara, Y., and Yuasa, M., 2013, Upwelling, rifting, and age-progressive magmatism from the Oki-Daito mantle plume: Geology, v. 41, p. 1011–1014. doi:10.1130/G34525.1

Ishizuka, O., Taylor, R.N., Yuasa, M., and Ohara, Y., 2011b, Making and breaking an island arc: A new perspective from the Oligocene Kyushu-Palau arc, Philippine Sea: Geochemistry, Geophysics, Geosystems, v. 12, p. Q05005. doi:10.1029/2010GC003440

Ishizuka, O., Uto, K., Yuasa, M., and Hochstaedter, A., 1998, K-Ar ages from the seamount chains in the back- arc region of the Izu-Ogasawara arc: Island Arc, v. 7, p. 408–421. doi:10.1111/j.1440-1738.1998.00199.x

Ishizuka, O., Uto, K., and Yuasa, M., 2003, Volcanic history of the back-arc region of the Izu-Bonin (Ogasawara) arc, *in* Larter, R.D., and Leat, P.H., eds., Intra-oceanic subduction systems: Tectonic and magmatic processes, Vol. 219, Geological Sociey, London, Special Publications, p. 187–205.

Johnson, K., Waldman, R., and Marsaglia, K.M., 2017, Data report: Sedimentary columns with facies and bedding for Units II–IV at IODP Site U1438, in Arculus, R.J., Ishizuka, O., Bogus, K., and the Expedition 351 Scientists, Izu-Bonin-Mariana Arc Origins, eds., Proceedings of the International Ocean Discovery Program, 351: College Station, TX (International Ocean Discovery Program). https://doi.org/10.14379/iodp.proc.351.201.2017

Kaiho, Y., No, T., Yamashita, M., Takizawa, K., Takahashi, N., Kodaira, S., and Kaneda, Y., 2007, MCS seismic profiling of an oceanic island arc in the southern Izu-Ogasawara arc-backarc area – KR0607 cruise: JAMSTEC Report of Research and Development, v. 5, p. 51–60.

Kawate, S., and Arima, S., 1998, Petrogenesis of the Tanzawa plutonic complex, central Japan: Exposed felsic middle crust of the Izu-Bonin- Mariana arc: Island Arc, v. 7, p. 342–358. doi:10.1111/iar.1998.7.issue-3

Keenan, T.E., and Encarnacíon, J., 2016, Unclear causes for subduction: Comment: Nature Geoscience, v. 9, p. 338–339. doi:10.1038/ngeo2703

Kennett, J.P., and Thunell, R.C., 1975, Global increase in Quaternary explosive volcanism: Science, v. 187, p. 497–502. doi:10.1126/science.187.4176.497

Kimura, J.I., Nagahashi, Y., Satoguchi, Y., and Chang, Q., 2015, Origins of felsic magmas in Japanese subduction zone: Geochemical characterizations of tephra from caldera-forming eruptions< 5 Ma: Geochemistry, Geophysics, Geosystems, v. 16, no. 7, p. 2147–2174.

Kodeira, S., Noguchi, N., Takahashi, N., Ishizuka, O., and Kaneda, Y., 2010, Evolution from fore-arc oceanic crust to island arc crust: A seismic study along the Izu-Bonin fore-arc: Journal of Geophysical Research, v. 115, p. B09102.

Koyama, M., and Kitazato, H., 1988, Paleomagnetic evidence for Pleistocene clockwise rotation in the Oiso Hills: A possible record of interaction between the Philippine Sea Plate and Northeast Japan: Rock Magnetism and Paleogeophysics, v. 15, p. 35–38.

Kuritani, T., Yokoyama, T., Kobayashi, K., and Nakamura, E., 2003, Shift and rotation of composition trends by magma mixing: 1983 eruption at Miyake-jima Volcano, Japan: Journal of Petrology, v. 44, no. 10, p. 1895–1916. doi:10.1093/petrology/egg063

Kurz, W., Ferre, E.C., Robertson, A., Avery, A., Christeson, G.L.S., Morgan, S., Kutterolf, S., Sager, W., Carvallo, C., and Shervais, J., Expedition 352 Scientists, 2015, Post-magmatic tectonic deformation of the outer Izu-Bonin-Mariana fore-arc system: Initial results of IODP Expedition 352: Vienna, Austria, European Geophysical Union General Assembly, Abstract.

Kutterolf, S., Jegen, M., Mitrovica, J.X., Kwasnitschka, T., Freundt, A., and Huybers, P., 2013, A detection of

Milankovitch frequencies in global volcanic activity: Geology, v. 41/2, p. 227–230. doi:10.1130/G33419.1

Kutterolf, S., Schindlbeck, J.C., Robertson, A.H.F., Avery, A., Baxter, A.T., Petronotis, K., and Wang, K.-L., 2017, Submitted to G-Cubed, Tephrostratigraphy and provenance from IODP Expedition 352, Izu-Bonin arc: Tracing tephra sources and volumes from the Oligocene to the Recent. Geochemistry, Geophysics, Geosystems.

Kutterolf, S., Schindlbeck, J.C., Robertson, A.H.F., Avery, A., Baxter, A.T., and Wang, K.-L. 2016, Tephrachronostratigraphy and provenance from IODP expedition 352, Izu-Bonin arc: variable tephra sources from the Oligocene to the Holocene, Goldschmidt Conference, Yokohama, Japan, Abstract.

Kutterolf, S., Schindlbeck, J.C., Scudder, R.P., Murray, R.W., Pickering, K.T., Freundt, A., Labanieh, S., Heydolph, K., Saito, S., Naruse, H., Underwood, M.B., and Wu, H., 2014, Large volume submarine ignimbrites in the Shikoku Basin: An example for explosive volcanism in the Western Pacific during the Late Miocene: Geochemistry, Geophysics, Geosystems, v. 15, p. 1837–1851. doi:10.1002/2014GC005263

Lallemand, S., 2016, Philippine sea plate inception, evolution, and consumption with special emphasis on the early stages of izu-bonin-mariana subduction: progress in earth and planetary science, v. 3, no. 15. doi: 10.1186/s40645-016-0085-6

Lee, J., Stern, R.J., and Bloomer, S.H., 1995, Forty million years of magmatic evolution in the Mariana arc: The tephra glass record: Journal of Geophysical Research, v. 100, no. B9, p. 17671–17687. doi:10.1029/95JB01685

Leng, W., and Gurnis, M., 2015, Subduction initiation at relic arcs: Geochemistry, Geophysics, Geosystems, v. 12, p. Q12018.

Liang, M., Gua, Z., Kahmann, A.J., and Oldfield, F., 2009, Geochemical characteristics of the Miocene eolian deposits in China: Their provenance and climate implications: Geochemistry, Geophysics, Geosystems, v. 10. doi:10.1029/2008GC002331.

Lin, P.-N., 1992, Trace element and isotopic characteristics of western Pacific pelagic sediments: Implications for the petrogenesis of Mariana Arc magmas: Geochimica Et Cosmochimica Acta, v. 56, p. 1641–1654. doi:10.1016/0016-7037(92)90231-7

Lowe, D.R., 1982, Sediment gravity flows: II. Depositional models with special reference to the deposits of high-density turbidity currents: Journal of Sedimentary Petrology, v. 52, p. 279–297.

Lyle, M., 2003, Neogene carbonate burial in the Pacific Ocean: Paleoceanography, v. 18, p. 1059. doi:10.1029/2002PA000777

Lyle, M., Dadey, K.A., and Farrell, J.W., 1995, The late Miocene (11–8 Ma) eastern Pacific carbonate crash: Evidence for reorganization of deep-water circulation by the closure of the Panama Gateway, *in* Pisias, N.G., Mayer, L.A., Janecek, T. R., Palmer-Julson, A., and Van Andel, T.H., eds, Proceedings of the Ocean Drilling Program, Scientific Results, Volume 138: College Station, TX, Ocean Drilling Program.

Machida, H., and Arai, F., 1983, Extensive ash falls in and around the Sea of Japan from large late Quaternary eruptions: Journal of Volcanology and Geothermal Research, v. 18, p. 151–164. doi:10.1016/0377-0273(83)90007-0

Mahony, S.H., Wallace, L.M., Miyoshi, M., Villamor, P., Sparks, R. S.J., and Hasenaka, T., 2011, Volcano-tectonic interactions during rapid plate-boundary evolution in the Kyushu region, SW Japan: Japanese Geological Society American Bulletin, v. 123, p. 2201–2223. doi:10.1130/B30408.1

Marsaglia, K.M., Barth, A.P., Brandl, P.A., Hickey-Vargas, R., Jiang, F., Kanayama, K., Kusano, Y., Li, H., McCarthy, A., Meffre, S., Savov, I.P., Tepley, F.J.I., and Yogodzinski, G.M. 2014, The sedimentary record of an intraoceanic magmatic arc, from inception through maturation to abandonment: IODP expedition 351, American Geophysical Union Meeting, San Francisco, California, Abstract T53A-4641.

Matsuda, T., 1978, Collision of the Izu-Bonin arc with central Honshu: Cenozoic tectonics of the Fossa Magna Japan: Journal of Physical Earth, v. 26, p. S409–S422. doi:10.4294/jpe1952.26.Supplement_S409

McLennan, S.M., Hemming, S., McDaniel, D.K., and Hanson, G. N., 1993, Geochemical approchaes to sedimentation, provenance, and tectonics, *in* Johnson, M.J., and Basu, A., eds, Processes Contolling the Composition of Clastic Sediments, Geological Society of America Special Paper, Volume . 284, p. 21–40.

Minai, Y., Matsumoto, R., and Tominaga, T., 1986, Geochemistry of deep sea sediments from the Nankai Trough, the Japan Trench and adjacent regions, *in* Kagami, H., Karig, D., Coulbourn, W.T., et al., eds., Initial reports of the deep sea drilling project, Volume 87: Washington D.C., U.S. Government Printing Office, p. 643–657.

Mori, R., and Ogawa, Y., 2005, Transpressional tectonics of the Mineoka Ophiolite Belt in a trench–trench–trench-type triple junction, Boso Peninsula: Island Arc, v. 14, p. 571–581. doi:10.1111/j.1440-1738.2005.00485.x

Mori, R., Ogawa, Y., Hirano, N., Tsunogae, T., Kurosawa, M., and Chiba, T., 2011, Role of plutonic and metamorphic block exhumation in a forearc ophiolite mélange belt: An example from the Mineoka belt, Japan, *in* Wakabayashi, J., and Dilek, Y., eds, Mélanges: Processes of formation and societal significance, Geological Society of America Special Paper, Volume Vol. 480, p. 95–115.

Mulder, T., and Alexander, J., 2001, The physical character of subaqueous sedimentary density flows and their deposits: Sedimentology, v. 48, p. 269–299. doi:10.1046/j.1365-3091.2001.00360.x

Najman, Y., Appel, E., Boudagher-Fadel, M., Bown, P., Carter, A., Garzanti, E., Godin, L., Han, J., Liebke, U., Oliver, G., Parrish, R., and Vezzoli, G., 2010, Timing of India-Asia collision: Geological, biostratigraphic, and palaeomagnetic constraints: Journal of Geophysical Research, v. 115, p. B12416. doi:10.1029/2010JB007673

Nathan, S.A., and Leckie, R.M., 2009, Early history of the Western Pacific warm pool during the middle to late Miocene (~13.2-5.8 Ma): Role of sea-level change and implications for equatorial circulation: Palaeogeography, Palaeoclimatology, Palaeoecology, v. 274, p. 140–159. doi:10.1016/j.palaeo.2009.01.007

Natland, J.H., and Tarney, J., 1982, Petrologic evolution of the Mariana arc and back-arc basin system—A synthesis of drilling results in the South Philippine Sea, *in* Hussong, D. M., Uyeda, S., et al., eds., Initial reports of the deep sea drilling project, Volume 60: Washington D.C., U.S. Government. Printing Office, p. 877–908.

Nesbitt, H.W., and Young, G.M., 1982, Early Proterozoic climates and plate motions inferred from major element chemistry of lutites: Nature, p. 715–717. doi:10.1038/299715a0.

Ohara, Y., Kato, Y., Yoshida, T., and Nishimura, A., 2015, Geoscientific characteristics of the seafloor of the southern ocean of Japan revealed by Japan's continental shelf survey: Journal of Geography (Chigaku Zasshi), v. 124, pp. 687–709. (In Japanese with English abstract.

Ogawa, Y., Horiuchi, K., Taniguchi, H., and Kaka, J., 1985, Collision of the izu arc with honshu and the effects of oblique subduction the miura-boso peninsulas: tectonophysics, v. 119, p. 349–379. doi:10.1016/0040-1951(85)90046-0

Ogawa, Y., and Sashida, K., 2005, Lower Cretaceous radiolarian bedded chert from the Mineoka Belt, Boso Peninsula, Japan: The Journal of the Geological Society of Japan, v. 111, p. 624–627. doi:10.5575/geosoc.111.624

Ogawa, Y., and Takahashi, A., 2004, Seafloor spreading, obduction and triple junction tectonics of the Mineoka ophiolite, Central Japan: Tectonophysics, v. 392, p. 131–141. doi:10.1016/j.tecto.2004.08.007

Ogawa, Y., Takami, Y., and Takazawa, S., 2008, Oblique subduction in island arc collision setting: Unique sedimentation, accretion and deformation processes in the Boso TTT-type triple junction area, NW Pacific, *in* Draut, A.E., Clift, P. D., and Scholl, W.D., eds, Formation and Applications of the Sedimentary Record in Arc Collision Zones: Geological Society of America Special Paper, Volume. 436, p. 155–170.

Ogawa, Y., and Taniguchi, H., 1989, Origin and emplacement of basaltic rocks in the accretionary complexes in SW Japan: Ofioliti, v. 14, p. 177–193.

Pälike, H., Lyle, M.W., Nishi, H., Raffi, I., Ridgwell, A., Gamage, K., Klaus, A., Acton, G., Anderson, L., Backman, J., Baldauf, J., Beltran, C., Bohaty, S.M., Bown, P., Busch, W., Channell, J.E.T., Chun, C.O.J., Delaney, M., Dewangan, P., Dunkley Jones, T., Edgar, K.M., Evans, H., Fitch, P., Foster, G.L., Gussone, N., Hasegawa, H., Hathorne, E.C., Hayashi, H., Herrle, J.O., Holbourn, A., Hovan, S., Hyeong, K., Iijima, K., Ito, T., Kamikuri, S.-I., Kimoto, K., Kuroda, J., Leon-Rodriguez, L., Malinverno, A., Moore, T.C., Jr, Murphy, B.H., Murphy, D.P., Nakamura, H., Ogane, K., Ohneiser, C., Richter, C., Robinson, R., Rohling, E.J., Romero, O., Sawada, K., Scher, H., Schneider, L., Sluijs, A., Takata, H., Tian, J., Tsujimoto, A., Wade, B.S., Westerhold, T., Wilkens, R., Williams, T., Wilson, P.A., Yamamoto, Y., Yamamoto, S., Yamazaki, T., and Zeebe, R.E., 2012, A Cenozoic record of the equatorial Pacific carbonate compensation depth: Nature, v. 488, p. 609–614. doi:10.1038/nature11360

Pearce, J., and Robinson, P.T., 2010, The Troodos ophiolitic complex probably formed in a subduction initiation, slab edge setting: Gondwana Research, v. 18, p. 60–81. doi:10.1016/j.gr.2009.12.003

Pearce, J., Van Der Laan, S.R., Arculus, R.J., Murton, B.J., Ishii, T., Peate, D.W., and Parkinson, I.J., 1992, Boninite and Harzburgite from Leg 125 (Bonin-Mariana Forearc): A case study of magma genesis during the initial stages of subduction, *in* Fryer, P., Pearce, J., Stokking, L.B., et al., eds., Proceedings ODP, scientific results, Volume 125: College Station, Texas, Ocean Drilling Program, p. 623–659.

Peters, J.L., Murray, R.W., Sparks, J., and Coleman, D.S., 2000, Terrigenous matter and dispersed ash in sediment from the Caribbean Sea: Results from Leg 165: Proceedings, Ocean Drilling Program Scientific Results, v. 165, p. 115–124.

Petronotis, K.E., Acton, G.D., Jovane, L., Li, Y., and Zhao, X., 2015, Data report: Magnetic properties of sediments and basalts from the Costa Rica subduction margin (Expeditions 334 and 344), *in* Harris, R.N., Sakaguchi, A., Petronotis, K.E., et al., eds., Proceedings IODP, Volume Initial reports of the Deep Sea Drilling Project: College Station, TX, Integrated Ocean Drilling Program.

Pickering, K.T., and Hiscott, R.N., 2016, Deep marine environments-clastic sedimentation and Tectonics: London, Unwin Hyman.

Pickering, K.T., Stow, D.A.V., Watson, M., and Hiscott, R.N., 1986, Deep-water facies, processes, and models: A review and classification scheme for modern and ancient sediments: Earth-Science Reviews, v. 23, p. 75–174. doi:10.1016/0012-8252(86)90001-2

Pickering, K.T., Underwood, M.B., Saito, S., Naruse, H., Kutterolf, S., Scudder, R.P., Park, J.-O., Moore, G., and Slagle, A., 2013, Depositional architecture, provenance and tectonic/eustatic modulation of Miocene submarine fans in the Shikoku Basin: Results from Nankai seismogenic zone experiment: Geochemistry, Geophysics, Geosystems, v. 14, p. 1722–1739. doi:10.1002/ggge.20107

Pike, C.R., Roberts, A.P., and Verosub, K.L., 1999, Characterizing interactions in fine magnetic particle systems using first order reversal curves: Journal of Applied Physics, v. 85, p. 6660–6667. doi:10.1063/1.370176

Plank, T., 2005, Constraints from Thorium/Lanthanum on sediment recycling at subduction zones and the evolution of the continents: Journal of Petrology, v. 46, p. 921–944. doi:10.1093/petrology/egi005

Plank, T., Kelley, K.A., Murray, R.W., and Stern, L.Q., 2007, Chemical composition of sediments subducting at the Izu–Bonin trench: Geochemistry, Geophysics, Geosystems, v. 8, p. Q04I16. doi:10.1029/2006GC001444

Prueher, L.M., and Rea, D.K., 2001, tephrachronology of the kamchatka-kurile and aleutian arcs: evidence for volcanic episodicity: journal volcanology and geothermal research, v. 106, p. 67–84.

Reagan, M.K., Hanan, B.B., Heizler, M.T., Hartman, B.S., and Hickey-Vargas, R., 2008, Petrogenesis of volcanic rocks from Saipan and Rota, Mariana Islands, and implications for the evolution of nascent island arcs: Journal of Petrology, v. 49, p. 441–464. doi:10.1093/petrology/egm087

Reagan, M.K., Ishizuka, O., Stern, R.J., Kelley, K.A., Ohara, Y., Blichert-Toft, J., Bloomer, S.H., Cash, J., Fryer, P., and Hanan, B.B., 2010, Fore-arc basalts and subduction initiation in the Izu-Bonin-Mariana system: Geochemistry: Geophysics, Geosystems, v. 11, p. Q03X12.

Reagan, M.K., McClelland, W.C., Girard, G., Goff, K.R., Peate, D. W., Ohara, Y., and Stern, R.J., 2013, The geology of the southern Mariana fore-arc crust: Implications for the scale of Eocene volcanism in the western Pacific: Earth and Planetary Science Letters, v. 380, p. 41–51. doi:10.1016/j.epsl.2013.08.013

Reagan, M.K., Pearce, J.A., Petronotis, K., Almeev, R.R., Avery, A. J., Carvallo, C., Chapman, T., Christeson, G.L., Ferré, E.C., Godard, M., Heaton, D.E., Kirchenbaur, M., Kurz, W., Kutterolf, S., Li, H., Li, Y., Michibayashi, K., Morgan, S., Nelson, W.R., Prytulak, J., Python, M., Robertson, A.H.F., Ryan, J.G., Sager, W.W., Sakuyama, T., Shervais, J.W.,

Shimizu, K., and Whattam, S.A., 2017, Subduction initiation and Ophiolite Crust: New insights from IODP drilling: International Geology Review, v. 59, P. 1439–1450. doi:10.1080/00206814.2016.1276482.

Reagan, M.K., Pearce, J.A., Petronotis, K., and Scientists, E. 2015, Izu-Bonin-Mariana Fore Arc., Proceedings of the International Ocean Discovery Program, 352: College Station, TX (International Ocean Discovery Program)., 10.14379/iodp.proc.14352.12015.

Richter, C., and Ali, J.R., 2015, Philippine sea plate motion history: Eocene-Recent record from ODP Site 1201, central West Philippine basin: Earth and Planetary Science Letters, v. 410, p. 165–173. doi:10.1016/j.epsl.2014.11.032

Roberts, A.P., Chang, L., Heslop, D., Florindo, F., and Larrasoana, J.C., 2012, Searching for single domain magnetite in the "pseudo-single-domain" sedimentary haystack: Implications of biogenic magnetite preservation for sediment magnetism and relative paleointensity determinations: Journal of Geophysical Research, v. 117, p. B08104. doi:10.1029/2012JB009412

Roberts, A.P., Pike, C.R., and Verosub, K.L., 2000, First-order reversal curve diagrams: A new tool for characterizing the magnetic properties of natural samples: Journal of Geophysical Research, v. 105, p. 28461–28475. doi:10.1029/2000JB900326

Robertson, A.H.F., 1975, Cyprus umbers: Basalt-sediment relationships on a Mesozoic ocean ridge: Journal of Geological Society, London, v. 131, p. 511–531. doi:10.1144/gsjgs.131.5.0511

Robertson, A.H.F., 1977, Tertiary uplift history of the Troodos massif, Cyprus: Geological Society of America Bulletin, v. 88, p. 1763–1772. doi:10.1130/0016-7606(1977)88<1763:TUHOTT>2.0.CO;2

Robertson, A.H.F., and Hudson, J.D., 1973, Cyprus umbers: Chemical precipitates on a tethyan ocean ridge: Earth and Planetary Science Letters, v. 18, p. 93–101. doi: 10.1016/0012-821X(73)90039-3.

Robertson, A.H.F., Kutterolf, S., Petronotis, K., Avery, A., Baxter, A.T., Schindlbeck, J.C., Wang, K.-L., and Acton, G.D. 2016, Geological development of the Izu-Bonin forearc since the eocene based on biostratigraphic, rock magnetic, and sediment provenance observations from IODP expedition 352 drill cores, American Geophysical Union Meeting, San Francisco, California, Abstract V13C-2860.

Rollinson, H., 1993, Using geochemical data: Evaluation, presentation, interpretation: Burnt Mill, Harlow, Essex, Longman Group, Geochemistry series, 352.

Sager, W.W., Clark, R.W., and Carvallo, C., 2017, Data report: Paleomagnetic direction measurements on Expedition 352 igneous core samples. In Reagan, M.K., Pearce, J.A., Petronotis, K.E., and the Expedition 352 Scientists, Izu-Bonin-Mariana Fore Arc, eds., Proceedings of the International Ocean Discovery Program, 352: College Station, TX (International Ocean Discovery Program). http://dx.doi.org/ 10.14379/ iodp.proc.352.202.2017

Sasaki, T., Yamazaki, T., and Ishizuka, O., 2014, A revised spreading model of the West Philippine basin: Earth, Planets and Space, v. 66, p. 83. doi:10.1186/1880-5981-66-83

Savov, I.P., Hickey-Vargas, R.M.D.A., Ryan, J.G., and Spadea, P., 2006, Petrology and geochemistry of West Philippine Basin basalts and early Palau–Kyushu arc volcanic clasts from ODP Leg 195, Site 1201D: Implications for the early history of the Izu–Bonin–Mariana arc: Journal of Petrology, v. 47, p. 277–299. doi:10.1093/petrology/egi075

Sayles, F.L., and Bischoff, J.L., 1973, Ferromanganoan sediments in the equatorial East Pacific: Earth and Planetary Science Letters, v. 19, p. 330–336. doi:10.1016/0012-821X(73)90083-6

Schindlbeck, J.C., Kutterolf, S., Freundt, A., Scudder, R.P., Pickering, K.T., and Murray, R.W., 2013, Emplacement processes of submarine volcaniclastic deposits (IODP Site C0011 Nankai Trough): Marine Geology, v. 343, p. 115–124. doi:10.1016/j.margeo.2013.06.017

Schindlbeck, J.C., Kutterolf, S., Straub, S., Andrews, G., and Wang, K.-L., 2017, Provenance of the 1 Ma - Recent Tephra Record at IODP Sites U1436 and U1437: Insights into explosive volcanism from the Japan and Izu arcs. The Island Arc. doi:10.1111/iar.12244

Scudder, R.P., Murray, R.W., and Plank, T., 2009, Dispersed ash in deeply buried sediment from the northwest Pacific Ocean: An example from the Izu–Bonin arc (ODP Site 1149): Earth and Planetary Science Letters, v. 284, p. 639–648. doi:10.1016/j.epsl.2009.05.037

Scudder, R.P., Murray, R.W., Schindlbeck, J.C., Kutterolf, S., Hauff, F., and McKinley, C.C., 2014, Regional-scale input of dispersed and discrete volcanic ash to the Izu-Bonin and Mariana subduction zones: Geochemistry, Geophysics, Geosystems, v. 15, p. 4369–4379. doi:10.1002/2014GC005561

Scudder, R.P., Murray, R.W., Schindlbeck, J.C., Kutterolf, S., Hauff, F., Underwood, M.B., Gwizd, S., Lauzon, R., and McKinley, C.C., 2016, Geochemical approaches to the quantification of dispersed volcanic ash in marine sediment: Progress in Earth and Planetary Science, v. 3, p. 1–32. doi:10.1186/s40645-015-0077-y

Sdrolias, M., Roest, W.R., and Müller, R.D., 2004, An expression of Philippine Sea plate rotation: The Parece Vela and Shikoku Basins: Tectonophysics, v. 394, p. 69–86. doi:10.1016/j.tecto.2004.07.061

Seno, T., and Maruyama, S., 1984, Paleogeographic reconstruction and origin of the Philippine sea: Tectonophysics, v. 102, p. 53–84. doi:10.1016/0040-1951(84)90008-8

Shih, T.-C., 1980, Marine magnetic anomalies from the West Philippine Sea: Implications for the evolution of marginal basins, *in* Hayes, D.E., ed., The tectonic and geologic evolution of Southeast Asian Seas and Islands, Volume 23: Washington, DC, AGU Geophyical Monograph, p. 49–76.

Sibuet, J.C., Letouzey, J., Barbier, F., Charvet, J., Foucher, J.P., and Hilde, T.W., 1987, Back arc extension in the Okinawa Trough: Journal of Geophysical Research, v. 92, p. B14041–14063. doi:10.1029/JB092iB13p14041

Sigurdsson, H., Sparks, R.S.J., Carey, S.N., and Huang, T.C., 1980, Volcanogenic sedimentation in the lesser antilles arc: Journal of Geology, v. 88, p. 523. doi:10.1086/628542

Soh, W., Nakayama, K., and Kimura, T., 1998, Arc-arc collision in the Izu collision zone, central Japan, deduced from the Ashigara Basin and adjacent Tanzawa Mountains: Island Arc, v. 7, p. 330–341. doi:10.1111/j.1440-1738.1998.00193.x

Stern, R.J., 2004, Subduction initiation: Spontaneous and induced: Earth and Planetary Science Letters, v. 226, p. 275–292. doi:10.1016/S0012-821X(04)00498-4

Stern, R.J., and Bloomer, S.H., 1992, Subduction zone infancy: Examples from the Eocene Izu-Bonin-Mariana and Jurassic California arcs: Geological Society of America Bulletin, v.

104, p. 1621–1636. doi:10.1130/0016-7606(1992)104<1621:SZIEFT>2.3.CO;2

Straub, S.M., 1997, Multiple sources of Quaternary tephra layers in the Mariana Trough: Journal of Volcanology and Geothermal Research, v. 76, p. 251–276. doi:10.1016/S0377-0273(96)00075-3

Straub, S.M., 2003, The evolution of the Izu Bonin - Mariana volcanic arcs (NW Pacific) in terms of major element chemistry: Geochemistry, Geophysics, Geosystems, v. 4, p. 1018. doi:10.1029/2002GC000357

Straub, S.M., and Schmincke, H.U., 1998, Evaluating the tephra input into Pacific Ocean sediments: Distribution in space and time: Geologische Rundschau, v. 87, p. 461–476. doi:10.1007/s005310050222

Straub, S.M., Woodhead, J.D., and Arculus, R.J., 2015, Temporal evolution of the Mariana arc: Mantle Wedge and subducted slab controls revealed with a tephra perspective: Journal of Petrology, v. 56, p. 409–439. doi:10.1093/petrology/egv005

Taira, A., 2001, Tectonic evolution of the Japanese island arc system: Annual Review of Earth and Planetary Sciences, v. 29, p. 109–134. doi:10.1146/annurev.earth.29.1.109

Taira, A., Okada, H., Whitaker, J.H.M., and Smith, A.J., 1982, The Shimanto Belt of Japan: Cretaceous–lower Miocene active-margin sedimentation, *in* Leggett, J.K., ed., Trench-forearc geology, Geological society of London Special Publication, v. 10, p. 5–26.

Taira, A., Tokoyma, H., and Soh, W., 1989, Accretion tectonics and evolution of Japan, *in* The Evolution of the Pacific Ocean margins: Oxford University Press, p. 100–123.

Takahashi, M., and Saito, K., 1997, Miocene intra-arc bending at an arc-arc collision zone, central Japan: Island Arc, v. 6, p. 168–182. doi:10.1111/j.1440-1738.1997.tb00168.x

Takahashi, M., and Saito, K., 1999, Miocene intra-arc bending at an arc-arc collision zone, central Japan: Reply: Island Arc, v. 8, p. 114–123. doi:10.1046/j.1440-1738.1999.t01-1-00227.x

Takahashi, N., Kodeira, Y., Tatsumi, Y., Yamashita, M., Sato, T., Kaiho, Y., Miura, S., No, T., Takizawa, K., and Kaneda, Y., 2009, Structural variations of arc crusts and rifted margins in the southern Izu-Ogasawara arc–back arc system: Geochemistry, Geophysics, Geosystems, v. 10, p. Q09X08. doi:10.1029/2008GC002146

Tamura, Y., Barker, A., Busby, C., Berger, J., Blum, P., Bongiolo, E., Guèrin, G., Bordiga, M., Andrews, G., and DeBari, S. 2014, Izu-Bonin-Mariana Rear Arc-The missing half of the subduction factory: IODP Preliminary Report 350.

Tamura, Y., Busby, C.J., and Blum, P., and the Expedition 350 Scientists, 2015. *Proceedings of the International Ocean Discovery Program, Expedition 350: Izu-Bonin-Mariana Rear Arc*: College Station, TX (International Ocean Discovery Program). http://dx.doi.org/10.14379/iodp.proc.350.2015

Tamura, Y., Gill, J., Tollstrup, D., Kawabata, H., Shukuno, H., Chang, Q., Miyazaki, T., Takahashi, T., Hirahara, Y., Kodaira, S., Ishizuka, O., Suzuki, T., Kido, Y., Fiske, R.S., and Tatsumi, Y., 2009, Silicic Magmas in the Izu-Bonin oceanic arc and implications for crustal evolution: Journal of Petrology, v. 50, p. 685–723. doi:10.1093/petrology/egp017

Tamura, Y., Tani, K., Chang, Q., Shukuno, H., Kawabata, H., Ishizuka, O., and Fiske, R., 2007, Wet and dry basalt magma evolution at Torishima Volcano, Izu–Bonin Arc, Japan: The possible role of phengite in the downgoing Slab: Journal of Petrology, v. 48, no. 10, p. 1999–2031. doi:10.1093/petrology/egm048

Tamura, Y., Tani, K., Ishizuka, O., Chang, Q., Shukuno, H., and Fiske, R., 2005, Are arc basalts dry, wet, or both? Evidence from the Sumisu caldera volcano, Izu–Bonin arc, Japan: Journal of Petrology, v. 46, no. 9, p. 1769–1803. doi:10.1093/petrology/egi033

Taylor, B., Fujioka, K., et al., 1992, Proc. ODP, Sci. Results, 126: College Station, TX, Ocean Drilling Program. doi:10.2973/odp.proc.sr.126.1992.

Taylor, B., and Goodliffe, A.M., 2004, The West Philippine Basin and the initiation of subduction, revisited: Geophysical Research Letters, v. 31, p. L12602. doi:10.1029/2004GL020136

Taylor, B., Huchon, P., Klaus, A., et al., 1999, Proceedings of the Ocean Drilling Program, Scientific Results, v. 180: College Station Texas, Ocean Drilling Program.

Taylor, R.N., and Nesbitt, R.W., 1998, Isotopic characteristics of subduction fluids in an intra-oceanic setting, Izu–Bonin Arc, Japan: Earth and Planetary Science Letters, v. 164, no. 1, p. 79–98. doi:10.1016/S0012-821X(98)00182-4

Taylor, S.R., and Mc Lennan, S.M., 1985, The Continental Crust: Its composition and evolution, Proceedings ODP, Scientific Results Volume 126: College Station, TX, Ocean Drilling Progam.

Tollstrup, D., Gill, J., Kent, A., Prinkey, D., Williams, R., Tamura, Y., and Ishizuka, O., 2010, Across-arc geochemical trends in the Izu-Bonin arc: Contributions from the subducting slab, revisited: Geochemistry, Geophysics, Geosystems, v. 11, no. 1. doi:10.1029/2009GC002847.

Uyeda, S., and Ben-Avraham, Z., 1972, Origin and development of the Philippine sea: Nature, v. 240, p. 176–178.

Whittaker, J., Muller, R., Leitchenkov, G., Stagg, H., Sdrolias, M., Gaina, C., and Goncharov, A., 2007, Major Australian-Antarctic plate reorganization at Hawaiian-Emperor bend time: Science, v. 318, no. 5847, p. 83–86. doi:10.1126/science.1143769

Wortel, M.J.R., and Spakman, W., 2000, Subducting slab detachment in the Mediterranean-Carpathian region: Science, v. 290, no. 5498, p. 1910–1917. doi:10.1126/science.290.5498.1910

Wu, J., Suppe, J., Lu, R., and Kanda, R., 2016, Philippine sea and east Asian plate tectonics since 52 Ma constrained by new subducted slab reconstruction methods: Journal of Geophysical Research, v. 121, p. B4670–4741.

Xu, J., Ben-Avraham, Z., Kelty, T., and Yu, H.-S., 2014, Origin of marginal basins of the NW Pacific and their plate tectonic reconstructions: Earth Science Reviews, v. 130, p. 154–196. doi:10.1016/j.earscirev.2013.10.002

Yamamoto, Y., and Kawakami, S., 2005, Rapid tectonics of the Late Miocene Boso accretionary prism related to the Izu–Bonin arc collision: Island Arc, v. 14, p. 178–198. doi:10.1111/j.1440-1738.2005.00463.x

Yamamoto, Y., Ogawa, Y., Uchino, T., Muraoka, S., and Chiba, T., 2007, Large-scale chaotically mixed sedimentary body within the Late Pliocene to Pleistocene Chikura Group, Central Japan: Island Arc, v. 16, p. 505–507. doi:10.1111/iar.2007.16.issue-4

Yamazaki, T., Takahashi, M., Iryu, Y., Sato, T., Oda, M., Takay-Anagi, H., Chiyonobu, S., Nishimura, A., Nakazawa, T., and

Ooka, T., 2010, Philippine Sea Plate motion since the Eocene estimated from paleomagnetism of seafloor drill cores and gravity cores: Earth, Planets and Space, v. 62, p. 495–502. doi:10.5047/eps.2010.04.001

Yokoyama, T., Kobayashi, K., Kuritani, T., and Nakamura, E., 2003, Mantle metasomatism and rapid ascent of slab components beneath island arcs: Evidence from ^{238}U - ^{230}Th - ^{226}Ra disequilibria of Miyakejima volcano, Izu arc, Japan: Journal of Geophysical Research, Solid Earth, v. 108. doi:10.1029/2002JB002103.

Yokoyama, T., Kuritani, T., Kobayashi, K., and Nakamura, E., 2006, Geochemical evolution of a shallow magma plumbing system during the last 500 years, Miyakejima volcano, Japan: Constraints from ^{238}U–^{230}Th–^{226}Ra systematics: Geochimica Et Cosmochimica Acta, v. 70, no. 11, p. 2885–2901. doi:10.1016/j.gca.2006.02.027

Zahirovic, S., Seton, M., and Müller, R.D., 2014, The Cretaceous and Cenozoic tectonic evolution of Southeast Asia: Solid Earth, v. 5, p. 227–273. doi:10.5194/se-5-227-2014

Ziegler, C.L., and Murray, R.W., 2007, Geochemical evolution of the central Pacific Ocean over the past 56 Myr: Paleoceanography, v. 22, p. PA2203. doi:10.1029/2006PA001321

Ziegler, C.L., Murray, R.W., Hovan, S.A., and Rea, D.K., 2007, Resolving eolian volcanogenic and authigenic components in pelagic sediment from the Pacific Ocean: Earth and Planetary Science Letters, v. 254, p. 416–432. doi:10.1016/j.epsl.2006.11.049

Zimmermann, U., and Bahlburg, H., 2003, Provenance analysis and tectonic setting of the Ordovician clastic deposits in the southern Puna Basin, NW Argentina: Sedimentology, v. 50, p. 1079–1104. doi:10.1046/j.1365-3091.2003.00595.x